IN SITU ELECTRON, PROTON, AND ULTRAVIOLET RADIATION EFFECTS ON THERMAL CONTROL COATINGS

FINAL REPORT FOR THE PROGRAM

SPACE ENVIRONMENT EFFECTS
ON THERMAL CONTROL COATINGS

CONTRACT NO. NAS5-9650

GODDARD SPACE FLIGHT CENTER

CONTRACTING OFFICER: Peter Videnieks

TECHNICAL MONITOR: Charles H. Duncan

PREPARED BY:

Lawrence B. Fogdall
TECHNICAL LEADER

Sheldon S. Cannaday
PRINCIPAL INVESTIGATOR

Richard P. Brown
PROGRAM MANAGER

THE BOEING COMPANY
AEROSPACE GROUP
SEATTLE, WASHINGTON

FOR

GODDARD SPACE FLIGHT CENTER
GREENBELT, MARYLAND

IN SITU ELECTRON, PROTON, AND ULTRAVIOLET RADIATION EFFECTS ON THERMAL CONTROL COATINGS

FINAL REPORT FOR THE PROGRAM

SPACE ENVIRONMENT EFFECTS
ON THERMAL CONTROL COATINGS

CONTRACT NO. NAS5-9650

PREPARED BY
THE BOEING COMPANY
AEROSPACE GROUP
SEATTLE, WASHINGTON

FOR

GODDARD SPACE FLIGHT CENTER
GREENBELT, MARYLAND

ABSTRACT

This document constitutes the final report for NASA Goddard Contract NAS5-9650. Included is a description of and results from tests conducted for the research program, "Space Environment Effects on Thermal Control Coatings," accomplished during the period 15 September 1965 through 15 July 1968. During this research program, electron, proton and ultraviolet radiation exposures were conducted on 21 types of thermal control coatings. Measurements of spectral reflectance in the wavelength region from 240 to 2500 millimicrons were obtained in situ on a total of about 200 samples, before exposures began, periodically during exposures, and both in vacuum and in air, following exposures. Data obtained from these measurements were analyzed for spectral reflectance changes, for solar absorptance changes, for irradiation rate effects, and for synergistic effects.

The program has resulted in many significant results and conclusions. From the electron exposure tests we conclude that:

(1) The specular surfaces tested and the leafing aluminum—silicone coating tested are relatively "hard" to reflectance degradation under 50-keV electron exposure.

(2) Excepting leafing aluminum, the diffuse coatings or paints tested are subject to severe, in-air recoverable degradation in the infrared wavelength region, and to substantial visible-region reflectance losses which are less recoverable or "bleachable" upon re-exposure of test samples to air.

(3) Coatings employing methyl silicone binders sustain the greatest degree of reflectance degradation in the infrared wavelength region. Coatings using potassium silicate binders suffer the largest electron-induced reflectance losses in the visible region.

(4) Over the wide range of fluxes and fluences used (4×10^8 to 1.7×10^{12} electrons/cm^2/sec, and 10^{13} to 8×10^{15} electrons/cm^2) no irradiation rate effects from 50-keV electrons are evident from in situ measurements of

hemispherical spectral reflectance obtained with an integrating sphere reflectometer. Thus, to an acceleration factor of 10^3 or so, laboratory exposures of the tested coatings to 50-keV electrons at rates greater than those in space are valid.

From the "ultraviolet" exposure tests we conclude that:

(5) The specular surfaces and leafing aluminum are resistant to reflectance change in the infrared wavelength region, but undergo substantial, permanent reflectance losses in the visible and ultraviolet wavelength regions.

(6) The diffuse coatings tested are subject to reflectance degradation over much or all of the measured 0.24- to 2.5-micron wavelength region.

(7) Damage thresholds and rates of damage buildup vary widely among the classes and types of coatings tested. Within their class, titanium dioxide—methyl silicone sample types show the widest variation in effects, of all classes of samples tested. One TiO_2—methyl silicone coating type was the most resistant of the diffuse samples to reflectance changes from ultraviolet radiation.

(8) Upon re-exposure to air following exposure to ultraviolet-rich electromagnetic radiation, only a few types of tested coatings (B, F_3, L, O, P, and Y) recover fairly close to their respective preirradiation reflectance values. In the majority of coatings exposed to ultraviolet, there is little evidence of increased reflectance in air when compared to post-irradiation in situ reflectance values.

(9) Separate tests show that UA-series long-arc mercury, and Pek long-arc xenon, ultraviolet sources are about equally effective for inducing reflectance losses in selected thermal control coatings.

From the proton exposure test we conclude that:

(10) The specular surfaces and leafing aluminum are quite resistant to reflectance changes across the 0.24- to 2.5-micron wavelength region.

(11) S-13G and Pyromark exhibit severe reflectance losses in the visible wavelength region. Only partial recovery of reflectance occurs in air.

From the combined electron-ultraviolet tests we conclude that:

(12) Reflectance changes resulting from coating exposure to a combined electron-ultraviolet environment are less than additive, whether the combined irradiation occurs simultaneously or sequentially.

(13) Increasing the ultraviolet-to-electron intensity radio during an exposure, or having ultraviolet exposure follow exposure to electrons causes partial restoration of reflectance in some types of coatings. Exposure to ultraviolet before electron exposure favorably preconditions some coatings to resist later changes due to the presence of the electron flux. This suggests the possibility of pre-exposing properly configured thermal control coatings on the ground, in order to obtain reduced degradation later in space.

From the overall testing program we conclude that:

(14) Optimum formulation of coatings in a given class (e.g., TiO_2—methyl silicone) must be determined by iterative steps, since radiation-induced degradation is strongly dependent upon seemingly minor variations in such parameters as coating thickness, ratio of pigment to binder, and (for samples with mixed constituents) relative amounts of pigment or binder components.

(15) Wavelength regions in which the largest reflectance changes occur are substantially different for the three cases of electron, proton, and ultraviolet radiation. Exposure to 50-keV electrons causes the greatest reflectance losses in most diffuse coatings to occur in the infrared. Ultraviolet radiation and proton radiation result in more damage at

shorter wavelengths, particularly at any existing ultraviolet absorption edge. Degradation from protons is more likely to extend as one band to longer wavelengths in a given type of coating, while separate bands of increased absorptance are more likely to result from incident ultraviolet radiation.

(16) Reflectance recovery phenomena following electron, proton, and ultraviolet exposure are likewise diverse. This diversity of both reflectance loss and reflectance recovery phenomena indicates that more than one damage mechanism may be operating in the types of coatings tested.

(17) The sequencing of combined environment exposures affects significantly the degradation that results. Except for simulating missions actually encountering a sequence of ultraviolet and electrons in space, test standardization on simultaneous exposure to electrons and ultraviolet is essential to prevent drawing false conclusions about performance of coatings in the existing, multiconstituent space environment. Future selection of coatings for space use should be even more strongly mission-dependent and based upon the anticipated relative intensities of constituents in the space environment.

(18) The results of these tests on thermal control coatings tie together (a) the results of early in-air tests in which specimens exposed to high fluences evidenced lasting effects mainly in the visible region, and (b) the more recent results of in situ testing that indicate that contamination-free exposures to electrons show reflectance changes in the infrared region as well.

The work performed for this program establishes the basis for making the following recommendations:

(1) A study of the dependence of surface reflectance degradation upon the incident energy of protons and electrons between 2 and 80 keV should be performed as follow-on work to this contract.

(2) A study of rate effects from ultraviolet radiation should be made from one to five or more space ultraviolet suns, to provide baseline data of a scope comparable to electron data available from this program.

(3) Data from (1) and (2) will provide a strong base for a properly-planned (i.e., related to orbital environments expected to be encountered) multiple radiation environment test program.

(4) A study of in-vacuum (in situ) reflectance changes with time following exposure of thermal control coatings to electromagnetic and particle radiation should be performed to provide more basic data on possible damage mechanisms.

(5) Based upon evidence of micro-pitting in selected coatings following proton exposure, an investigation of light trapping from such pitting as a potential mechanism for increased absorptance (reflectance degradation) should be made.

ACKNOWLEDGMENTS

The technical leaders and principal investigators for the research performed on this contract wish to thank Mrs. Ruby Lee, Mrs. Joanne Arrowood, Mrs. Esther Taylor, Miss Betty Barry, Mr. C. R. Brittain, Jr., Mr. E. D. Sullivan, and Mr. Loren D. Milliman for their assistance in obtaining and analyzing test data, and in preparing this report.

KEY WORDS

CRETC
Curing
Contamination control
Damage mechanisms
Electron gun
Electron radiation
Equivalent sun hour
Filters
Fluence
Flux
Hemispherical
In situ
In situ spectral monitor
In situ reflectometer
Monochromator
Proton radiation
Radiation
Rate effects
Reflectance
Reflectance recovery
Solar simulation
Source spectra
Spectral
Spectrum
Standardize
Thermal control coatings
Ultraviolet
Vacuum

TABLE OF CONTENTS

LIST OF FIGURES

LIST OF FIGURES (continued)

LIST OF FIGURES (continued)

LIST OF FIGURES (continued)

LIST OF FIGURES (continued)

LIST OF FIGURES (continued)

LIST OF FIGURES (continued)

LIST OF TABLES

1.0 SUMMARY OF PROGRAM

1.1 PROGRAM DESCRIPTION

The overall objective of the program has been a survey of the effects of electrons, protons, and ultraviolet radiation on a great variety of thermal control coatings, in the presence of environmental conditions similar to those encountered in space. The environment criterion selected has been that for a near-earth orbiting spacecraft. Those features selected for simulation have been ultrahigh vacuum, temperature, ultraviolet radiation, and magnetically trapped electrons. The specific objectives of the program have been to:

(1) Study the effects of simultaneous electron and ultraviolet irradiation on the thermophysical properties of thermal control coatings.

(2) Establish the validity of accelerated-rate laboratory irradiation of coatings through a study of electron radiation damage as a function of exposure rate.

(3) Conduct surveys of coating degradation phenomena following exposure to protons, ultraviolet radiation from xenon arc sources, and ultraviolet radiation from mercury arc sources.

(4) Investigate physical property changes as well as optical characteristic changes due to irradiation in a simulated space environment.

Approximately 1,000 test specimens have been supplied by the Thermophysics Branch of NASA Goddard. These samples have been exposed to electrons, protons, and ultraviolet radiation, both singly and together, using the Combined Radiation Effects Test Chamber (CRETC). To meet the program objectives the following tests have been conducted:

(1) A screening test involving exposure of 17 sample types at 22°C, to 50-keV electrons at fluences from 1.6×10^{13} to 8.5×10^{14} electrons cm^{-2}.

(2) An electron rate test, again using 50-keV electrons at fluxes from 4×10^{8} to 1.7×10^{12} electrons cm^{-2} sec^{-1}, to establish the equivalence between effects produced by accelerated laboratory exposures and the lower flux levels of space exposure, on 13 sample types at 20°C. The fluence range covered was 1×10^{13} to 8×10^{15} electrons cm^{-2}.

(3) An ultraviolet radiation effects study to provide information needed to determine if the effects of low energy electrons and ultraviolet radiation are additive for simultaneous or sequential irradiations. Forty-one samples of 14 program types, plus five samples of two types of current interest to the OAO program, were exposed to ultraviolet-rich electromagnetic energy, and measured at levels from 18 to 1,130 equivalent UV-sun hours, while their substrates were maintained at 20°C.

(4) An electron-ultraviolet intensity ratio study to determine the influence of this ratio on damage and damage rates. Periodic reflectance measurements were made on selected types of coatings in vacuum at 20°C during combined ultraviolet and 50-keV electron exposure tests.

(5) A proton effects test, to survey the degradation caused by 20-keV protons in selected types of coatings. Seven coating types were exposed to fluences from 10^{14} to 10^{17} protons cm^{-2}.

(6) A xenon lamp continuum effects comparison performed on selected coatings. Nine types of samples were exposed up to 85 ESH from xenon sources and the degradation compared to that observed in Test 3.

Hemispherical spectral reflectance measurements of test and control samples have been made in situ over the 240 to 2500 millimicron wavelength region before, periodically during, and after irradiation. Spectral reflectance data obtained have been analyzed to determine changes in reflectance. On appropriate samples the existence of rate effects or synergistic effects has been investigated. On selected samples the recovery of lost reflectance upon re-exposure to air has been determined. Physical changes have been noted in certain samples.

1.2 TEST FACILITY DEVELOPMENT

Concurrent with the execution of this research program was the developmental evolution of a combined radiation effects test chamber (CRETC). Inherent in considerations guiding its development was a desire not only to incorporate judiciously recent innovations of contemporary facilities but also to validate several original concepts. This endeavor culminated in the creation of a uniquely flexible in situ test facility that is sufficiently versatile to respond to changing requirements of environmental conditions and test methods, and yet be commensurate with both the specific program objectives of the contracted study and of ensuing, follow-on programs.

Several of the salient features of the CRETC are cited to indicate the spectrum of its capabilities.

(1) The CRETC provides not only the environments (vacuum, temperature, ultraviolet radiation, and electron radiation) to the degree specified in the original technical proposal, but also provides simultaneous exposure by positive ions (protons and alpha particles). Thermally-generated electrons are also available to simulate charge neutralization phenomena associated with the solar wind.

(2) The large chamber concept with its inherent advantage of large capacity permits:

   (a) The testing of hundreds of specimens while maintaining identical vacuum and temperature conditions for all samples at all times during radiation exposure and measurement of reflectance.

   (b) The uniform exposure of large groups of specimens with simultaneously combined types of radiation while concurrently uniformly exposing other groups of specimens to the separate component types of radiation (all specimens being in the same residual gas environment).

(c) The rotation of a second group of samples into an undisturbed radiation beam such that the new specimens are in the exact positions occupied by corresponding samples of the first group (with the ability to alter other aspects of the environment).

(d) The exposure of different groups of samples to the radiation of different types of ultraviolet lamp sources, in order to correlate the resultant changes in reflectance with the emission spectra.

(3) In addition to furnishing the more conventional, modern dosimetry techniques for charged particles, an in situ ultraviolet lamp monitoring system has been devised for high resolution spectral measurements of the actual electromagnetic intensity incident on the sample plane.

(4) An effective anticontamination baffle is available to eliminate cross-contamination of specimens subjected to exposure conditions. The large chamber concept employed in the CRETC is believed to diminish significantly self-contamination and other forms of external contamination often observed in small-volume chambers.

(5) The acquisition of test data from the CRETC reflectometer and Beckman DK-2A spectrophotometer employs automated equipment, enabling significant time and cost savings as well as increased accuracy. The Datex data handling system installed treats and feeds data to an IBM 526 card punch. The result is the simultaneous compilation of raw data (conventional reflectance charts) and the implementation of computer-aided data reduction.

The integration of a low energy particle accelerator (LEPA) with the CRETC is shown in Figure 1. The dual Plasmatron source of ions is mounted external to the CRETC to facilitate magnetic energy analysis and mass separation of positive ions. Both the very low energy ("thermal") electron source (utilized for charge neutralization) and the electron accelerator (shown in Figure 2) are mounted inside of the vacuum chamber, to minimize the influence of drift fields. Electrons

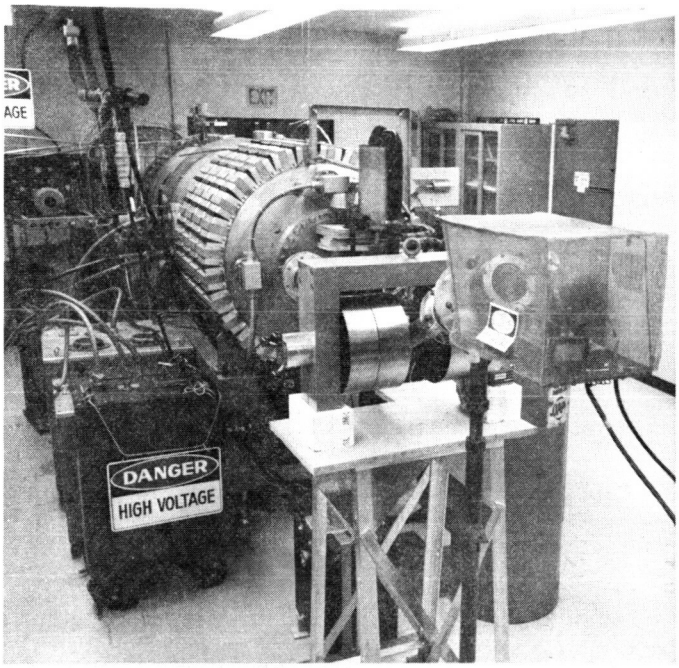

Figure 1. Low Energy Particle Accelerator and Combined Radiation Effects Test Chamber

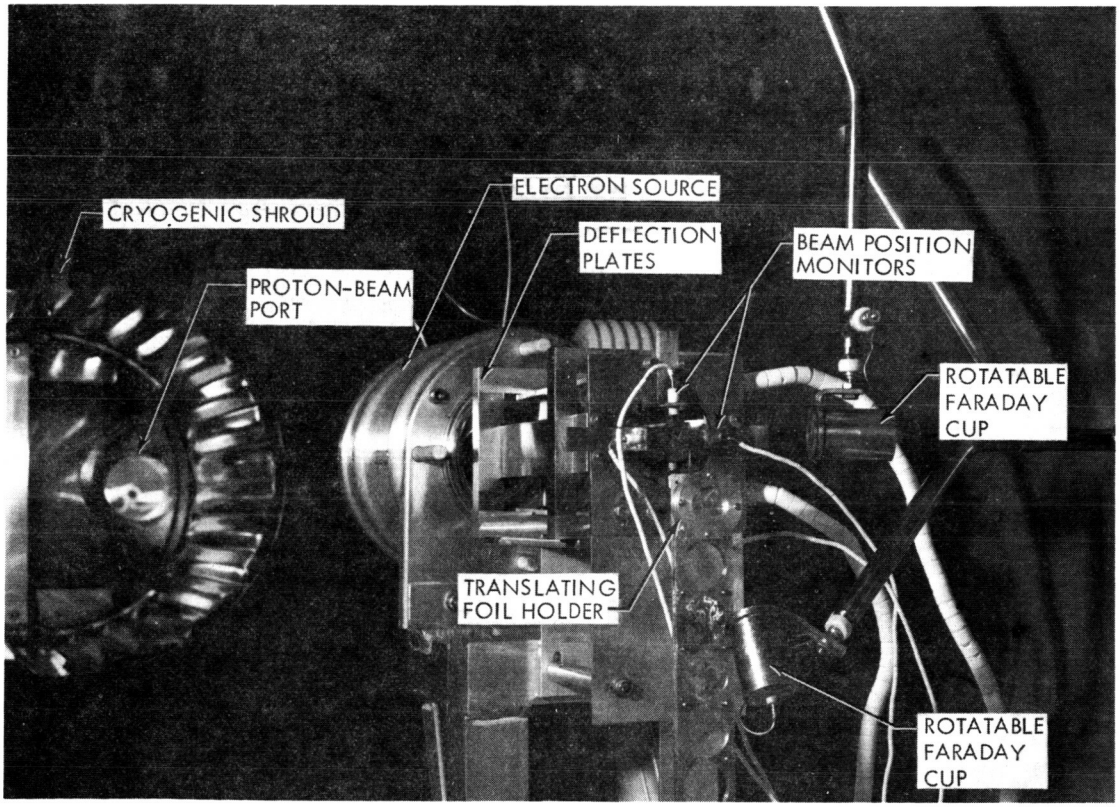

Figure 2. CRETC Electron Accelerator and Beam Handling System

and positive ions available from the major radiation sources encompass the energy range from below 1 keV up to 100 keV. To obtain higher energies, the CRETC external beam port is designed to join the beam handling systems of the existing Dynamitron (energies to 3 MeV) and the Linac (energies to 25 MeV),

The interior of the three-feet-diameter CRETC is shown in Figure 3. Shown is the temperature-controlled specimen wheel (containing mounted arrays of samples), the housing assembly for the integrating sphere (utilized in reflectance measurements), foils for electron beam scattering, and an array of water-cooled UA-3 and UA-11 mercury-vapor lamps. Figure 4 shows a pair of xenon lamps mounted in the same chamber, and the very low energy electron source.

The in situ spectral monitoring system for ultraviolet-rich electromagnetic energy sources is diagrammed in Figure 5. This system, calibrated against standard light sources, can record high-resolution spectral information at wavelengths as short as 1650 Angstroms, and as long as 3.5 microns (35,000 Angstroms). An example is shown in Figure 6.

Shown in Figure 7 is the anticontamination baffle used extensively during this program. The temperature of this baffle can be controlled by selected coolants. Evaluation of the reflectance stability of standard specimens and radiation-resistant control specimens shows no evidence of either external or cross-contamination.

Measurement of spectral reflectance is performed using a Beckman Far UV DK-2A spectrophotometer, external to the CRETC, in conjunction with an integrating sphere located within the vacuum chamber. The interior wall of the integrating sphere is a composite—electrostatically-smoked magnesium oxide power over a zinc oxide-potassium silicate paint base. This system is depicted diagrammatically in Figure 8. High-resolution spectral reflectance charts can be obtained, as evidenced by the data presented in Figure 9. The automatic spectral data collection system (whose control console is shown in Figure 10), in conjunction with an IBM 526 card punch, accelerates data acquisition and analysis. Accuracy is enhanced by employing computer programs that can display reflec-

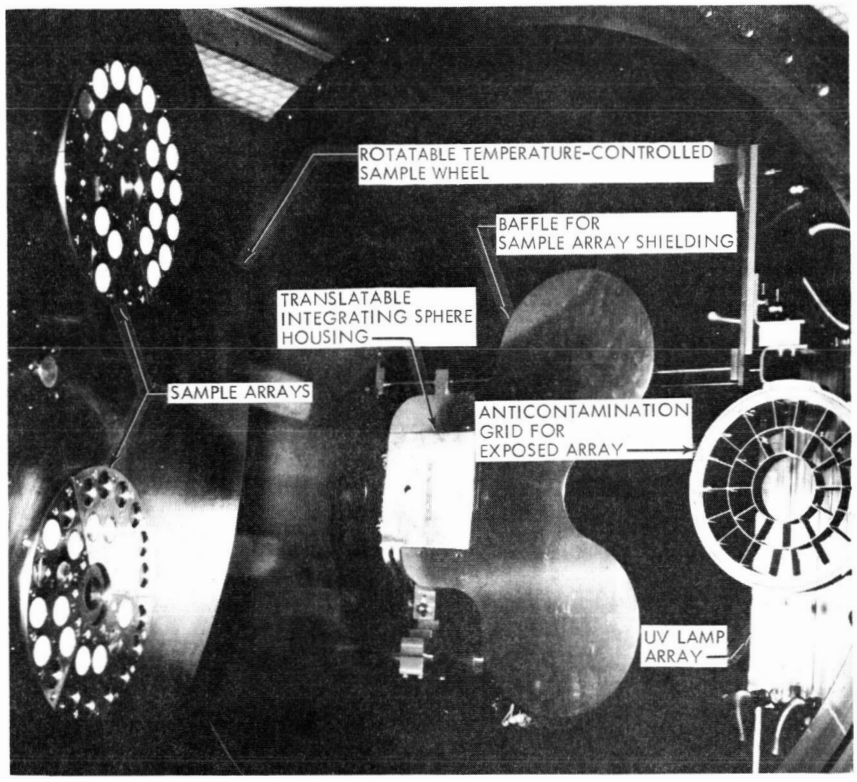

Figure 3. CRETC Interior

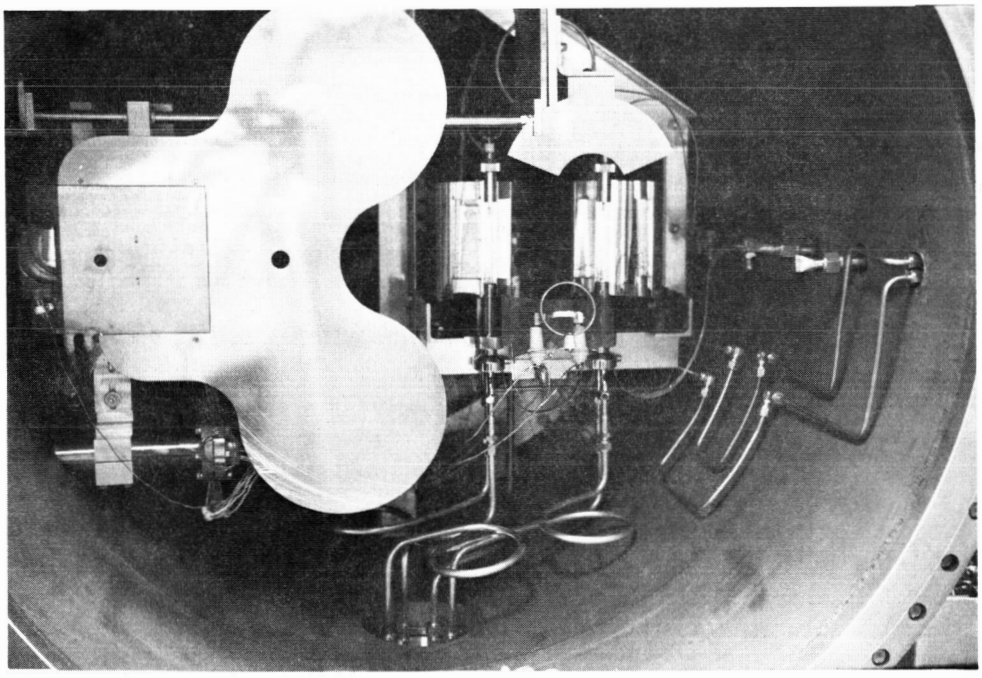

Figure 4. CRETC Integrating Sphere, Xenon Ultraviolet Sources, and Thermal Electron Source

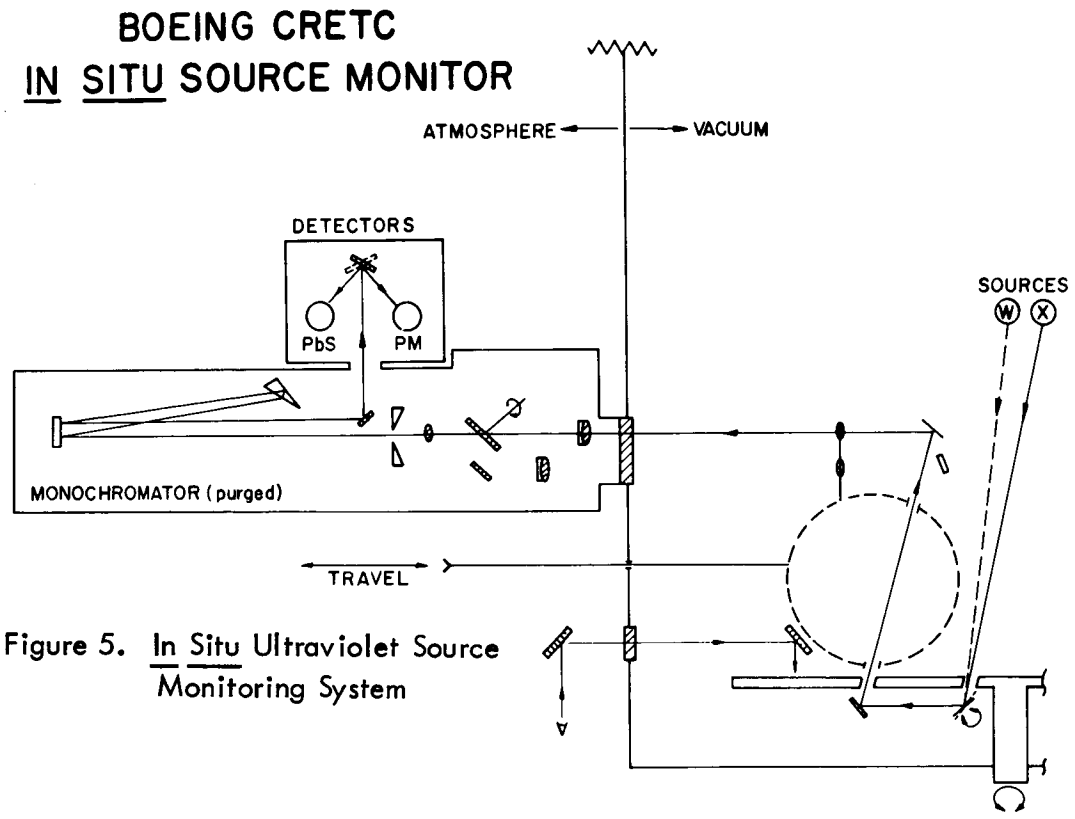

Figure 5. In Situ Ultraviolet Source Monitoring System

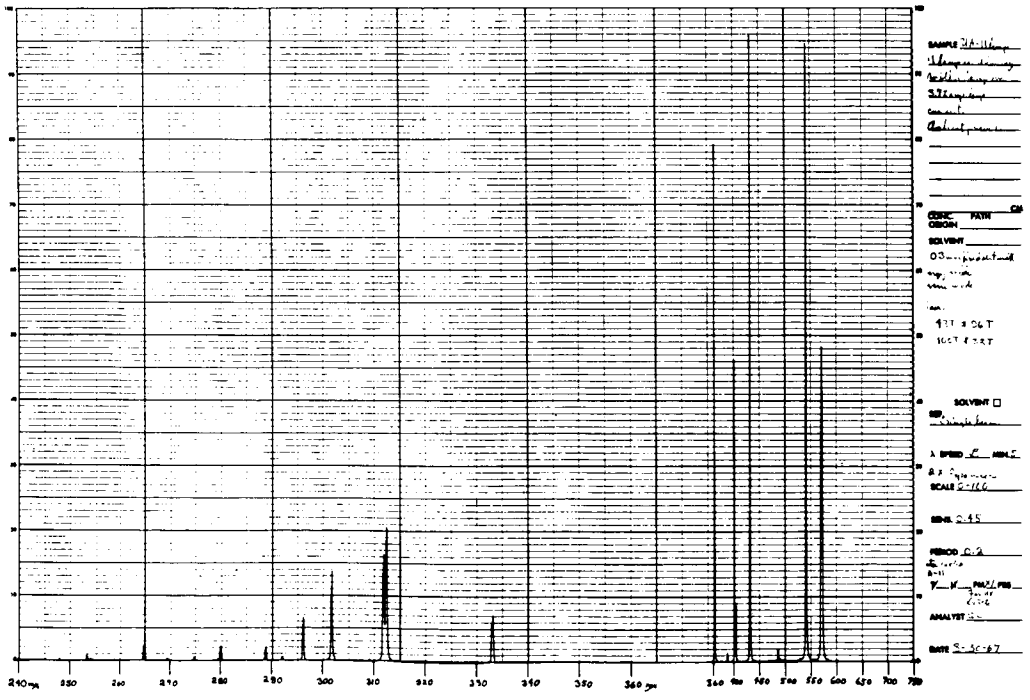

Figure 6. In Situ Monitoring of Ultraviolet Source. Visible and Ultraviolet Regions

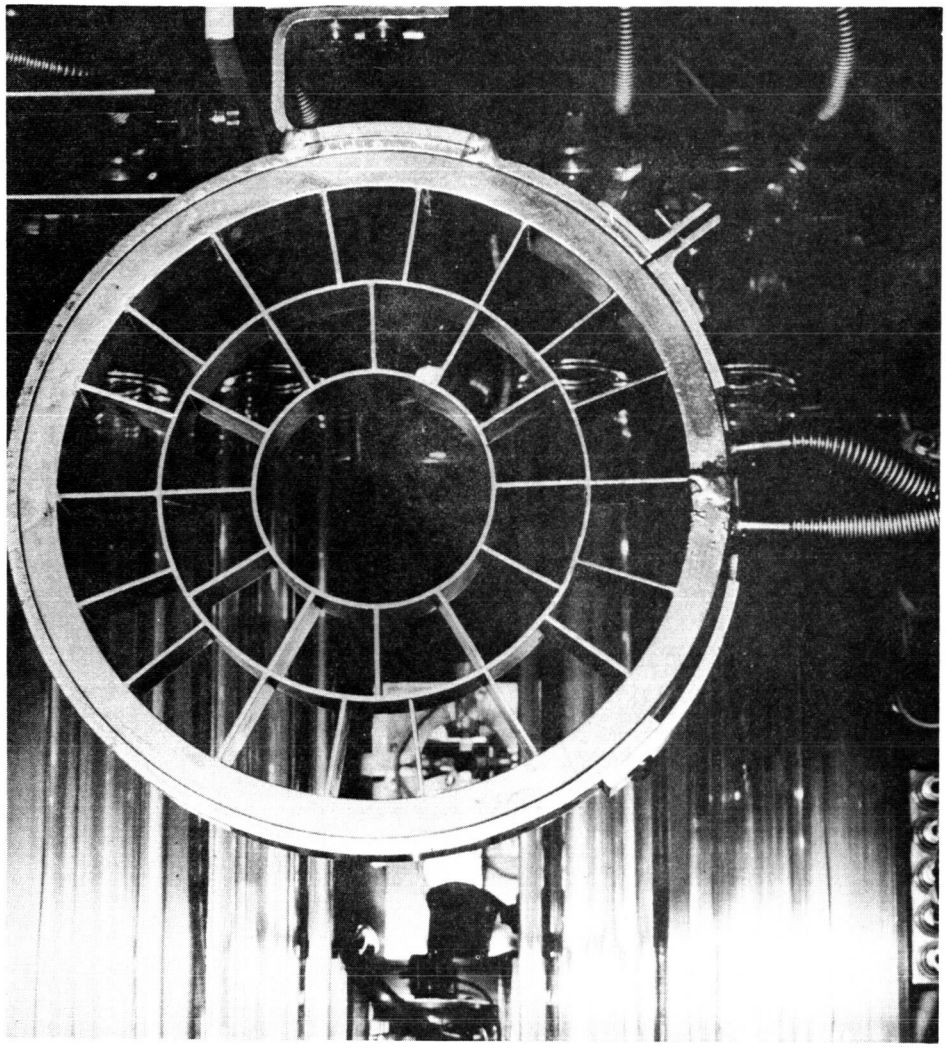

Figure 7. Sample Anticontamination Baffle

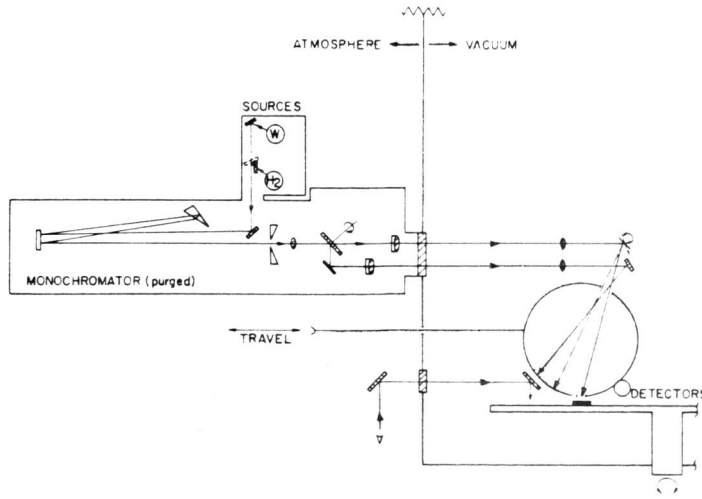

Figure 8. Diagram of the In Situ Reflectance Measurement System

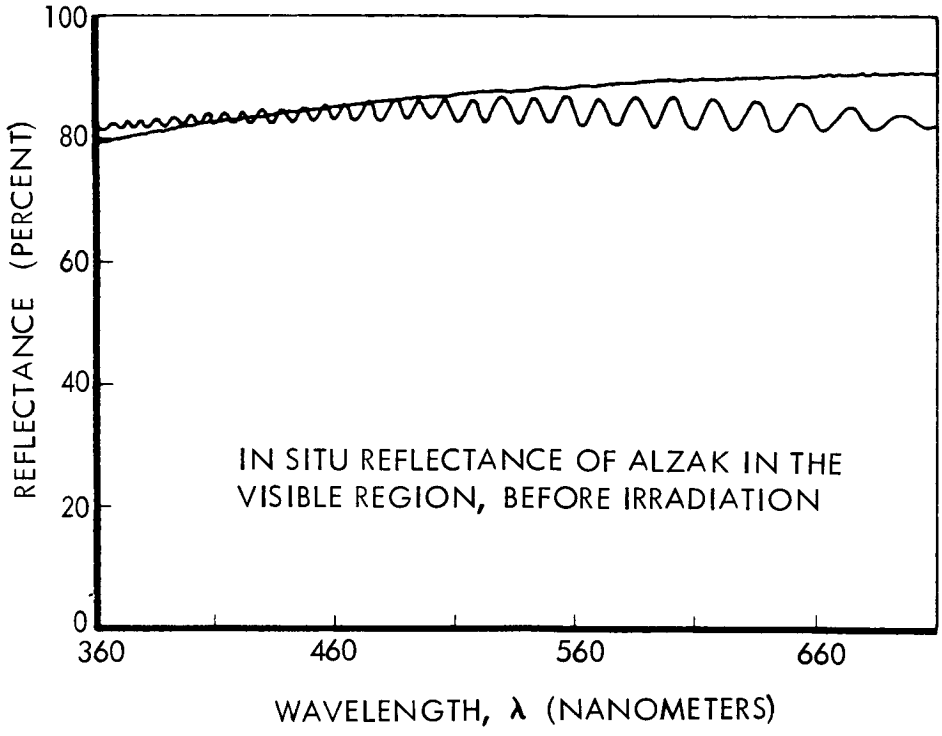

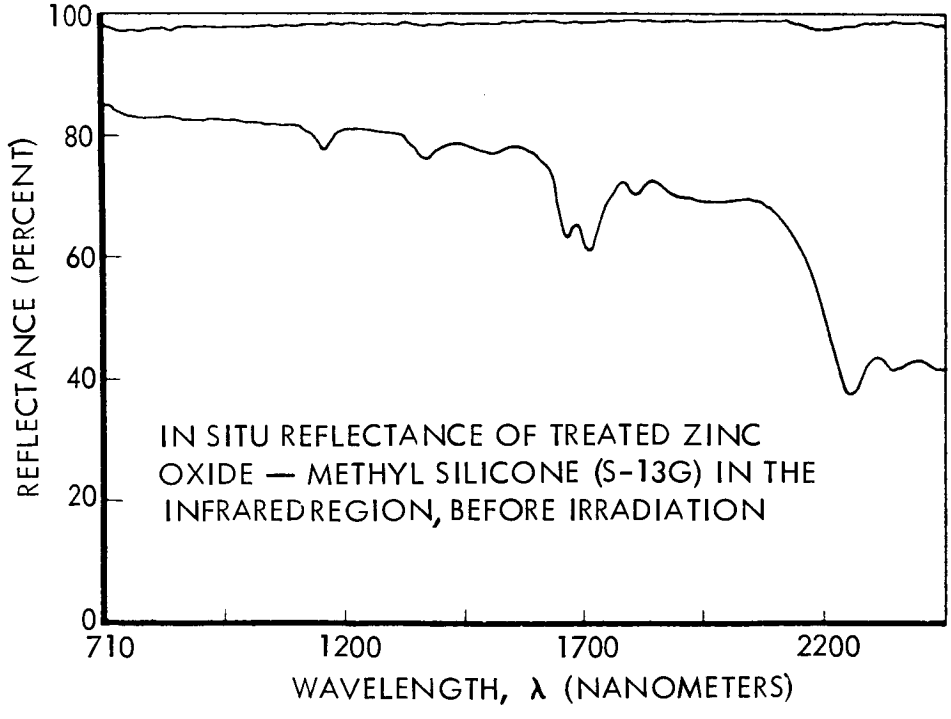

Figure 9. Spectral Reflectance Measurements Made In Situ

Figure 10. Spectrophotometer Data Recording System Console

tance data in a variety of ways and can compute absolute reflectance using data from reflectance standards and normalization factors. Folding of the solar spectrum into output data is readily performed by the computer to obtain solar absorptance.

Figures 50 through 59, and 66 through 68 in this report are computer-processed plots of changes in reflectance, obtained using the automatic data collection system.

2.0 DETAILED REPORT OF PROGRAM RESULTS

The main effort of this program has been directed toward obtaining in situ test results of changes in the spectral reflectance of some 22 types of thermal control coatings exposed to single and/or multiple constituents of the space radiation environment.

2.1 TEST SPECIMENS

Table 1 lists and describes the 22 types of coatings exposed to various radiation sources during the different phases of the program. Upon receipt from NASA-Goddard, test samples were secured and stored in a clean environment. When being placed in sample holders in preparation for exposure, each sample was handled on edge by persons wearing clean, white gloves. Copper shims placed behind the aluminum substrate of each test sample assured maximum thermal contact with the CRETC's temperature-controlled copper sample wheel throughout tests. Figure 3 (in Section 1.2) shows the configuration of mounted samples.

More detailed descriptions of sample preparation procedures for coating types D_3, E_3, F_3, H, I, and J are given in Tables 2, 3, 4, and 5.

2.2 TESTS IN ELECTRON-ONLY ENVIRONMENT

Two groups of exposure tests were conducted on the majority of the coatings listed in Table 1: an initial electron screening test, and a series of electron rate tests. All exposures were made using a 50-keV electron beam obtained from an electron gun mounted in the CRETC. The electron beam was scattered through a thin aluminum foil to obtain uniform exposure (axial symmetry) of samples mounted in test arrays like those shown in Figure 3. Voltage on the accelerating electrode was adjusted so that the energy of the electrons would be 50 keV after passing through the scattering foil. Direct beam current was measured in a fixed Faraday cup located behind the sample wheel. The hole in the center of each sample array (see Figure 3) serves as an aperture for that insulated Faraday cup. Thus the cup can also be used to monitor the forward scattered beam during exposure in order to

Table 1. Coating Types And Radiation Environments In Which Tested

Type Code	Description of Coating (Pigment--binder)	Exposed to			
		Electrons	UV	Electrons -UV	Protons
A	Anatase titanium dioxide-Dow Corning Q92-0090 methyl silicone, mixed 3 parts paint to 1 part catalyst. Approx. 2 mils of paint on top of 2 mils of Cat-a-Lac white primer.	x			
B S-13	Zinc oxide—methyl silicone. Approx. 9 mils of S-13 on top of a thin coat of GE S54044 primer.	x	x	x	
C	Zinc oxide—Dow Corning Q92-016 methyl silicone. Approx. 10 mils of paint on top of 2 mils of Cat-a-Lac white primer.	x			
D_3	Alpha-phase aluminum oxide—PS-7 potassium silicate. Approx. 11 mils of paint, applied directly to substrate. (See Table 2 also.)	x	x	x	
E_3	Rutile titanium dioxide/aluminum oxide—PS-7 potassium silicate. Approx. 4 mils of paint, applied as with type D_3; see Table 2.	x	x		
F_3	Zinc oxide/aluminum oxide—PS-7 potassium silicate. Approx. 5 mils of paint, applied as with type D_3; see Table 2.	x	x		
G	Vapor-deposited aluminum oxide (11,000 Å) on top of 1000 Å of aluminum evaporated onto a buffed, chemically cleaned, and glow discharge cleaned, substrate. (Prepared by Dr. Georg Hass of Fort Belvoir.)	x			x
H	Silicon dioxide deposited in vacuum onto a buffed and degreased aluminum substrate. See Table 3 also.	x	x		x
I	Leafing aluminum—mixed Dow Corning 805 and 806A phenylated silicones. Approx. 3 mils total in 3 coats; see also Table 5.	x	x		x

Table 1. Coating Types And Radiation Environments In Which Tested (Continued)

Type Code	Description of Coating (pigment--binder)	Exposed to			
		Electrons	UV	Electrons -UV	Protons
J	Vapor-deposited aluminum on a lacquered aluminum substrate. See Table 4	x	x		x
K	Buffed and vapor-degreased aluminum substrate.	x	x		x
L_1	Anatase titanium dioxide—Dow Corning Q92-0090 methyl silicone, mixed 3 parts paint to 1 part catalyst. Like type A, but approx. 5 mils of paint on top of 2 mils of Cat-a-Lac white primer.	x	x		
L_2	One-half of the type L samples, stored with a black water-emulsified removable overcover until a few hours before exposure.	x	x		
M S-13G	Treated zinc oxide—methyl silicone. Approx. 10 to 12 mils of an early formulation of S-13G, over S54044 primer.	x	x		x
N	2-mil Kapton H-film over a thin aluminum coat on an aluminum substrate.	x	x		
O	Rutile titanium dioxide—GE RTV 602 methyl silicone, mixed 2 parts pigment to 1 part vehicle.	x	x		x
P	Rutile titanium dioxide—Dow Corning XR 6-3488 methyl silicone, mixed 3 parts pigment to 2 parts vehicle.	x	x		
Q	Zinc oxide and titanium dioxide pigments in a mixed silicone/silicate vehicle.	x	x		
R	Treated zinc oxide—methyl silicone Series 101-7-1		x		
Y	Antase titanium dioxide—methyl phenyl silicone (OAO Pyromark Standard White).	x	x	x	x
Z_1	0.29-mil anodized aluminum. Alzak specimen No. 21		x		
Z_2	0.10-mil anodized aluminum. Alzak specimen No. 26		x		

Table 2. Preparation of Alkali Silicate Samples (Type D_3, E_3, and F_3)

Preparation of Substrates

1. Abraded
2. Degreased using H_3PO_4, then rinsed
3. Residual H_3PO_4 neutralized with 50 percent solution of PS-7

Coating Constituents

	Series D_3	Series E_3	Series F_3
K_2SiO_3	52%	56%	56%
TiO_2	--	9	1
ZnO (SP-500)	--	--	8
Al_2O_3	27	24	24
KOH (27N)	2	1	1
H_2O	19	10	10
	100%	100%	100%

Coating Preparation Process

1. Add solids to KOH(27N) and water mixture — excess water.
2. Stir and heat for about 3 days.
3. Evaporate to a thick slurry.
4. Add silicate.
5. Stir and heat 2 days.
6. Monitor weight of combination until the correct water balance is obtained.
7. Allow mixture to stand for about 14 days.
8. Carefully remove liquor. The remaining contents may be sprayed.

Table 3. Preparation of SiO_x Samples (Type H)

Aluminum discs buffed to 85-87 percent reflectance and degreased.
Coating Procedure 1. SiO applied in vacuum - one quarter wavelength (550 mμ). 2. Evaporate aluminum to opacity. 3. SiO_x applied in air environment to thickness of 18 quarters wavelengths. 4. Coatings exposed to ultraviolet radiation for total of 5 hours; no further change seen in reflectance. Final coating therefore considered to be SiO_2. Total coating weight approximately 0.0018 gram.

Table 4. Preparation of Vapor-Deposited Aluminum Samples (Type J)

Preparation of Substrate 1. Abraded with 320 grit silicon carbide paper. 2. Cleansed with acetone. 3. Interchemical Corp. Paladin thermosetting black primer applied to thickness of 0.0005 inch and baked for one hour at 350°F. 4. Bee Chemical Co. Logo urea or melamine formaldehyde (modified) clear thermosetting type lacquer applied in 2 coats to approximate 0.007 - 0.008 inch thickness. Force dried one hour at 150°F, and baked one hour at 350°F.
Coating Process Aluminum deposited to a total weight of approximately 0.04 gram.

Table 5. Preparation of Leafing Aluminum-Silicone Samples (Type I)

Preparation of Substrate	
1. Abraded with 320 grit silicon carbide paper.	
2. Cleansed with acetone.	
Coating Constituents Formula	
	Parts by Weight
Metal's Disintegrating Company 5100 Leafing Aluminum Powder	18.7
Dow Corning Silicone Resin No. 805 50 percent solids -- phenylated	29.1
Dow Corning Silicone Resin No. 806A 50 percent solids -- phenylated	29.1
Xylene	9.0
Coating Process	
1. Stored in glass for maximum shelf stability.	
2. Mixing accomplished on a Brookfield Counterrotating Mixer.	
3. Applied directly to aluminum disc substrates. No primer used.	
4. Three coats, applied at 15-minute intervals, for total of 0.003 inch approximately.	
5. Baked 3 hours at 350°F. Coating weight approximately 0.05 - 0.06 gram.	

provide a means of obtaining total exposure fluence. Two remotely controlled Faraday cups (90° with respect to each other) are rotated in front of the scattering foil in order to map the Gaussian electron scattering.

2.2.1 Electron Screening Test

Table 6 indicates the irradiation test points obtained, and the sample measurements made, during the 50-keV electron screening test. In situ spectral reflectance measurements were made following electron exposures of 1.6×10^{13}, 2×10^{14}, and 8×10^{14} electrons cm^{-2}. Average exposure rates used in reaching these three fluences were 2×10^{10}, 1×10^{11}, and 5×10^{11} electrons cm^{-2} sec^{-1}, respectively. These exposure rates were sufficiently low that no significant heating occurred in the test samples (determined by calculation). The temperature of the sample wheel, monitored during the test, was 22°C.

Hemispherical spectral reflectance measurements spanning the 0.22- to 2.57-micron wavelength region were made as indicated in Table 6. From these measurements the following reflectance changes in the various types of tested coatings were noted:

Aluminum and oxide-coated aluminum sample types G, H, I, J, and K exhibited no significant loss in reflectance from 0.25 to 2.5 microns for exposures as great as 8×10^{14} electrons cm^{-2}. Kapton H-film (sample type N) showed some reflectance loss in the visible region, but serious degradation occurred only at the highest exposure fluence, 8×10^{14} electrons cm^{-2}.

Zinc oxide—methyl silicone sample types (B, C, and M) had their greatest losses of reflectance in the infrared region. These samples showed the greatest loss of reflectance in the infrared region of all types tested. Type M appears to be the most sensitive of the ZnO—methyl silicone specimens. However, the loss of reflectance by ZnO—methyl silicone samples in the visible region was much less and far below that of many other sample types.

Table 6

Irradiation Test Points and Measurements —

Electron Screening Test

TEST SAMPLES	PRE-IRRADIATION, IN AIR			PRE-IRRADIATION, IN VACUUM			1.6×10^{13} e/cm^2			2×10^{14} e/cm^2			8×10^{14} e/cm^2			POST IRRADIATION, IN AIR		
	UV	VIS	IR	UV	VIS	IR	UV	VIS	IR	UV	VIS	IR	UV	VIS	IR	UV	VIS	IR
A-3	X	X	X	X	X	X		X	X	X	X	X		X	X			X
B-3	X	X	X		X			X			X	X		X	X		X	X
C-3	X	X	X		X			X			X	X		X	X			X
D_3-3	X	X	X	X	X		X	X		X	X	X	X	X	X			X
G-3	X	X	X	X	X	X	X			X		X	X	X	X			
F_3-3	X	X	X		X	X		X	X	X	X	X		X	X		X	X
E_3-3	X	X	X		X		X	X		X	X	X		X	X		X	X
H-3	X	X	X	X	X		X	X		X	X	X	X	X	X	X		
I-1	X	X	X	X	X					X	X	X	X	X	X			X
J-1	X	X	X	X	X		X			X	X	X	X	X	X			
K-3	X	X	X	X	X					X	X	X	X	X	X	X	X	X
L_1-11	X	X	X		X			X			X	X		X	X			X
L_2-4	X	X	X		X						X	X		X	X		X	X
M-3	X	X	X	X	X	X		X	X	X	X	X	X	X	X		X	X
O-3	X	X	X		X			X			X	X		X	X		X	X
P-4	X	X	X		X	X		X	X		X	X		X	X		X	X
N-4	X	X	X	X	X	X		X		X	X	X	X	X	X		X	
CONTROLS																		
A-2					X	X					X	X		X				
B-2					X													
C-2																		
D_3-2				X									X					
G-2				X	X													
F_3-2					X	X		X				X			X			
E_3-2					X			X						X				
H-2				X	X	X						X				X		
I-2				X														
J-2				X										X				
K-2				X	X					X		X			X	X	X	X
L_1-2																		
L_2-3																		
M-2						X						X			X			
O-2																		
P-2					X	X						X			X			

X = Reflectance charts that were made.

Titanium dioxide—methyl silicone sample types (A, L_1, L_2, O and P) were found to be less sensitive to reflectance change in the infrared region than the ZnO —methyl silicone samples. They did suffer more significant reflectance loss in the visible region, however. The order of resistance of the TiO_2—methyl silicone samples to radiation damage turned out to be in correlation with the alphabetical listing of the TiO_2—methyl silicone types. Thus sample type A was observed to have sustained the greatest loss of reflectance. Sample type L_2, with the removable coating (removed prior to exposure), showed somewhat greater damage than L_1, but the differences in reflectance losses were not large, nor were they fully consistent at all exposure levels. Types O and P were most resistant to radiation damage.

Metal oxide-potassium silicate samples (D_3, E_3, and E_3) exhibited larger losses of reflectance in the visible region than in the infrared region. In the visible region, losses of reflectance at 8×10^4 electrons cm^{-2} were greater in E_3 and F_3 than for any of the other types of diffuse coatings tested. The most sensitive sample with potassium silicate binder was found to be type F_3, zinc oxide/aluminum oxide —potassium silicate.

The profile of damage (loss of reflectance) in type M, an early formulation of S-13G (treated zinc oxide—methyl silicone), shown in Figure 11, is typical of the in situ damage profile measured in the tested white diffuse coatings following electron exposure. The reflectance of sample type M was also monitored during and following the backfilling of the test chamber with dry air. Reflectance charts were obtained periodically and the resulting recovery of reflectance is also shown in Figure 11. Rapid reflectance recovery of sample type M in the infrared region was observed as opposed to much slower recovery in the visible region.

Selected in-air reflectance data was obtained on all sample types before and after electron exposure. Most of the samples showed significant recovery after 24 hours of reexposure to air. In many types, infrared reflectance returned nearly to preexposure values within 24 hours after reexposure to air, while reflectance in the visible wavelength region was restored only partially. A noted exception to nearly

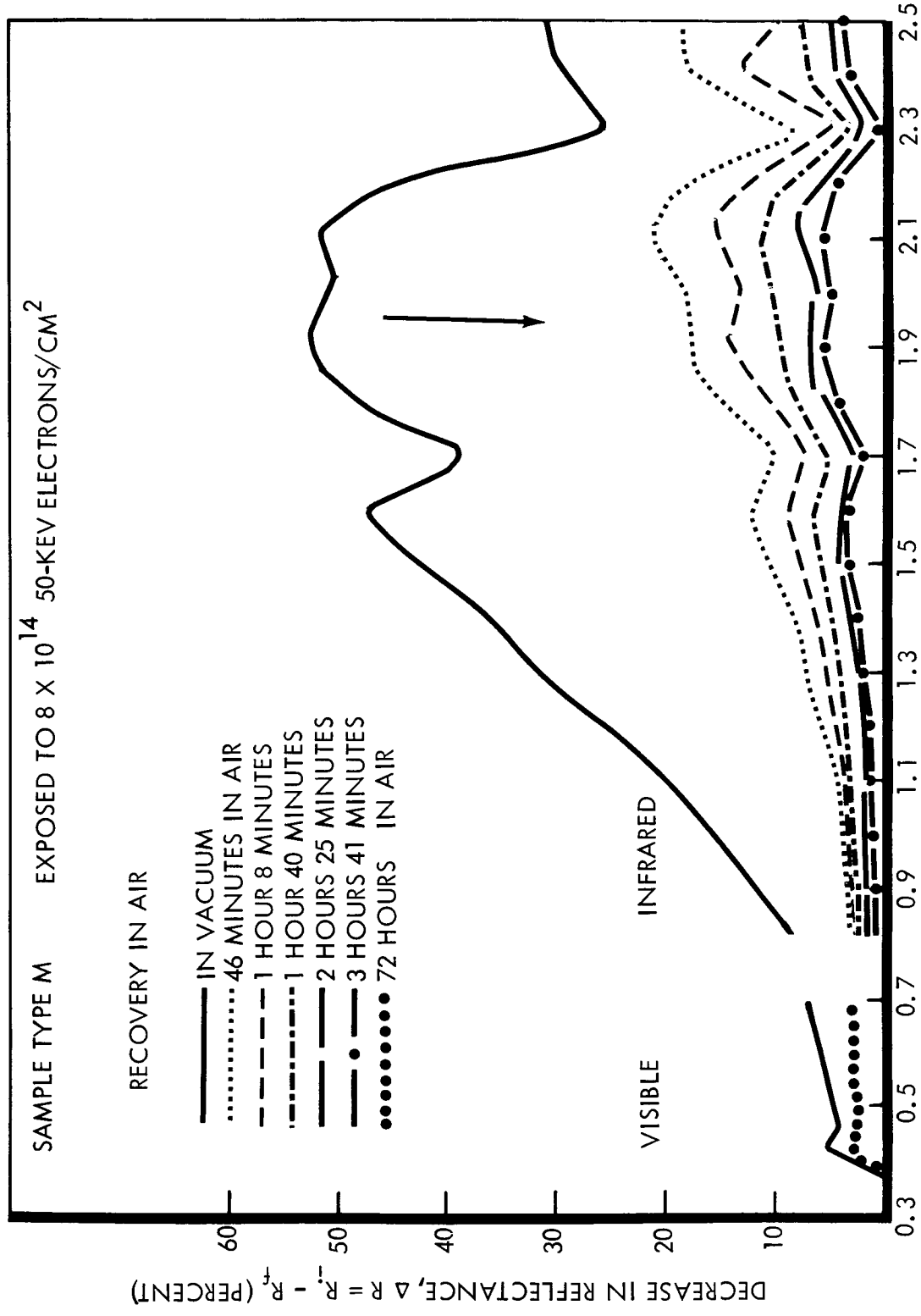

Figure 11. Damage Profile in S-13G Due to Electron Exposure, and Reflectance Recovery in Air

full recovery in the infrared was type L, which retained about half of its damage there and in the visible region also. Table 7 summarizes the observed in-air recovery properties.

Table 7. "Permanent" Reflectance Losses Measured After 24 Hours in Air, Following Exposure to 8×10^{14} 50-keV Electrons cm^{-2}

Sample Type	$\Delta R_{perm} = R_i - R_{post\ in\ air}$ (%) at		
	590 mμ	950 mμ	2100 mμ
A	-	0	1
E_3	4	2	4
F_3	4	1	5
L_1	-	4	10
L_2	6	5	15
M	3	1	3
O	0	1	2
P	1	1	2

(Note: No Significant changes in B, C, D, G, H, I, J and K.)

2.2.2 Electron Rate Studies

Table 8 shows the irradiation test points employed in these electron rate exposures, and the respective irradiation rates for each exposure which were used to establish the findings concerning electron rate effects. The findings are summarized by the statement that, for 50-keV electron fluxes ranging from those typical of peak space fluxes (4×10^8 electrons cm^{-2} sec^{-1}) to accelerated testing rates up to 1.7×10^{12} electrons cm^{-2} sec^{-1}, no significant rate effects exist in any of the 12 types of coatings tested.

The conclusion regarding absence of rate effects was obtained after detailed analysis of sample spectral reflectance data at four significant wavelengths, 590, 900, 950, and 2100 millimicrons. The wavelengths were chosen from continuous wavelength scan charts on the basis of significant reflectance changes and apparent operation of damage mechanisms in surrounding wavelength regions. Probable error

in the reflectance percentages expressed is plus or minus two percent. In the figures following, R_i is the preirradiation reflectance value, and R_f is the "final" in situ reflectance value at any given fluence. Each value has been corrected very nearly to absolute reflectance, by normalizing the integrating sphere MgO wall reference curve to 100 percent, and the sample reflectance data point proportionally.

Table 8. Exposure Rates Used For Electron Rate Study

Average Rates of and Exposures to 50-keV Electrons	
Fluence (electrons cm^{-2})	Flux (electrons cm^{-2} sec^{-1})
1×10^{13}	4×10^{8}, 1×10^{10}
1.6×10^{13}	2×10^{10}
5×10^{13}	2×10^{9}, 2×10^{10}
1×10^{14}	2×10^{9}, 2×10^{10}
2×10^{14}	2×10^{10}, 1×10^{11}
5.5×10^{14}	2×10^{10}
8.5×10^{14}	5×10^{11}
8×10^{15}	1.7×10^{12}

Figure 12 shows the building up of reflectance changes at 2100 mμ with increasing electron fluence in two zinc oxide—methyl silicone types of samples, S-13 (type B) and an early formulation of S-13G (type M). Data for each irradiation rate or flux bears a different symbol, allowing the determination to be made that exposures at all rates used cause equivalent manifestations of reflectance changes.

Figure 13 shows similar data at 2100 mμ for two types of titanium dioxide—methyl silicone coatings (L and P). Reflectance changes in L, an anatase TiO_2, are larger than those in P, a rutile TiO_2, at all but the highest fluence. Again, reflectance changes are seen to be independent of irradiation rate.

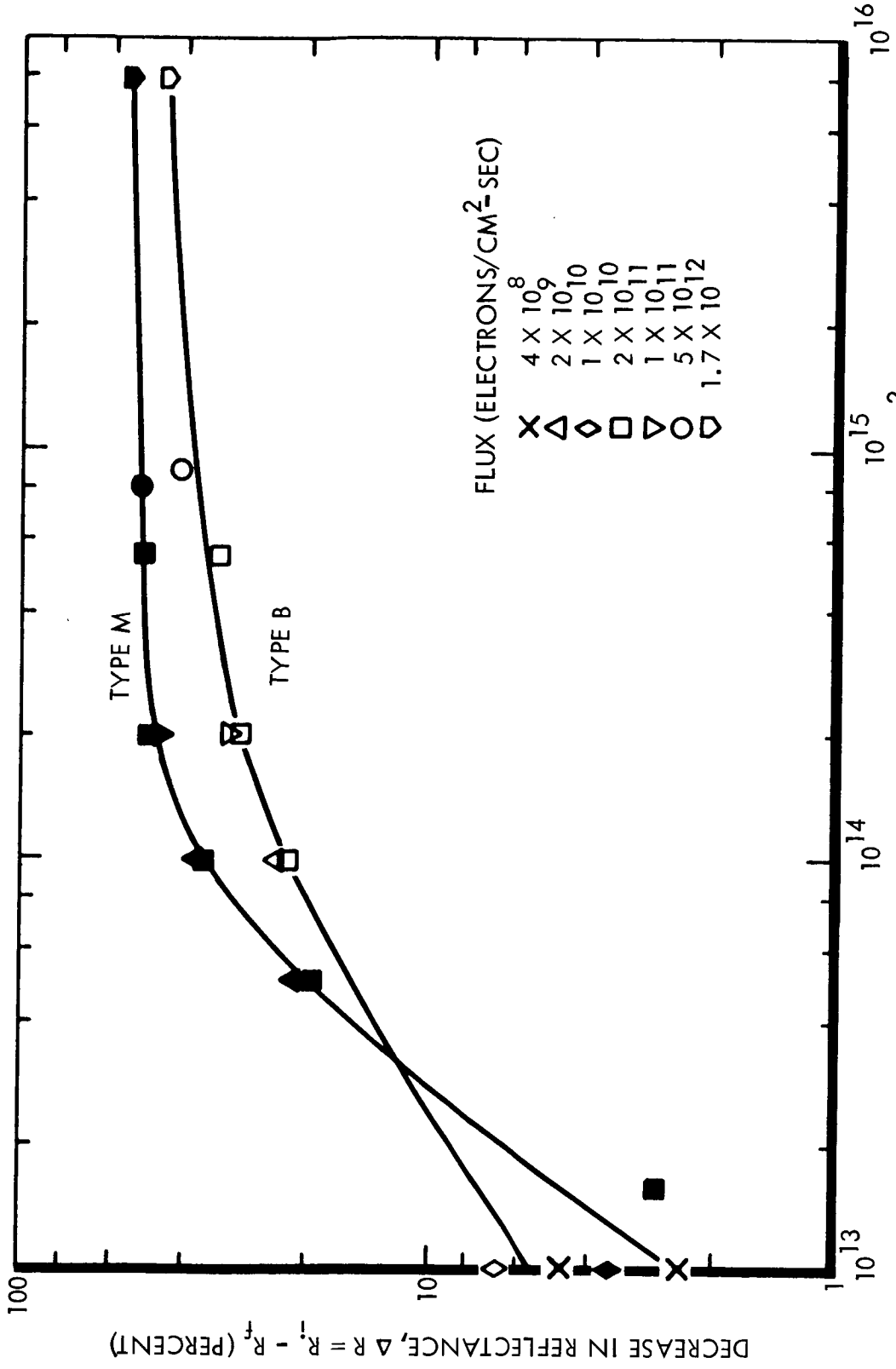

Figure 12. Electron Rate Study in Zinc Oxide – Methyl Silicone Coatings at 2100mμ

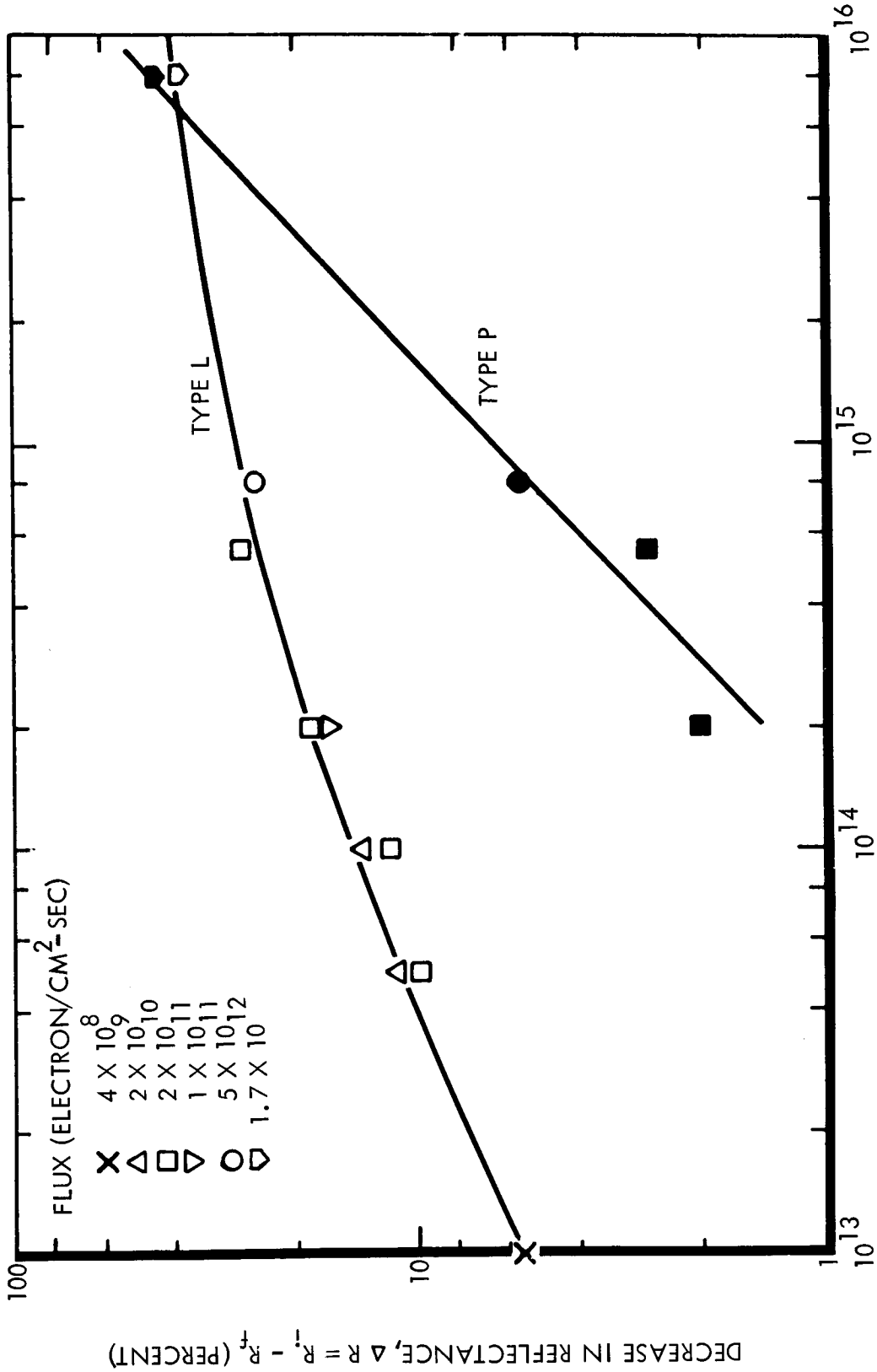

Figure 13. Electron Rate Study in Titanium Dioxide–Methyl Silicone Coatings at 2100mμ

Figure 14 shows data on two zinc oxide-pigmented sample types, M and F, at 950 mμ. The differences in damage buildup may be seen for zinc oxide/aluminum oxide—potassium silicate (F) as contrasted with zinc oxide—methyl silicone (M, S-13G). As in Figure 13, the data point spread is within experimental error.

Figure 15 contains near-infrared wavelength data for two titanium dioxide—methyl silicone coatings, L and P. The data for anatase TiO_2 (L), at 900 mμ, have the greatest spread seen in all groupings of reflectance values analyzed for rate effects phenomena. Because the spreads are within experimental error, however, there is again no evidence of irradiation rate effects.

Figure 16 shows reflectance data at 590 mμ for S-13G (M), zinc oxide—methyl silicone, and for type F, zinc oxide/aluminum oxide—potassium silicate. A comparison of the relative spreads of data from F and M is believed to point out greater sample-to-sample differences in M than in F. Figure 17 contains 590 mμ reflectance data for sample type L, TiO_2—methyl silicone.

Figure 18 shows total hemispherical reflectance data at 2100 mμ in two specular sample types, H (SiO_2 vapor-deposited onto aluminum) and K (buffed aluminum).

Figures 12 through 17 also provide additional data for characterizing coating degradation. Table 9 summarizes two aspects of degradation shown in the six figures: (1) extent of damage buildup before saturation, and (2) linear or non-linear presentation of reflectance changes when plotted on a log-log scale. Saturation of reflectance degradation is seen to take place after various amounts of reflectance change have occurred, and occasionally (such as type M at 2100 mμ) only as reflectance approaches zero. It is seen that reflectance changes in sample type F (zinc oxide/aluminum oxide—potassium silicate) can be plotted more linearly than changes in other coating types studied.

Tables 10, 11, and 12 indicate at the selected wavelengths of 2100, 950, and 590 mμ (chosen from 230 to 2500 mμ continuous-scan charts), the relative sensitivity to 50-keV electrons of the types of thermal control coatings tested during the

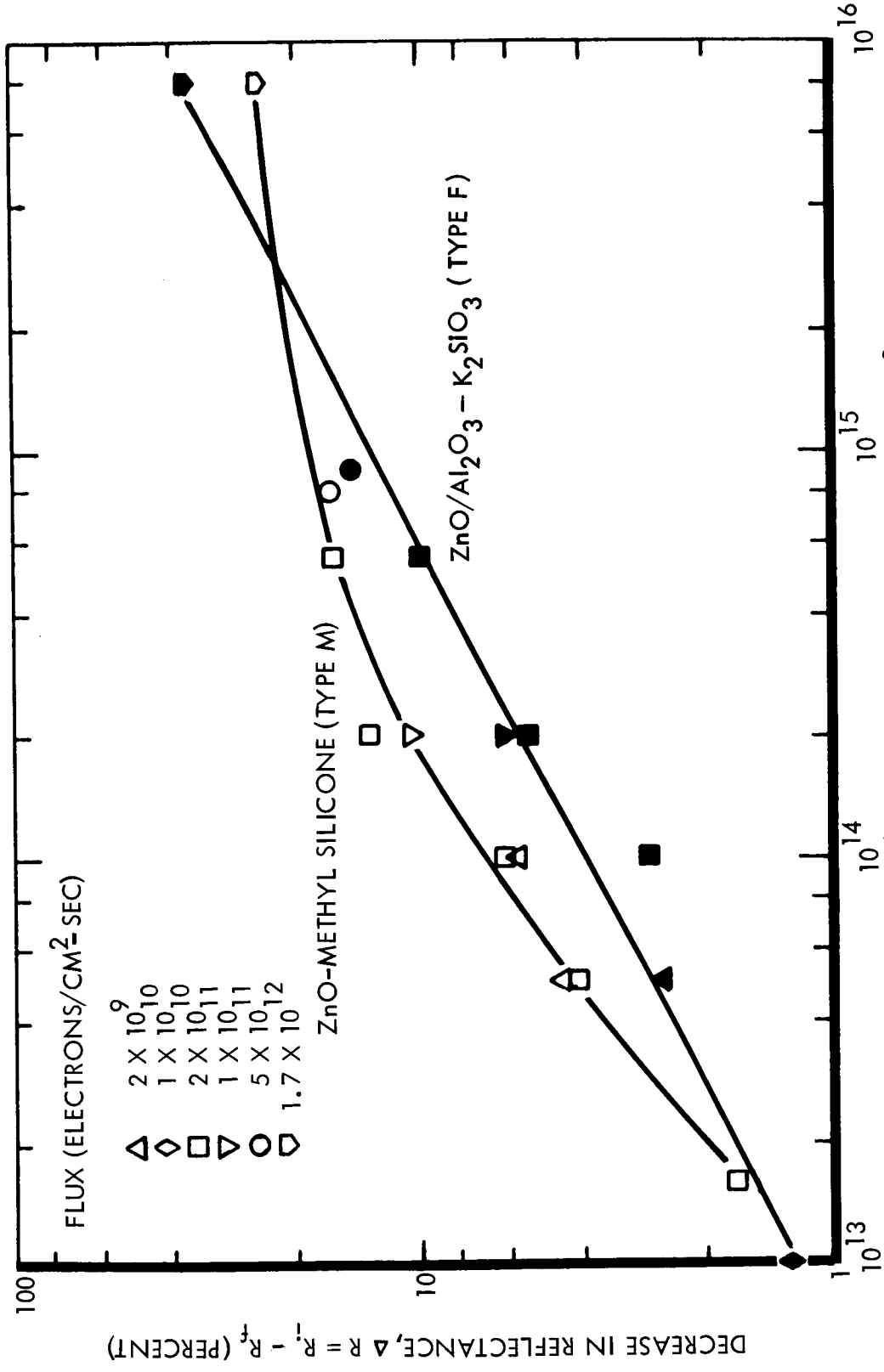

Figure 14. Electron Rate Study in Zinc Oxide-Pigmented Coatings at 950 mμ

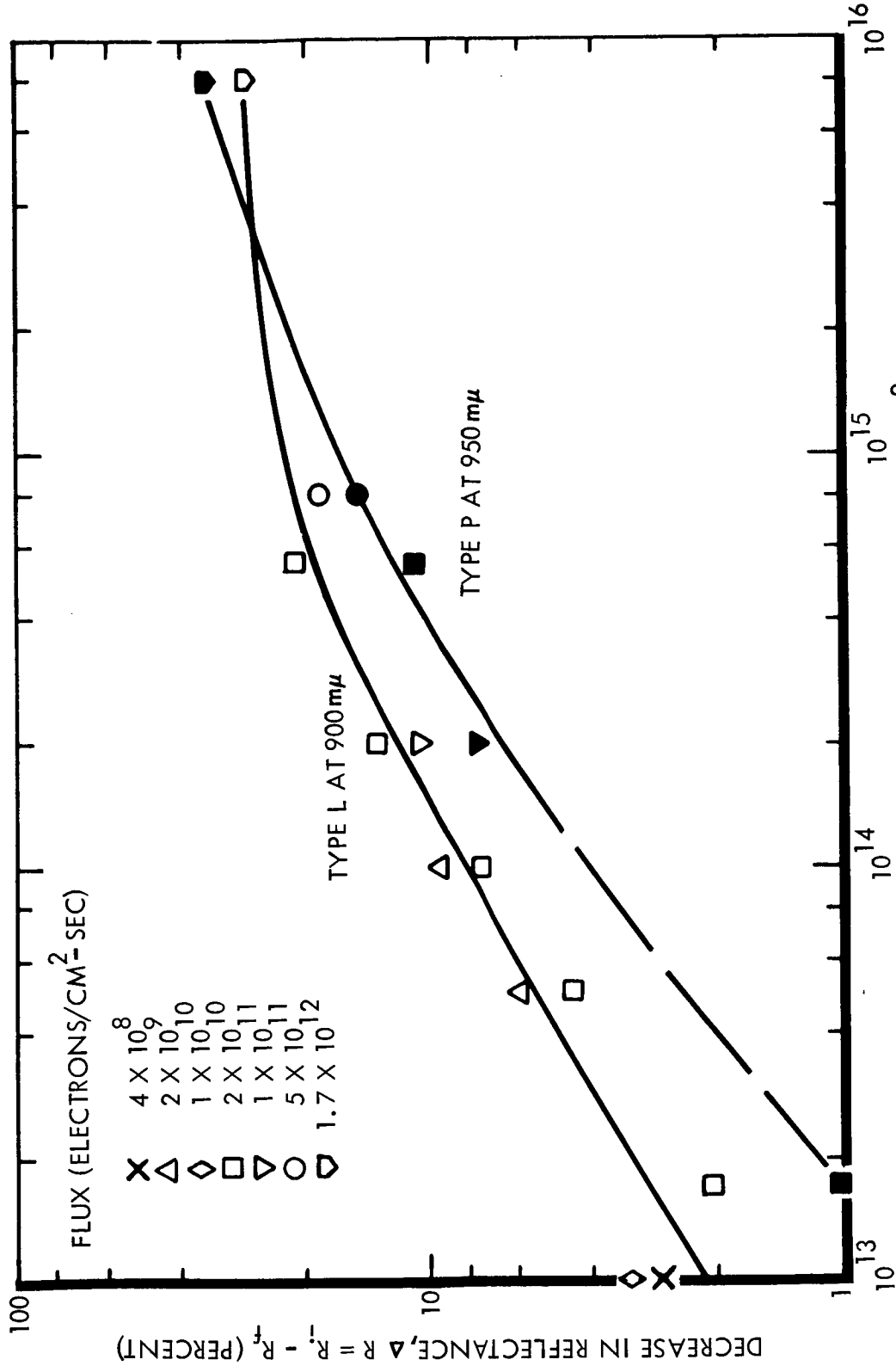

Figure 15. Electron Rate Study in Titanium Dioxide – Methyl Silicone Coatings

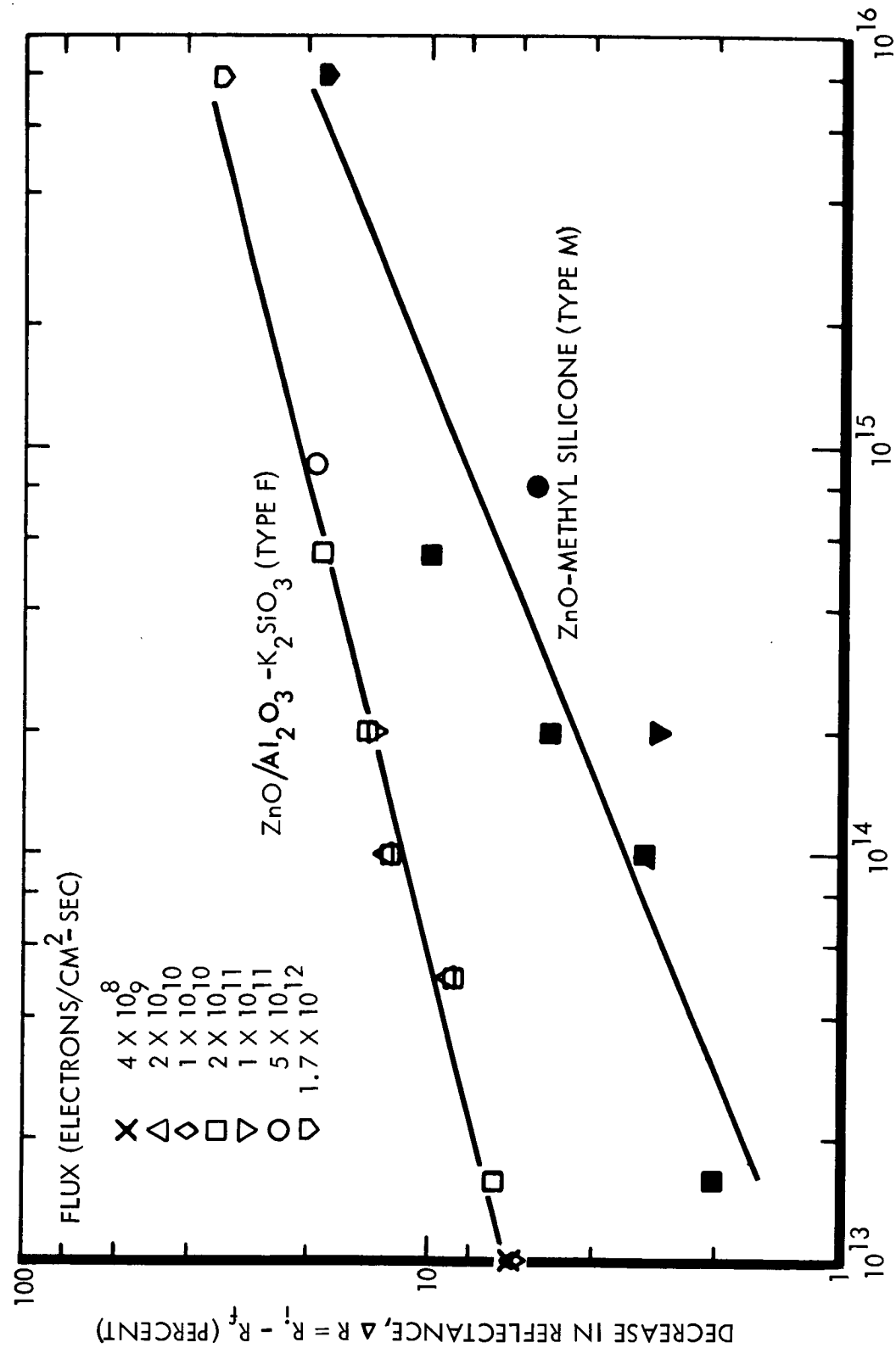

Figure 16. Electron Rate Study in Zinc Oxide-Pigmented Coatings at 590 mμ

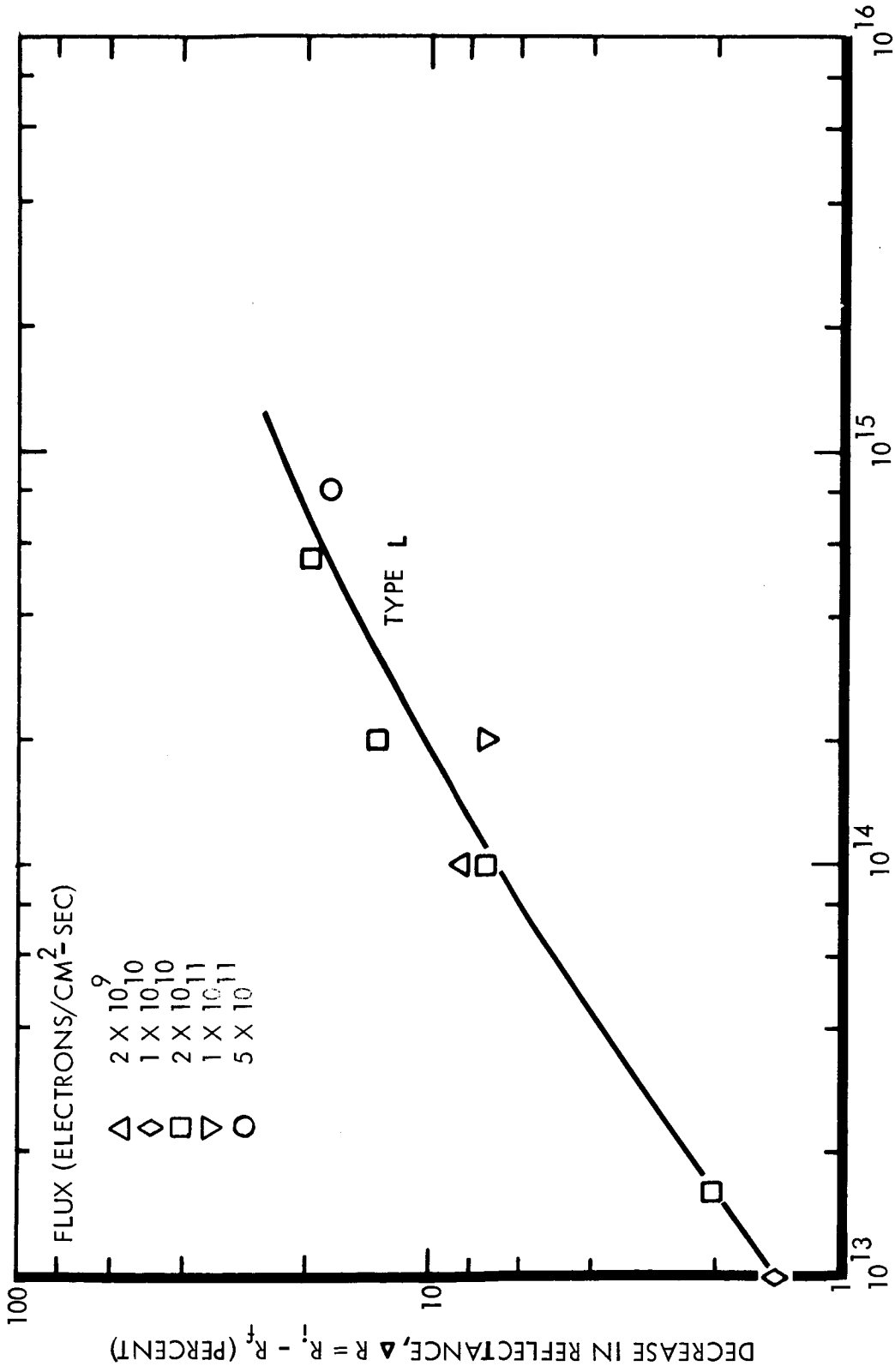

Figure 17. Electron Rate Study in Type L, Titanium Dioxide – Methyl Silicone, at 590mμ

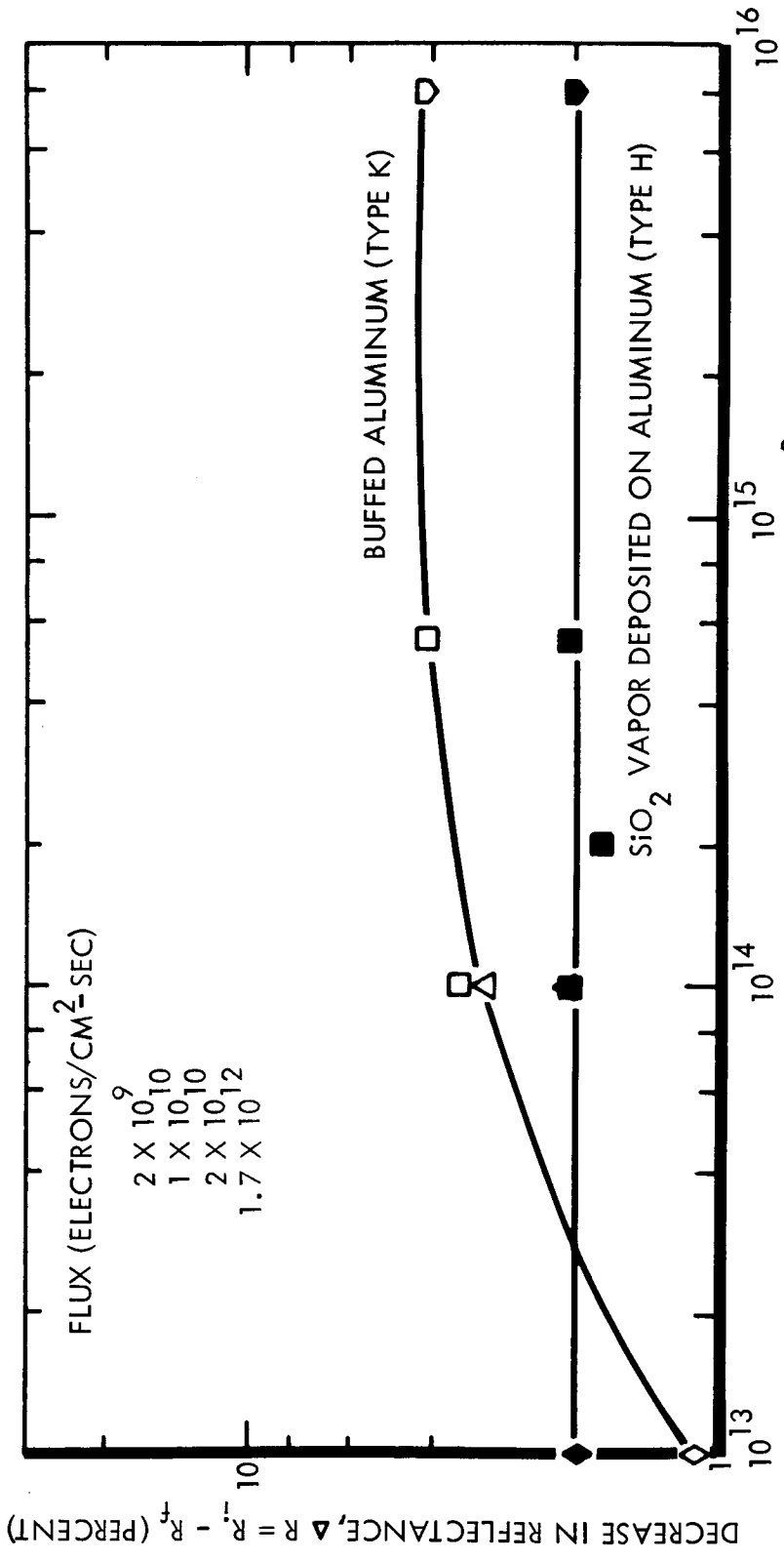

Figure 18. Electron Rate Study in Two Specular Coatings at 2100 mμ

Table 9. Characterization of Electron Degradation in Selected Coatings

Wavelength Region	Coating Type (Encircled number refers to Figure with that number)				
	L Anatase TiO_2-Methyl Silicone	P Rutile TiO_2-Methyl Silicone	B ZnO-Methyl Silicone	M Treated ZnO-Methyl Silicone	F_3 ZnO/Al_2O_3-Potassium Silicate
Middle Infrared	(13) Begins to saturate at $\Delta R \approx 40\%$.	Linear Presentation (within limits of data). (13)	Non-linear presentation (12) Begins to saturate at $\Delta R \approx 40\%$.	Non-linear presentation (12) Saturates at limit of reflectance.	(Mostly small reflectance changes.)
Near Infrared	Non-linear presentation (15) Begins to saturate above $\Delta R \approx 20\%$.	Non-linear presentation (15) Begins to saturate above $\Delta R \approx 20\%$.	(Small reflectance changes.)	Non-linear presentation (14) Begins to saturate at $\Delta R \approx 20\%$.	Linear presentation to highest fluence tested. (14)
Visible	Non-linear presentation (17) Begins to saturate above $\Delta R \approx 10\%$.	(Mostly small reflectance changes.)	(Very little reflectance change.)	Within data limits, linear presentation to highest fluence tested. (16)	Linear presentation to highest fluence tested. (16)

electron screening and rate studies. Buildup of degradation in these coatings can be summarized as follows:

(1) At 2100 mμ (Table 10) zinc oxide—methyl silicone coatings show the greatest sensitivity to damage. Of the titanium dioxide—methyl silicone coatings, sample type L is the most sensitive while types O and P exhibit much higher thresholds for damage. At 2,100 mμ type F is the least

Table 10. Decrease in Reflectance at 2100 mμ

Sample Type	$\Delta R = R_i - R_f$, (percent) for 50-keV electron exposures (electrons cm^{-2}) of:							
	$1x10^{13}$	$1.6x10^{13}$	$5x10^{13}$	$1x10^{14}$	$2x10^{14}$	$5.5x10^{14}$	$8x10^{14}$	$8x10^{15}$
A	--	3	--	--	14	--	20	--
B	6	--	--	23	30	33	41	45
C	--	--	--	--	13	--	19	--
F_3	--	2	--	0	5	7	8	29
H	2	--	--	2	2	2	--	2
I	--	--	--	--	--	3	--	8
J	--	--	--	--	--	3	--	7
K	1	--	--	3	3	4	--	4
L	6	0	11	13	17	28	25	39
M	3	3	20	37	47	51	51	55
N	--	--	--	--	0	0	--	--
O	--	--	--	--	1	2	--	37
P	0	--	--	--	2	3	--	43
Q	--	--	--	--	22	31	--	--
Y	--	--	--	--	2	12	--	--

Only small changes in D_3, E_3, G, H, I, J, K, N, O and P.

sensitive of the diffuse coatings to damage. Kapton H-film shows no evidence for degradation at that wavelength.

(2) The resistance to reflectance change is, in general, slightly greater at 950 mμ for most coatings (Table 11). The most notable exception is type F, which is significantly more sensitive to damage at 950 mμ .

(3) In the visible region (590 mμ) type F is the most sensitive and types B and O the least sensitive paints. Kapton H-film undergoes very large degradation, but only at very high fluences. See Table 12.

Table 11. Decrease in Reflectance at 950 mμ

Sample Type	$\Delta R = R_i - R_f$, (percent) for 50-keV electron exposures (electrons cm^{-2}) of:							
	1×10^{13}	1.6×10^{13}	5×10^{13}	1×10^{14}	2×10^{14}	5.5×10^{14}	8×10^{14}	8×10^{15}
A	--	4	--	--	13	--	17	--
B	--	0	--	0	2	2	8	9
C	--	0	--	--	3	--	11	--
D_3	--	0	--	--	1	--	1	--
E_3	--	2	--	--	8	--	20	--
F_3	1	0	2	2	6	10	15	37
L	3	3	5	8	13	21	21	28
M	--	2	4	6	12	16	17	24
N	0	--	0	0	0	6	--	17
O	--	--	--	--	4	9	--	46
P	--	0	--	--	7	11	15	35
Q	--	--	--	--	22	33	--	--
Y	--	--	--	--	6	18	--	--

Only small changes in G, H, I, J, and K.

Table 12. Decrease in Reflectance at 590 mμ

Sample Type	$\Delta R = R_i - R_f$, (percent) for 50-keV electron exposures (electrons cm^{-2}) of:							
	$1x10^{13}$	$1.6x10^{13}$	$5x10^{13}$	$1x10^{14}$	$2x10^{14}$	$5.5x10^{14}$	$8x10^{14}$	$8x10^{15}$
A	--	--	--	--	10	0	11	--
B	--	1	--	--	0	0	--	--
C	--	0	--	--	0	--	3	--
D	--	6	--	--	6	--	11	--
E	--	10	--	--	14	--	22	--
F	6	7	9	13	14	19	19	32
L	1	1	--	8	14	20	18	--
M	0	1	--	3	4	10	5	18
N	0	1	--	--	4	13	9	60
O	--	0	--	--	2	3	10	--
P	--	0	--	--	3	14	7	20

G, H, I, J, K: Very small changes, even after exposures of 8×10^{15} electrons cm^{-2}.

A multiplicity of 3 samples per coating type was used at most data points. Very close agreement was found between samples of the same type. No systematic differences were found between samples of type L which had or had not had a removable coating.

A detailed illustration of the buildup of degradation in sample type M (S-13G) with electron exposure up to 8×10^{15} electrons cm^{-2} is shown in Figure 19. There occurs in the infrared wavelength region an initially rapid decrease in reflectance, which eventually saturates at high ΔR values. In the visible region, however, the buildup of damage is slow at first and then more rapid at high exposure. Upon re-exposure to dry air, however, this coating exhibits contrasting behavior. A set of reflectance measurements was made on type M, treated zinc oxide-methyl silicone, while and after backfilling the chamber with dry air to an absolute pressure of one

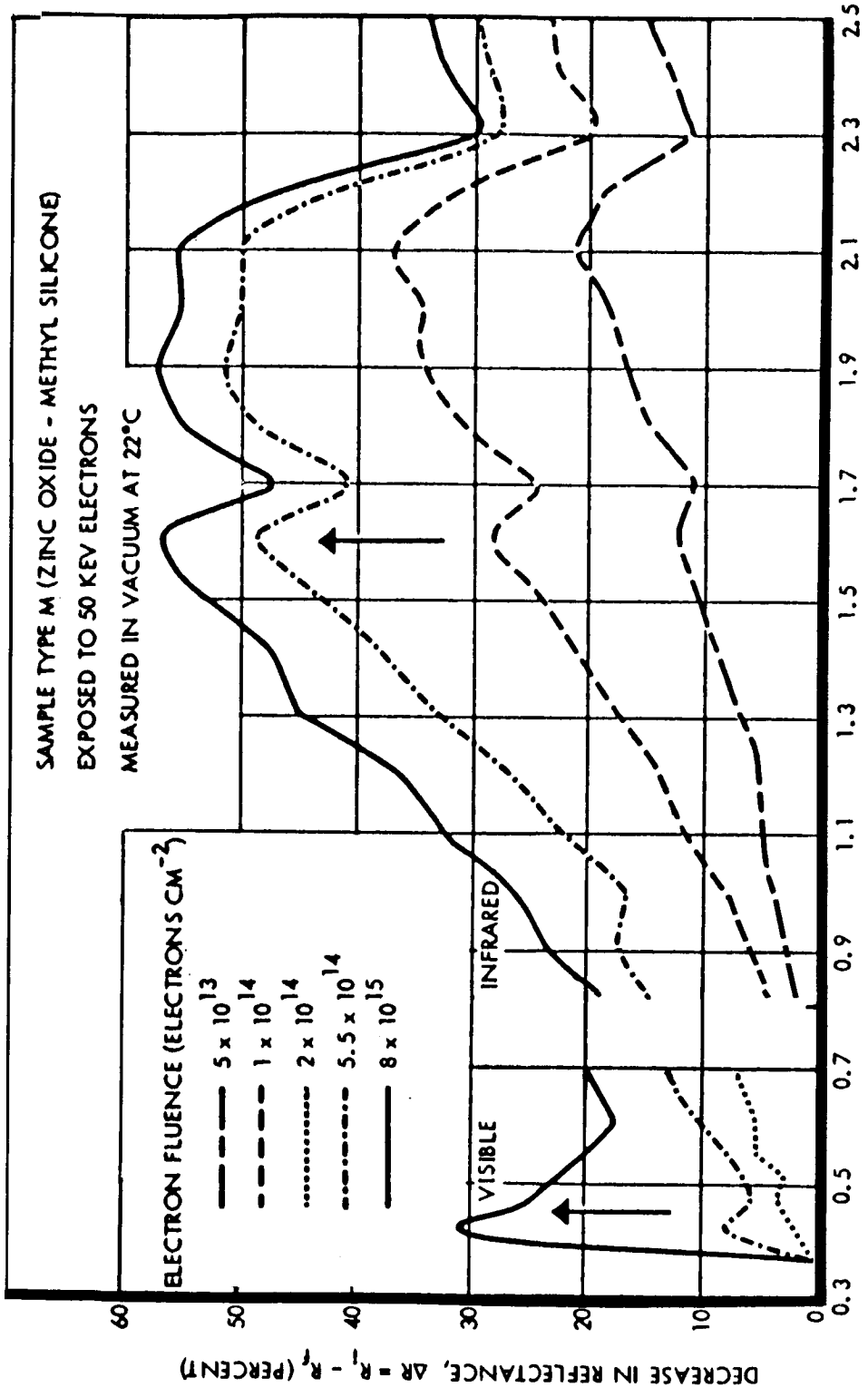

Figure 19. Buildup of Reflectance Degradation in Type M

atmosphere. This set of data is reduced to reflectance-change form in Figure 20. Reexposure to air causes a rapid rate of reflectance recovery in the infrared region; this rate decreases with time, as Figures 20 and 21 show. In the visible region, however, reflectance is restored much more slowly, with considerable "permanent" damage remaining in type M (and in the other diffuse coatings) even days after backfilling the chamber with air.

Table 13 contains in-air reflectance data on type M and on additional selected coatings as well, following exposure of different specimens to two distinct electron fluences. Measurements were taken several days following readmission of dry air into the chamber, and hence represent "permanent" reflectance losses in the selected coatings after stabilization in air.

The data presented herein is seen to be consistent with results from early in-air tests, in which coatings exposed to high fluences showed signs of permanent effects mainly in the visible wavelength region.

After completion of in-air reflectance measurements, the CRETC was re-evacuated in an attempt to confirm results reported elsewhere, to the effect that certain materials have a memory for damage sustained during a previous pumpdown.[1] In

Table 13. "Permanent" Reflectance Losses

Sample Types*	Approximate Loss of Reflectance (percent) for Exposure of:					
	5.5×10^{14} Electrons cm^{-2}			8×10^{15} Electrons cm^{-2}		
	U V Edge	Visible	Infrared	U V Edge	Visible	Infrared
B	0	0	0	4	0	0
F	0	1	0	3	1	1
M	0	0	0	4	0	0
O	6	0	0	6	4	0
P	4	3	0	6	4	0
L	2	6	13	7	9	20

*Types H, I, J, and K exhibited no permanent reflectance losses.

[1] J. E. Gilligan, oral remark at the 2nd AIAA Thermophysics Specialist Conference, New Orleans, Louisiana, April 19, 1967.

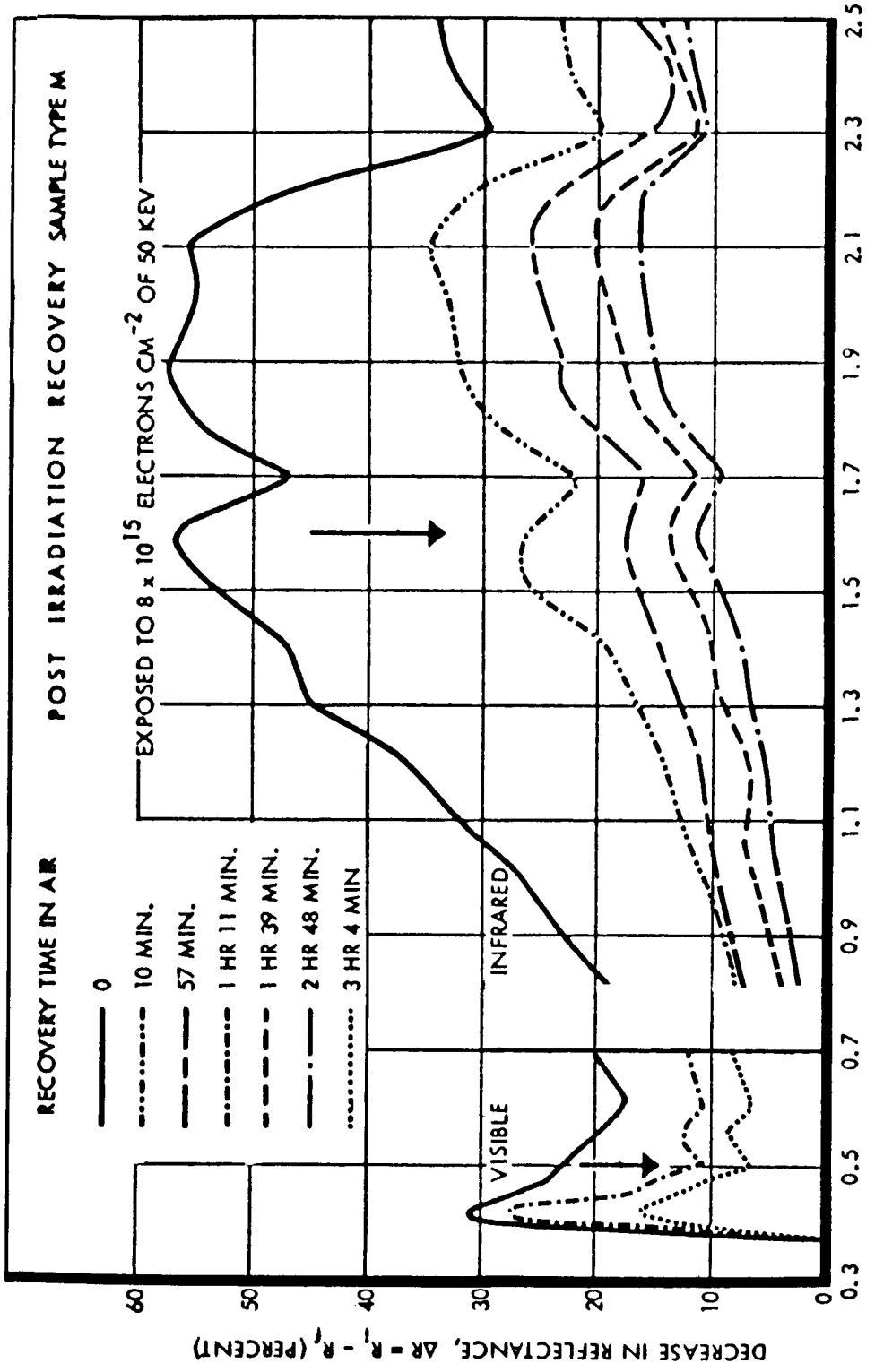

Figure 20. Post-Irradiation Reflectance Recovery Properties of S-13G When Reexposed to Air

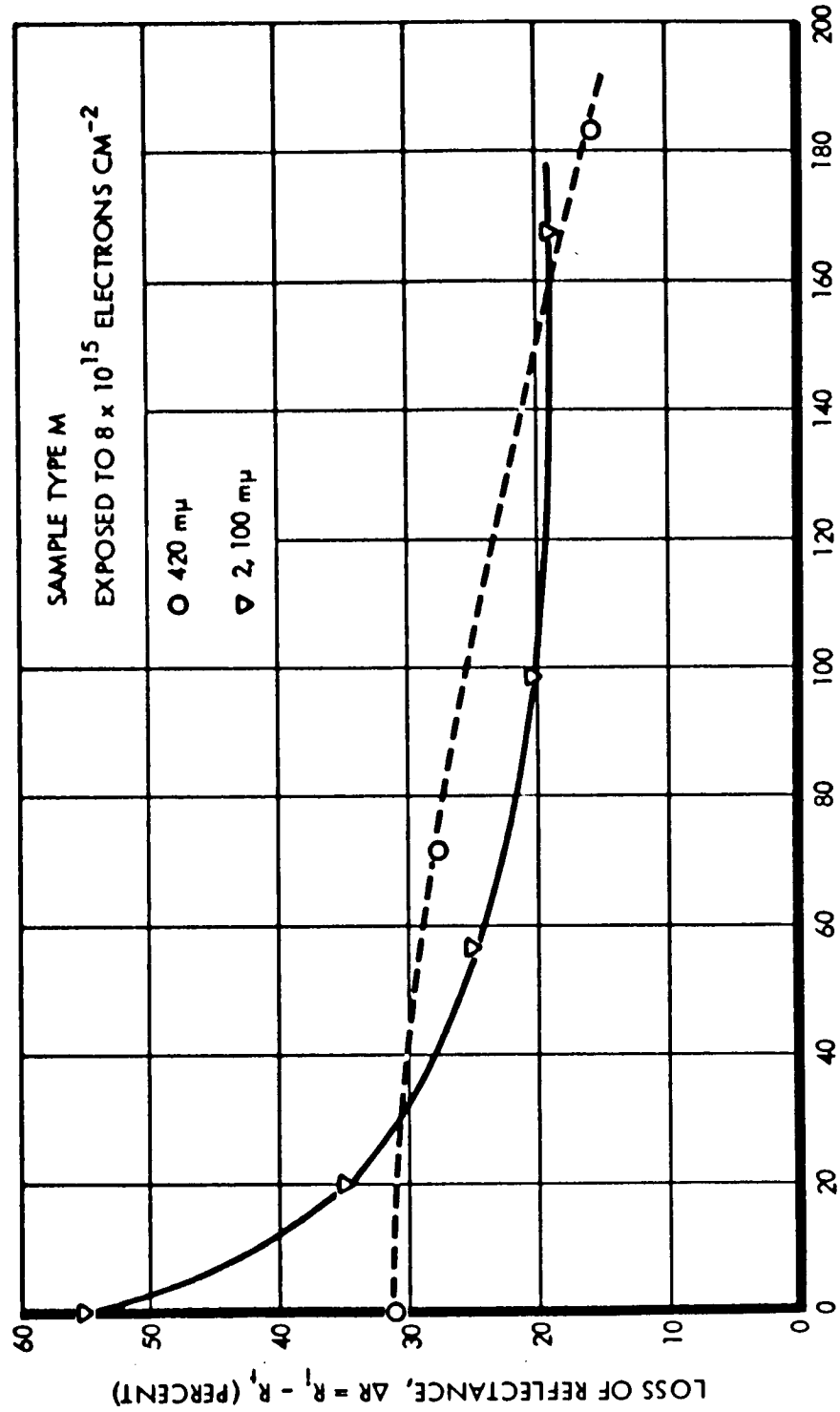

Figure 21. Rate of Reflectance Recovery of S-13G in Air

our tests, results were negative on all coatings measured, as no memory for previous damage was exhibited for the two cases of (1) pumpdown only, and (2) pumpdown followed by a brief electron exposure. (The exposure was made to see if it would "trigger" a return to the degraded state.)

More recent discussions with G. A. Zerlaut of IIT Research Institute have indicated that, when placed in vacuum a second time, unbound zinc oxide pigment has a memory for previous damage.

2.3 TESTS WITH ULTRAVIOLET-RICH ELECTROMAGNETIC RADIATION

A survey of effects of ultraviolet radiation from long-arc mercury sources was conducted on the majority of coatings listed in Table 1. Subsequently, comparative results were sought on selected coating types, using long-arc xenon ultraviolet sources.

2.3.1 Mercury-Arc Ultraviolet Radiation Studies

Figures 3 and 7 show the location, configuration, and details of the ultraviolet lamp array used for these tests. Four General Electric UA-11 and two UA-3 lamps were utilized to produce ultraviolet-rich electromagnetic radiation of uniform intensity in the sample plane and over an area larger than the sample array. Each UA lamp was enclosed in a water-cooled, double-walled quartz jacket and placed at the focus of a polished aluminum reflector. De-ionized distilled water was circulated through the lamp jackets via an external closed system consisting of pump, reservoir, ion and heat exchangers. Water samples could be drawn from the reservoir at any time to measure its spectral transmission if any change in the spectral distribution of the lamp array had been detected by the in situ electromagnetic radiation monitoring system.

The in situ spectral monitoring system has been employed during this program to determine the spectral character of ultraviolet sources used. As Figure 6 indicates, the determination that UA series ultraviolet sources have no excessive (relative to solar output) line emission at 2537 Å was based on measurements with this system. That the system's optical train and DK-2A spectrophotometer truly

pass energy at this wavelength was assured through experiments using the output of a small Penray lamp.

In detail, the in situ spectral monitor operates as follows: Energy from the ultraviolet source housed within the chamber is transferred to the entrance port of the integrating sphere via two shuttered holes in the sample wheel and two magnesium fluoride overcoated front surface aluminized mirrors. The energy then passes in a collimated beam through the integrating sphere's entrance and exit ports without impinging on its internal MgO surface. From this point on the energy utilizes the same transfer optics and far-ultraviolet spectrophotometer as when recording sample spectral reflectance. The spectrophotometer, however, is operated in the single beam energy mode rather than the usual double beam mode, and the energy traverses the monochromator in the direction opposite that normally used. Detectors are therefore located in the position on the spectrophotometer normally occupied by the instrument's energy sources. The detector housing contains a lead sulfide cell and a special far-ultraviolet photomultiplier tube. The detectors that are embedded in the integrating sphere wall and used when obtaining sample spectral reflectance, are disconnected when the instrument is measuring source spectra.

This system enables precise measurement of the spectral distribution of source energy impinging on the sample plane at any time and over the continuous wavelength region from 1650 Angstroms to 3.5 microns (35,000 Angstroms). Figure 6 is a reduced DK-2A chart of lamp spectra obtained during ultraviolet exposure of a sample array at a chamber pressure of 10^{-7} torr. Source emission lines in the ultraviolet region are resolved when separated by only a few Angstroms. This capability whether used to obtain source spectra or sample reflectance spectra, should not be confused with "spectral" measuring techniques which employ band-pass filters instead of a monochromator.

A TRW model DR-2 radiometer and a Corning type O-51 filter were used to measure the irradiance below 4000 Angstroms on the sample plane from the ultraviolet lamp array. Initial and final measurements were averaged and when divided by the

total solar energy below 4000 Angstroms, at zero air mass and one astronomical unit, resulted in a 4.7 UV-sun rate. While this is more or less "standard" procedure for determining sun rates and therefore employed, care must be taken in comparing sun rates derived for different UV lamp sources, due to the disparity in spectral match between any laboratory source and the extra-terrestrial sun.

The sample plane was mapped to determine its irradiance uniformity by placing the DR-2 radiometer head at each sample position as defined by the cells in the spider web contamination baffle. The receiving surface of the DR-2 was fitted with an aperture mask prior to the measurements so that its receiving area corresponded to the area irradiated by monochromatic energy during reflectance measurements. No significant departures from uniformity were found. The defocusing action of the lamp jackets enhances the array's characteristic uniformity but at the expense of ability to achieve sun rates much in excess of five at present source-to-sample distances.

Tables 14 and 15 show the total number of spectral reflectance charts produced in the ultraviolet, visible, and infrared wavelength regions, at the following times and exposure increments during the mercury-arc ultraviolet radiation effects study: pre-irradiation, in air; pre-irradiation, in situ; 135 ESH; 250 ESH; 490 ESH; 770 ESH; 1130 ESH; 18 ESH; 53 ESH; 120 ESH (all in situ); and post-irradiation, in air. These measurements, encompassing the 240 to 2500 millimicron wavelength region, were made using the Beckman DK-2A Far UV spectrophotometer and the CRETC reflectometer. At most exposure points, measurements were made on each of 3 samples of each type; no significant variations were observed among such sets of 3.

Throughout the ultraviolet radiation tests and measurement periods, each sample's substrate was maintained at 20 ± 1°C. Chamber pressure was lower than 4×10^{-7} torr at all times, and on the 10^{-8} torr range during measurement periods.

Figures 22 through 37 show normalized changes in reflectance over the 250 to 2450 millimicron wavelength region, for each type of coating tested. Each family of curves shows the buildup of reflectance changes during the course of exposure to

Table 14. Reflectance Measurements on Test Samples

TEST ARRAY SAMPLES	IN AIR, BEFORE IRRADIATION			IN VACUUM, BEFORE IRRADIATION			IN SITU, AFTER 135 ESH			INSITU, AFTER 250 ESH			IN SITU, AFTER 490 ESH			IN SITU, AFTER 770 ESH			IN SITU, AFTER 1130 ESH			IN AIR AFTER COMPLETION OF IN SITU TEST		
	UV	VIS	IR	UV	VIS	IR	UV	VIS	IR	UV	VIS	IR	UV	VIS	IR	UV	VIS	IR	UV	VIS	IR	UV	VIS	IR
Pyromark (#7)	X	X	X	X	X	X	X	X	X	X	X	X	X	X	X				X	X	X	X	X	X
Pyromark (#1)				X	X	X		X		X	X	X	X	X	X				X	X	X			
Alzak (#21)	X	X	X	X	X	X	X	X	X	X	X	X	X	X	X	X	X		X	X	X	X	X	X
B (#14)				X	X	X	X	X	X	X	X	X	X	X	X				X	X	X		X	X
D_3 (#4)	X			X	X	X	X	X	X	X	X	X	X	X	X				X	X	X	X	X	X
F_3 (#14)				X	X	X	X	X	X	X	X	X	X	X	X				X	X	X		X	X
H (#15)				X	X	X	X	X	X	X	X	X	X	X	X		X	X	X	X	X	X	X	X
H (#14)				X	X	X		X	X	X		X	X	X	X				X	X	X			
I (#8)	X			X	X	X	X	X	X	X	X	X	X	X	X	X	X		X	X	X	X	X	X
J (#16)				X	X	X				X			X						X	X	X			
J (#14)				X	X	X				X			X		X				X	X	X			
J (#15)				X	X	X	X	X	X	X	X	X	X	X	X				X	X	X	X	X	X
K (#9)				X	X	X		X	X	X	X	X	X	X	X	X			X	X	X	X	X	X
L_1 (#36)				X	X	X	X	X	X	X	X	X	X	X	X				X	X	X		X	X
L_2 (#9)				X	X	X				X	X	X	X	X	X				X	X	X	X	X	X
M (#15)				X	X	X	X	X		X	X		X	X	X		X	X	X	X	X		X	X
M (#38)				X	X	X		X	X		X	X		X	X				X	X	X			
M (#14)				X	X	X		X		X	X	X	X	X	X				X	X	X			
N (#1)				X	X	X		X			X		X	X					X	X	X			
N (#41)				X	X	X		X	X		X	X			X				X	X	X			
N (#55)				X	X	X	X	X	X	X	X	X	X	X	X	X	X	X	X	X	X	X	X	X
O (#15)				X	X	X		X	X	X	X	X	X	X	X		X	X	X	X	X		X	X
O (#16)				X	X	X		X	X		X	X		X	X				X	X	X			
O (#14)				X	X	X		X											X	X	X			
P (#27)				X	X	X		X		X	X	X	X	X	X				X	X	X		X	X
P (#24)				X	X	X	X	X	X	X	X	X	X	X	X		X	X	X	X	X	X	X	X
P (#26)				X	X	X		X											X	X	X			
Q (#4)	X	X	X	X	X	X	X	X	X	X	X	X	X	X	X		X	X	X	X	X		X	X
Q (#2)				X	X	X				X	X	X	X	X	X				X	X	X			
Q (#3)				X	X	X					X	X		X	X				X	X	X			

Table 15. Reflectance Measurements on Control Samples

CONTROL SAMPLES	IN VACUUM, BEFORE IRRADIATION			IN SITU, AFTER 135 ESH			IN SITU, AFTER 250 ESH			IN SITU, AFTER 490 ESH			IN SITU, AFTER 770 ESH			IN SITU, AFTER 1130 ESH			AFTER SHIFT TO EXPOSURE POSITION, AND AFTER EXPOSURE TO: 18 ESH			53 ESH			120 ESH			IN AIR, AFTER COMPLETION OF IN SITU TEST		
	UV	VIS	IR	UV	VIS	IR	UV	VIS	IR	UV	VIS	IR	UV	VIS	IR	UV	VIS	IR	UV	VIS	IR	UV	VIS	IR	UV	VIS	IR	UV	VIS	IR
Pyromark (#5)	X	X	X		X	X	X	X	X	X	X	X				X	X	X	X	X	X		X	X		X	X		X	X
Alzak (#26)	X	X	X	X	X		X	X	X	X	X	X				X	X	X	X	X	X	X	X	X	X	X	X	X	X	X
B (#15)	X	X	X	X	X	X		X	X	X	X	X				X	X	X		X			X	X		X	X		X	X
D_3 (#5)	X	X	X	X	X		X			X	X	X				X	X	X	X	X	X	X	X	X	X	X	X	X	X	X
F_3 (#15)	X	X	X		X		X		X		X	X				X	X	X								X			X	
H (#16)	X	X	X		X	X	X		X	X		X				X	X	X								X			X	
I (#9)	X	X	X				X		X	X		X			X	X	X	X							X			X		
J (#17)	X	X	X				X		X	X		X			X	X	X	X										X		
K (#10)	X	X	X	X		X	X	X	X	X		X	X		X	X	X	X							X			X		
L_1 #37	X	X	X		X	X		X	X	X	X	X		X	X	X	X	X	X	X	X		X	X		X	X		X	X
L_2 (#10	X	X	X		X	X		X	X	X	X	X		X	X	X	X	X	X	X	X		X	X		X	X		X	X
M (#17	X	X	X		X				X	X	X	X				X	X	X											X	X
N (#6	X	X	X				X		X	X	X	X			X	X	X	X								X			X	
O (#17	X	X	X						X	X	X	X				X	X	X												
P (#23	X	X	X			X					X	X		X		X	X	X												
Q (#5	X	X	X							X	X	X				X	X	X												

the ultraviolet-rich electromagnetic radiation. In each figure, the notation $\Delta R = R_i - R_f$ designates difference in percentage of incident energy which is hemispherically reflected after a given ESH exposure ("final"), relative to the pre-irradiation, in situ ("initial") value. Each entry has been rounded to the nearest percent, after being corrected very nearly to change in absolute reflectance. This is accomplished by multiplying the raw data point by that factor (greater than unity) which brings the integrating sphere MgO wall reference curve up to 100 percent.

Considering each coating type in turn, the following results have been obtained:

Aluminum sample types (I, J, and K) exhibit significant reflectance losses in the ultraviolet region, beginning with 135 ESH of UV exposure. See Figures 22, 23, and 24.

Coated aluminum sample types (H and Alzak) have reflectance losses over wider wavelength regions, and at exposure levels as low as 18 ESH. In H the losses extend from the near ultraviolet through the visible region. Type H also has small reflectance increases in portions of the ultraviolet and infrared regions, as Figure 25 indicates. Losses in reflectance for Alzak take place throughout the ultraviolet and visible regions.

The two Alzak specimens tested (#21, called Z_1, and #26, called Z_2) exhibit different reflectance loss rates when exposed to ultraviolet radiation, as a comparison of Figures 26 and 27 shows. Original reflectance charts confirm different surface characteristics for these two specimens—a 0.29-mil overcoating thickness for #21 and a 0.10-mil thickness for #26. The thicker coating exhibits the faster rate of damage buildup.

Reflectance decreases indicated in the tables and figures for H and Alzak are average values, based on interference minima and maxima near the wavelength which each table represents. In type H each minimum and maximum shifts with exposure to shorter wavelengths. For example, a local minimum at 740 mμ before exposure began shifts to 700 mμ at 1130 ESH.

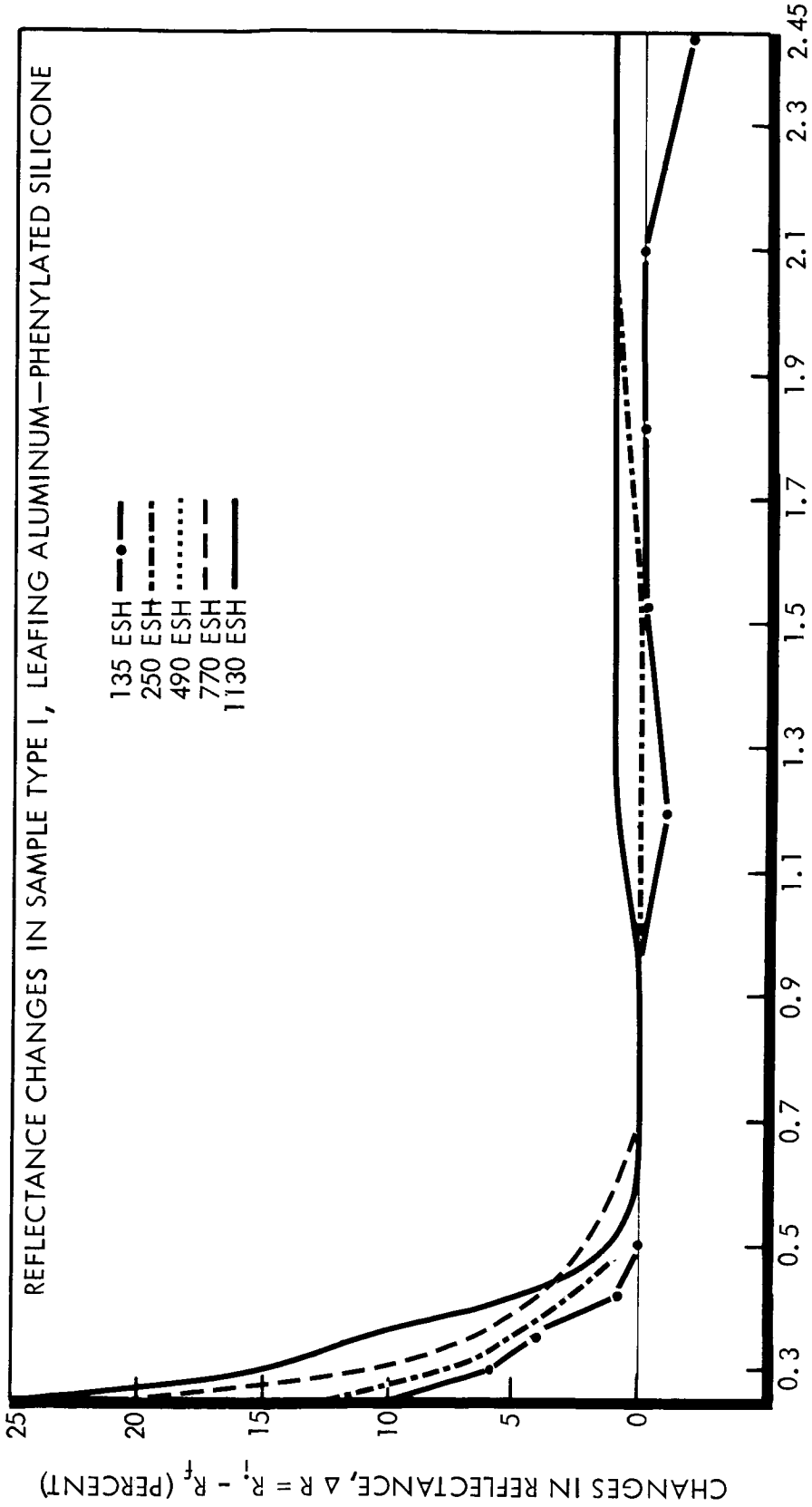

Figure 22. Spectral Reflectance Changes in Leafing Aluminum—Phenylated Silicone (Type I), Following Exposure to Ultraviolet Radiation

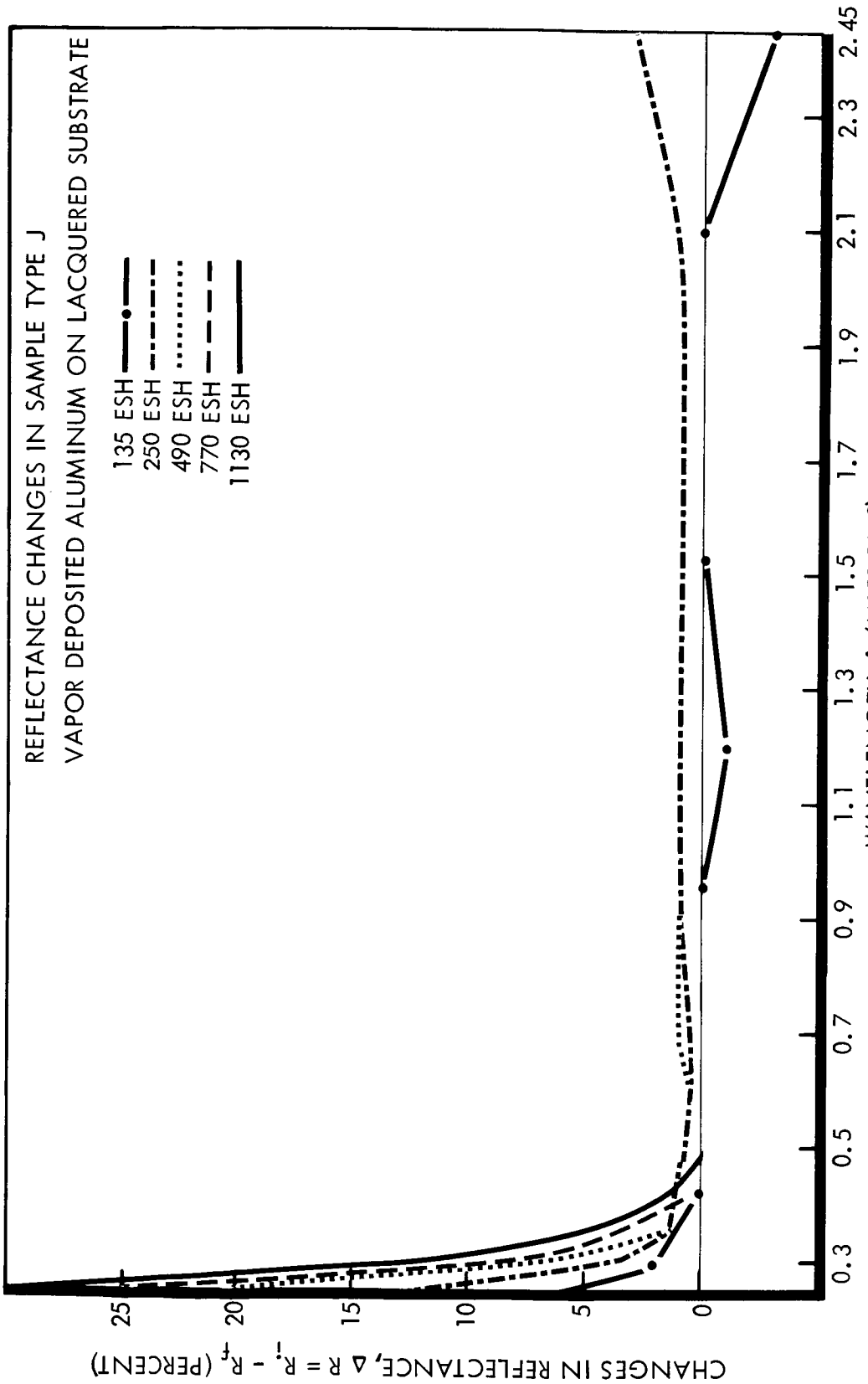

Figure 23. Spectral Reflectance Changes in Vapor-Deposited Aluminum on Lacquer (Type J), Following Exposure to Ultraviolet Radiation

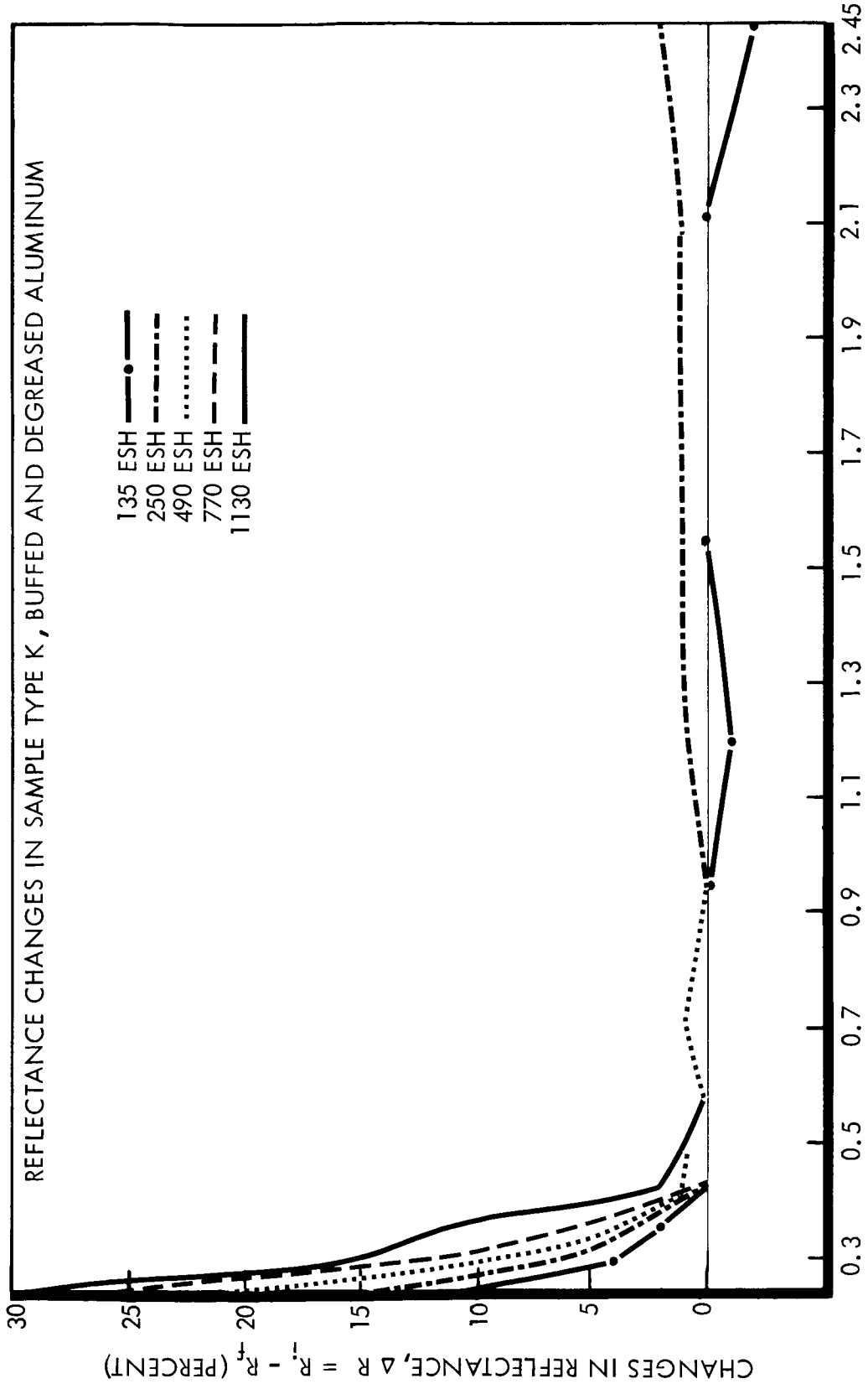

Figure 24. Spectral Reflectance Changes in Buffed and Degreased Aluminum (Type K), Following Exposure to Ultraviolet Radiation

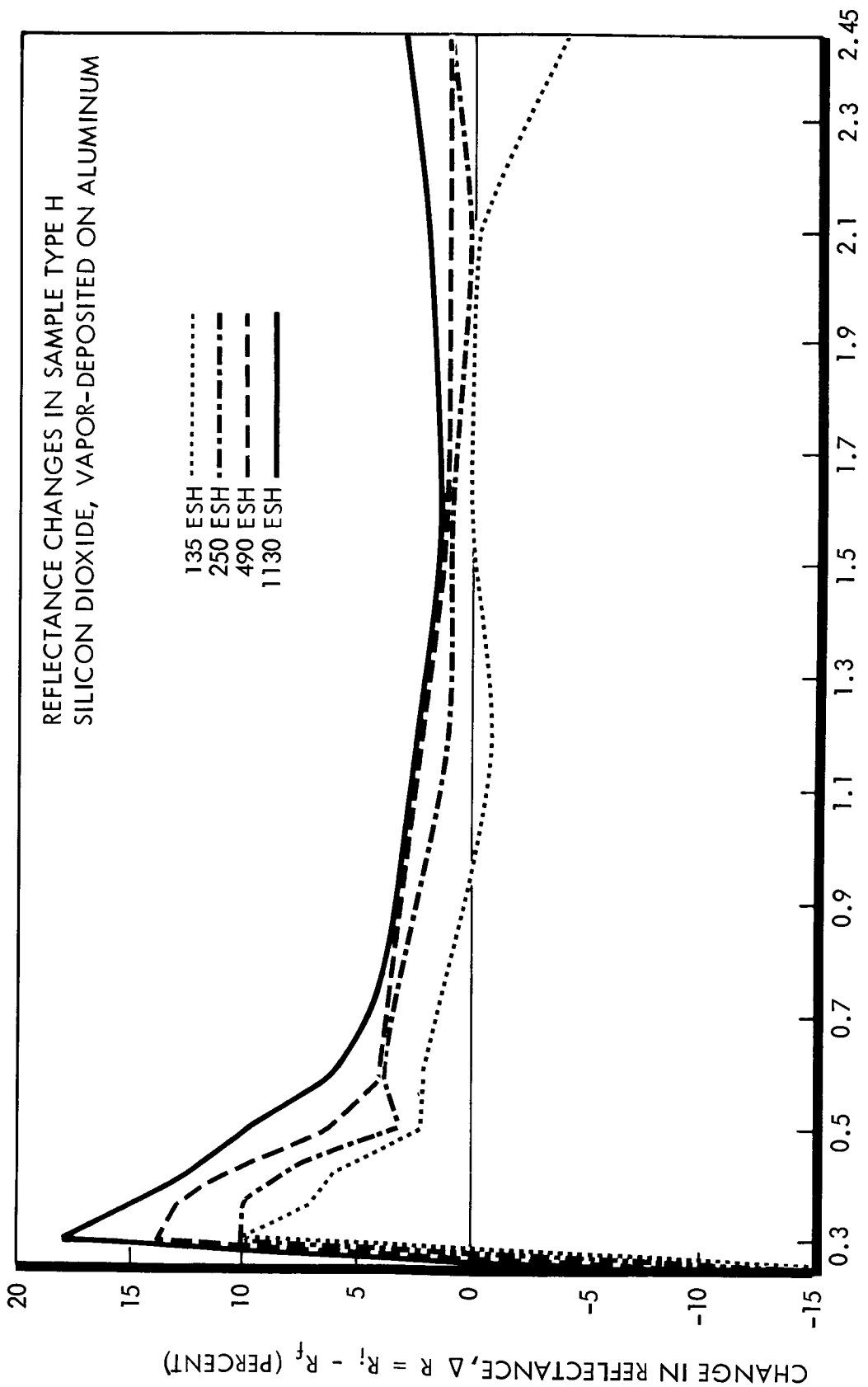

Figure 25. Spectral Reflectance Changes in Silicon Dioxide Vapor-Deposited on Aluminum (Type H), Following Exposure to Ultraviolet Radiation

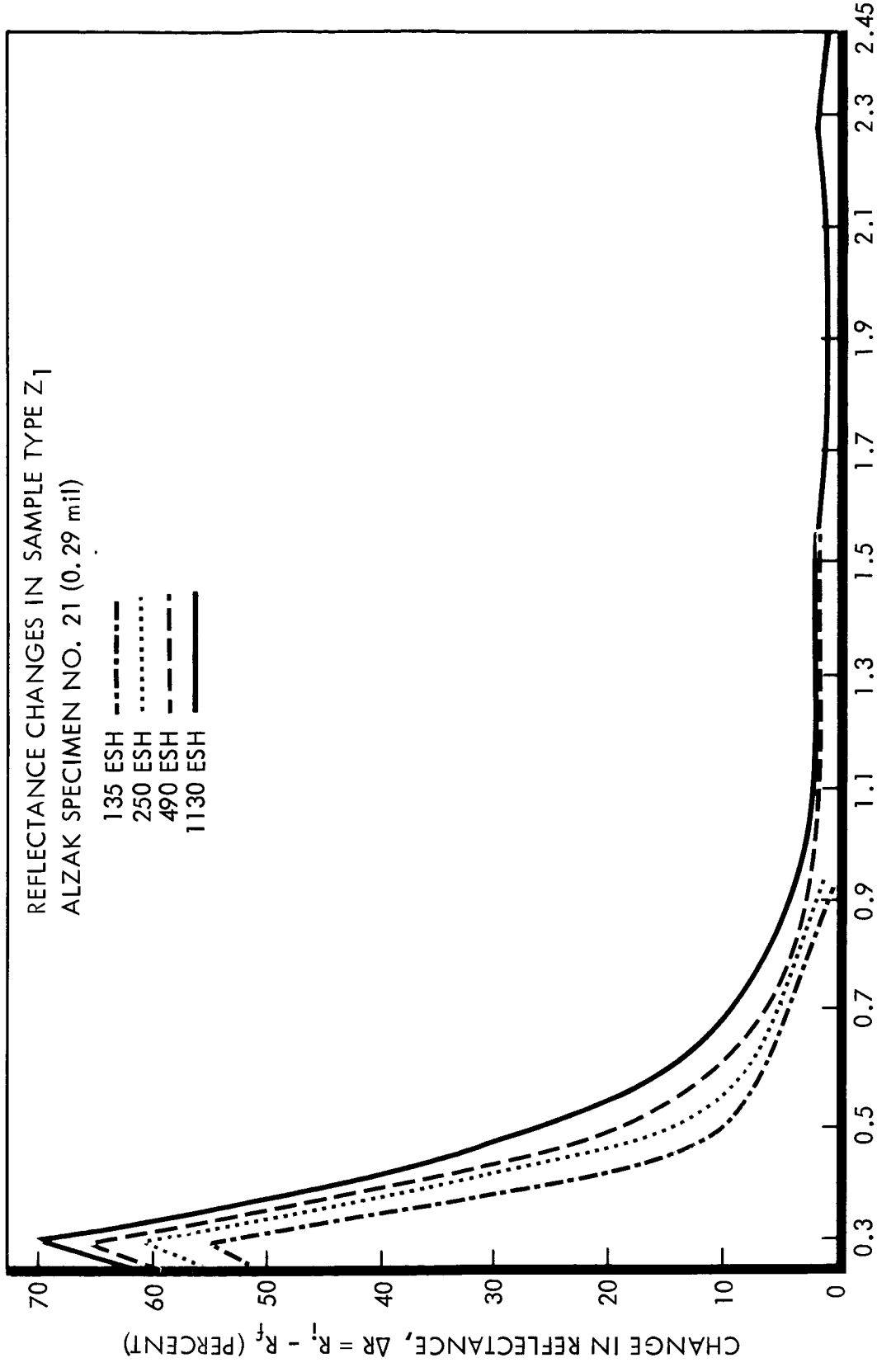

Figure 26. Spectral Reflectance Changes in 0.29-Mil Alzak (Type Z_1), Following Exposure to Ultraviolet Radiation

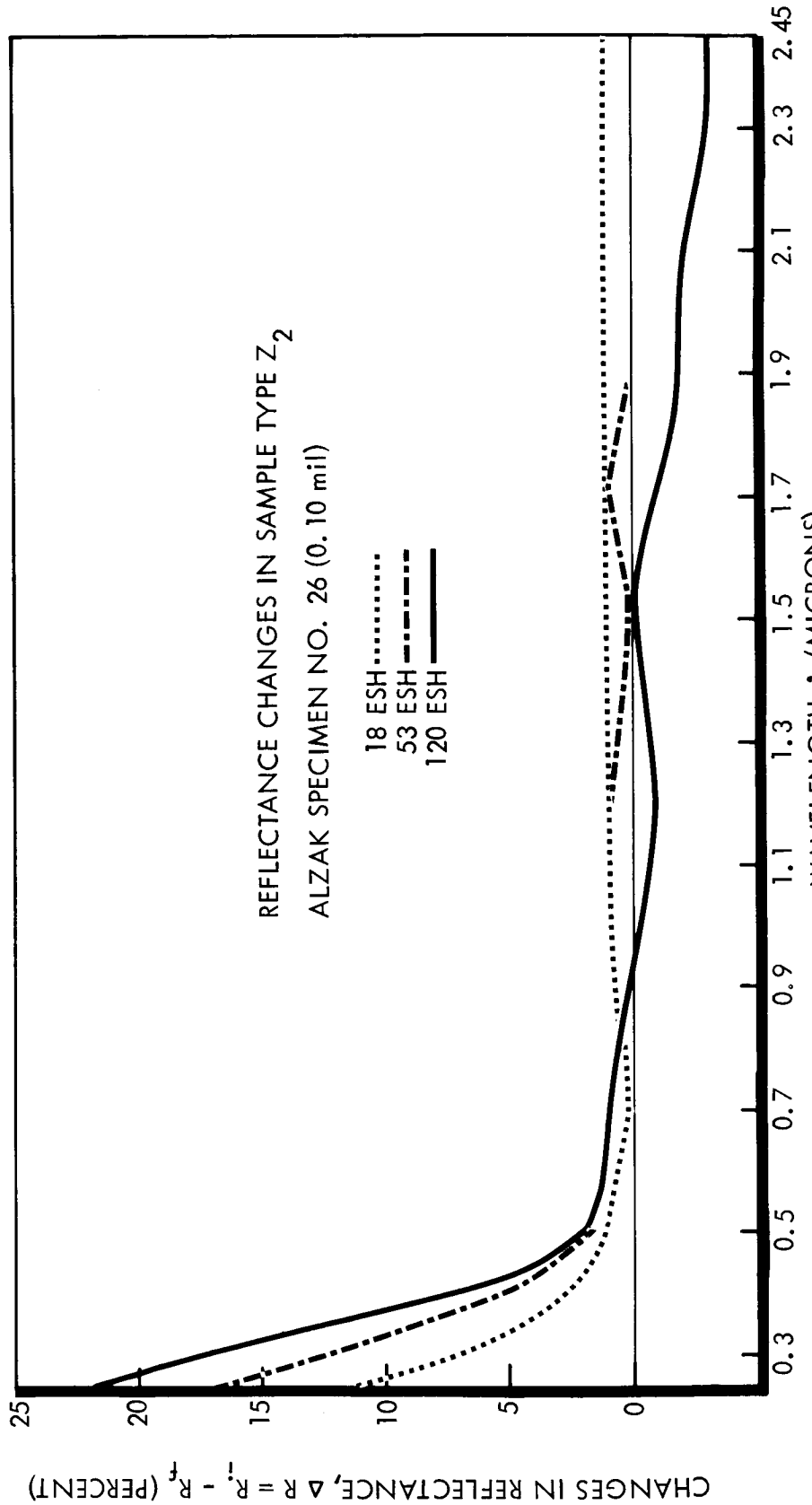

Figure 27. Spectral Reflectance Changes in 0.10-Mil Alzak (Type Z_2), Following Exposure to Ultraviolet Radiation

Similar to H, there occur in Alzak wavelength shifts with exposure, for each minimum and maximum. Typical of shifts in the visible region is that of a local maximum from 694 mμ before irradiation, to 689 mμ after 1130 ESH. In the infrared, a typical shift is that of a maximum from 1195 mμ to 1185 mμ.

Kapton H-film (sample type N) shows some reflectance loss in the ultraviolet, but more important for solar absorptance purposes are its moderate reflectance changes, both increases and decreases, in the visible and infrared regions. See Figure 28.

Of all classes of sample types tested, titanium dioxide—methyl silicone sample types exhibit the most variability in response, from severe degradation (L_1 and L_2) to great resistance (P). Type P undergoes only small changes across most of the region measured, even at 1130 ESH. Type O is somewhat worse, showing in the 400-500 millimicron wavelength region the usual characteristic of larger reflectance changes. Types L_1 and L_2 undergo very large changes throughout the visible and infrared regions. Comparisons can be made from Figures 29, 30, and 31.

Zinc oxide—methyl silicone sample types (B is 9 mils of S-13, while M is 10 to 12 mils of S-13G) have significant losses across the visible region. In the infrared, however, B degrades much more severely than M. Compare Figures 32 and 33.

Metal oxide—potassium silicate sample types (D_3 and F_3) also exhibit significant reflectance changes, as shown in Figures 34 and 35. Type F_3 (zinc oxide/aluminum oxide—potassium silicate) has moderate reflectance losses across most of infrared region measured, and has the customarily greater losses in the short-wavelength visible region.

Originally having a high reflectance in the ultraviolet region, D_3 (aluminum oxide—potassium silicate) is subject to and undergoes large reflectance losses in the ultraviolet wavelength region. These losses extend through the visible and into the near infrared, but are of small magnitude there. Between 1.6 and 2.5 microns there is no reflectance loss in D_3. In spite of its large reflectance losses, however, it should be noted that the solar reflectance of type D at 1130 ESH is still no less than that of type F_3.

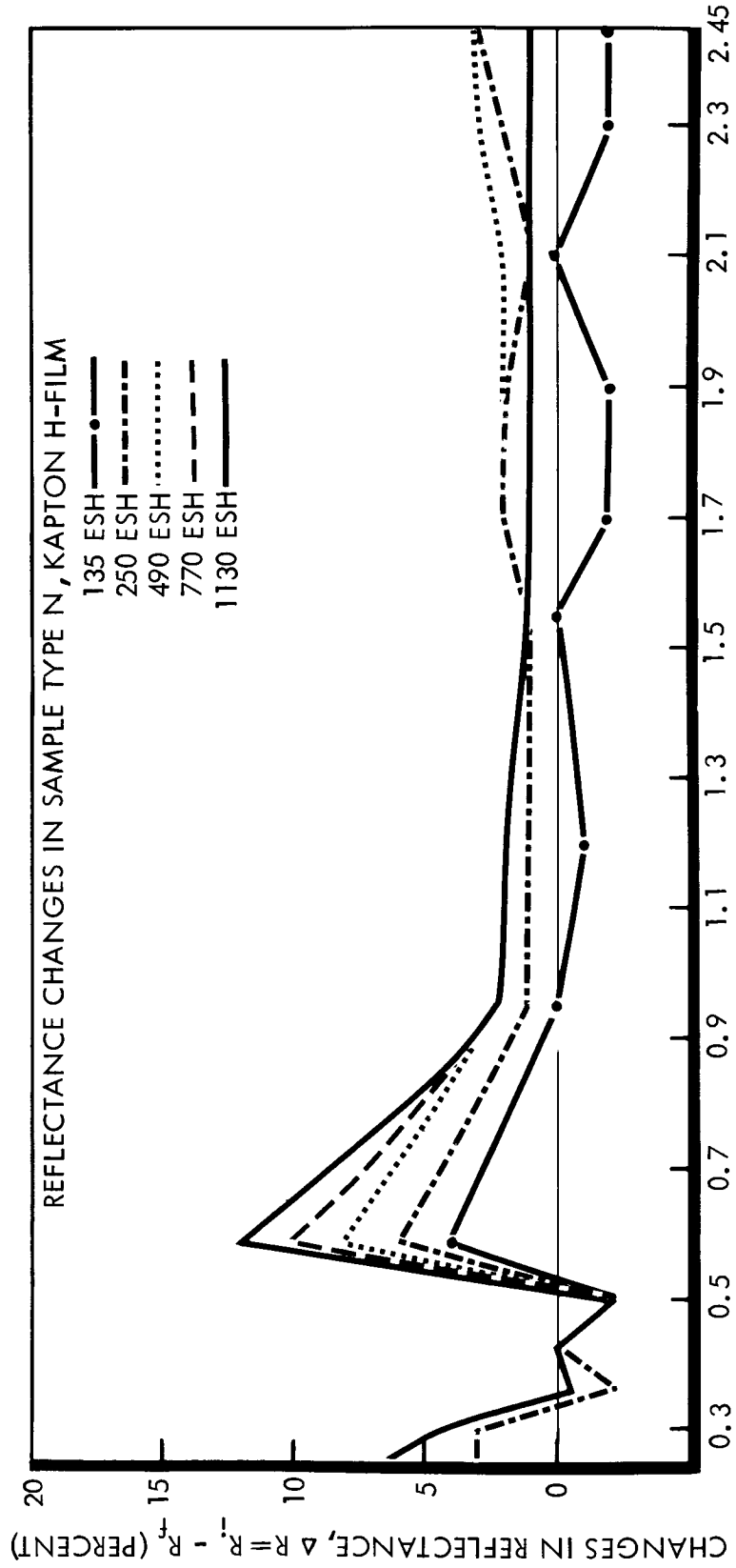

Figure 28. Spectral Reflectance Changes in Kapton H-Film (Type N), Following Exposure to Ultraviolet Radiation

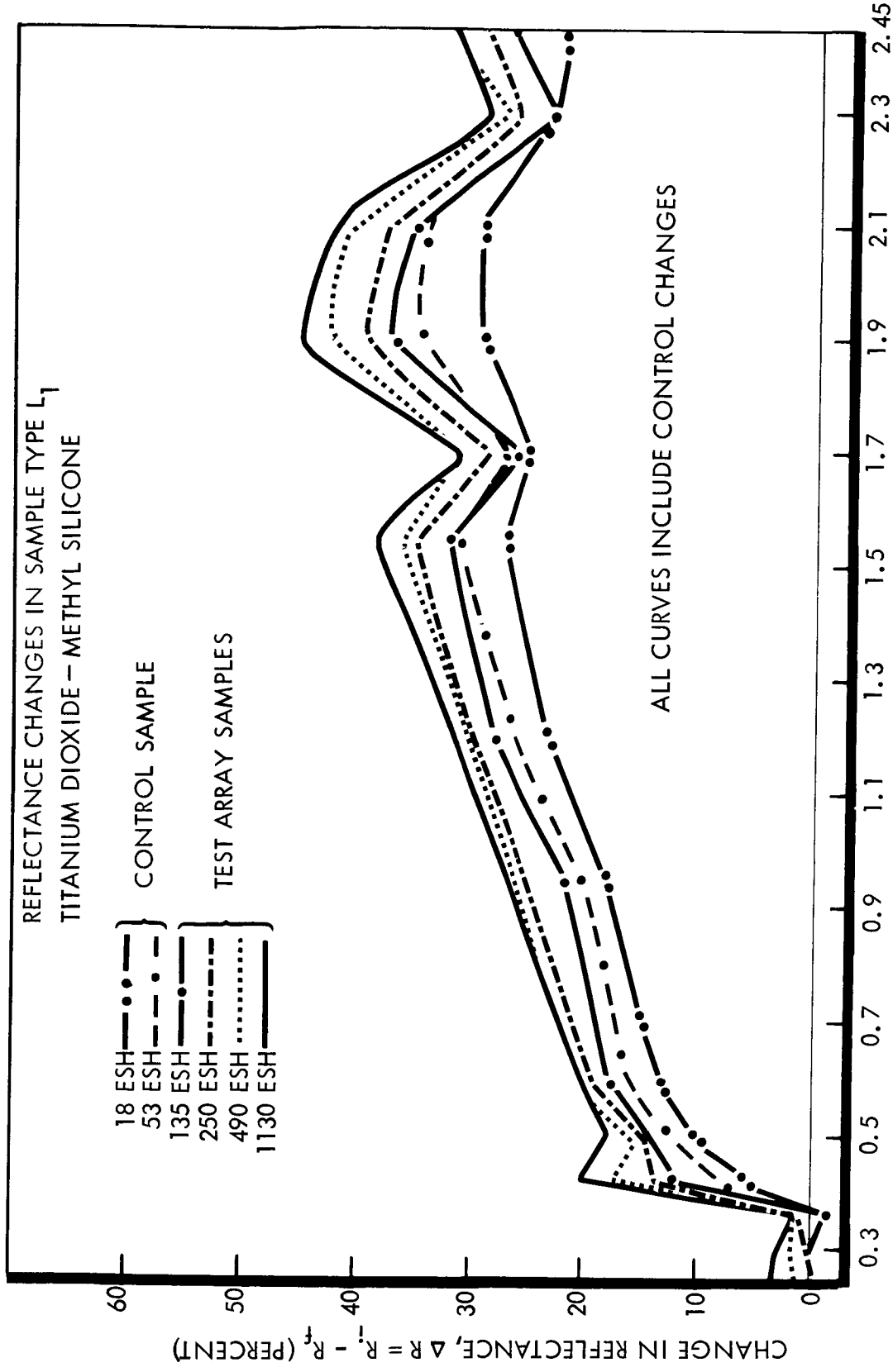

Figure 29. Spectral Reflectance Changes in Titanium Dioxide–Methyl Silicone (Type L_1), Following Exposure to Ultraviolet Radiation

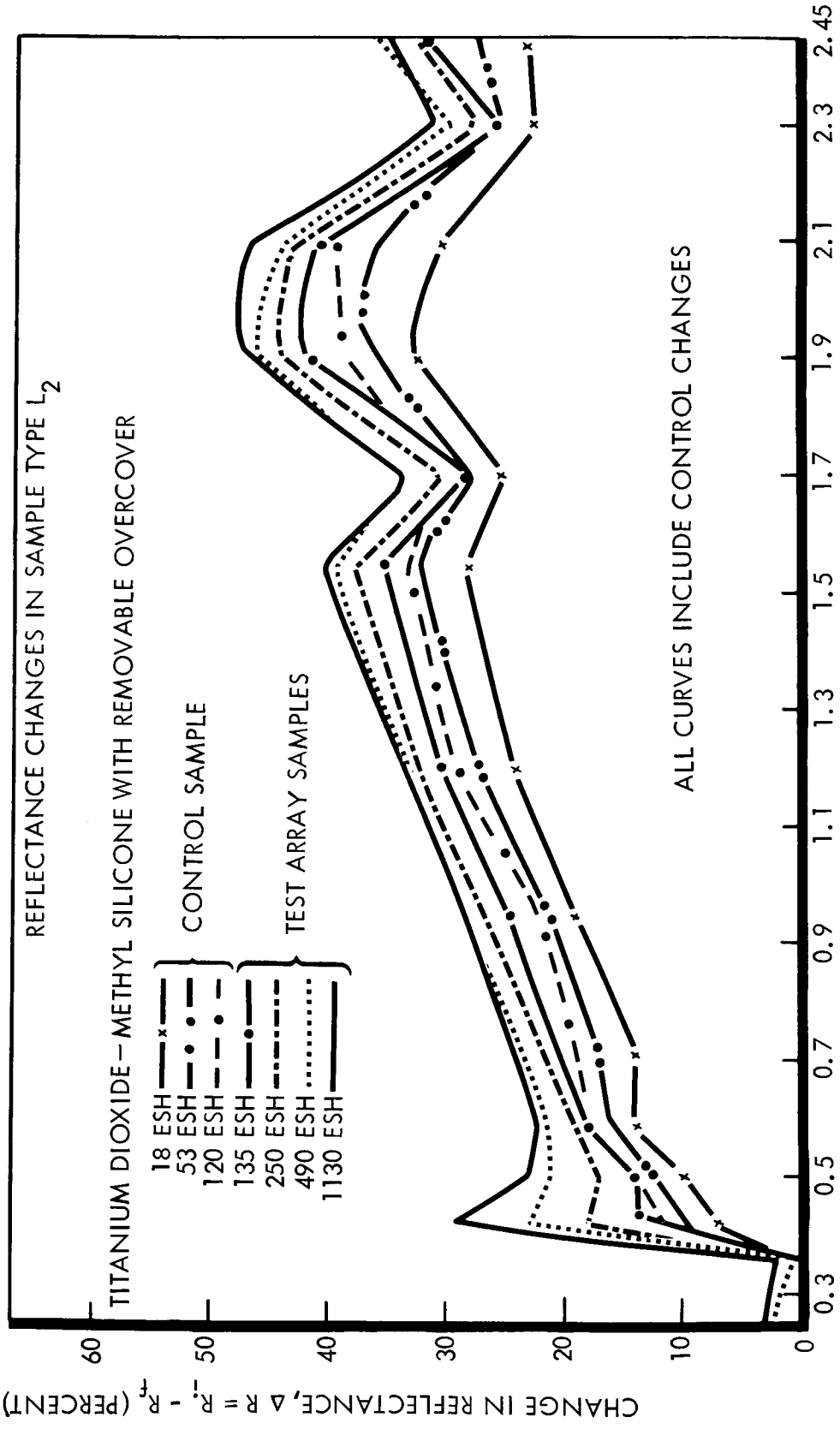

Figure 30. Spectral Reflectance Changes in Titanium Dioxide – Methyl Silicone (Type L_2), Following Exposure to Ultraviolet Radiation

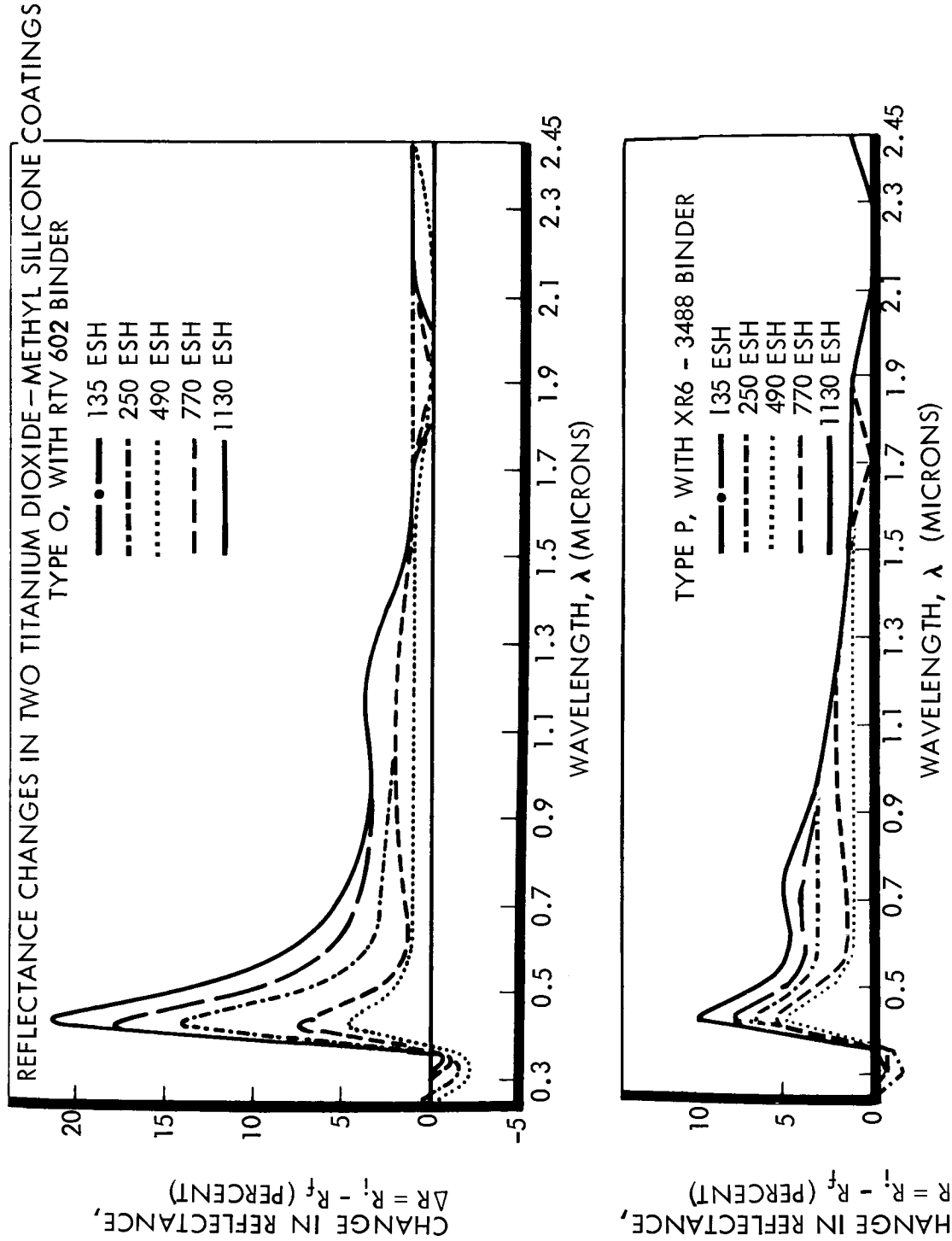

Figure 31. Spectral Reflectance Changes in Two Titanium Dioxide – Methyl Silicone Coatings (Types O and P), Following Exposure to Ultraviolet Radiation

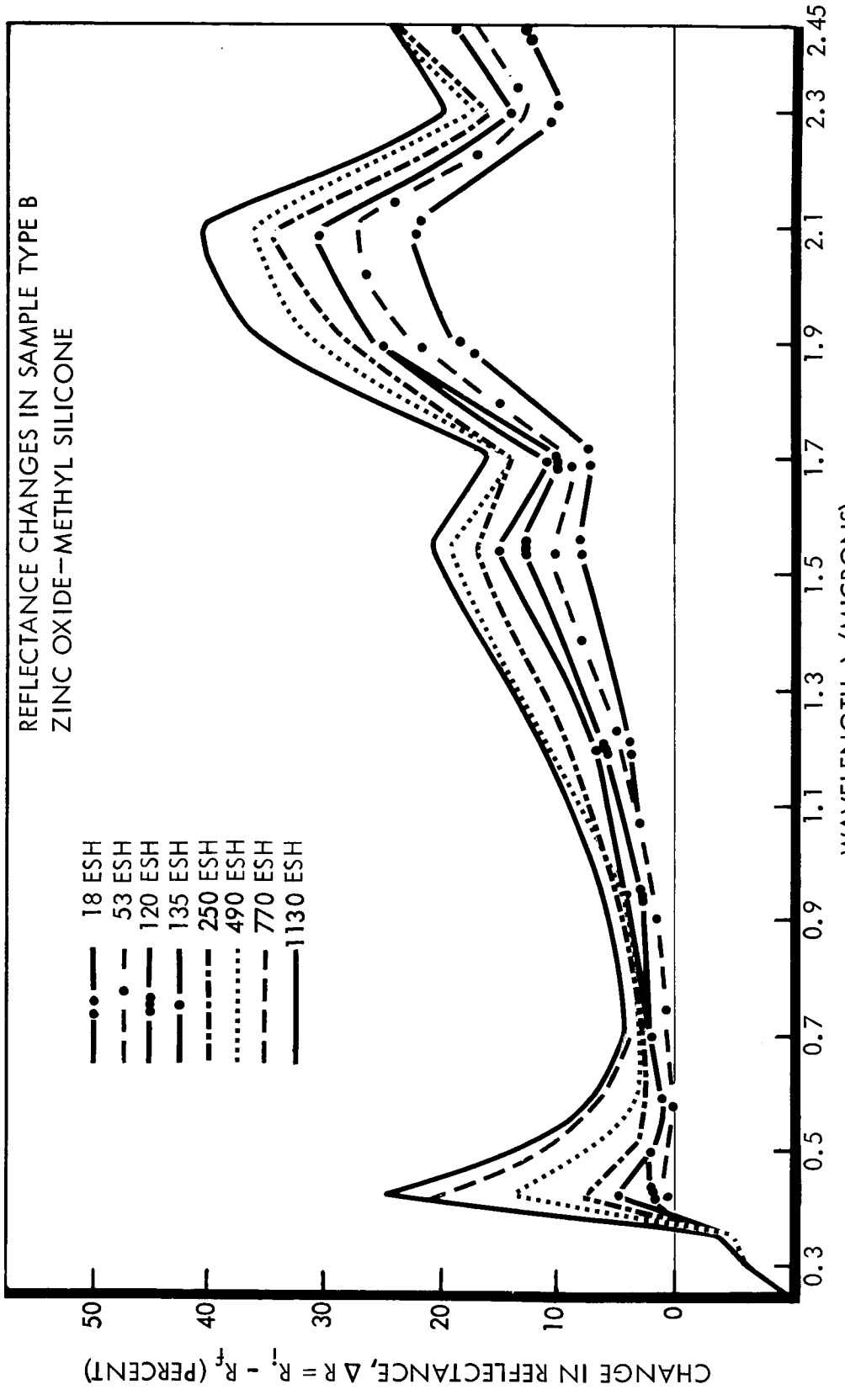

Figure 32. Spectral Reflectance Changes in Zinc Oxide – Methyl Silicone, S-13 (Type B), Following Exposure to Ultraviolet Radiation

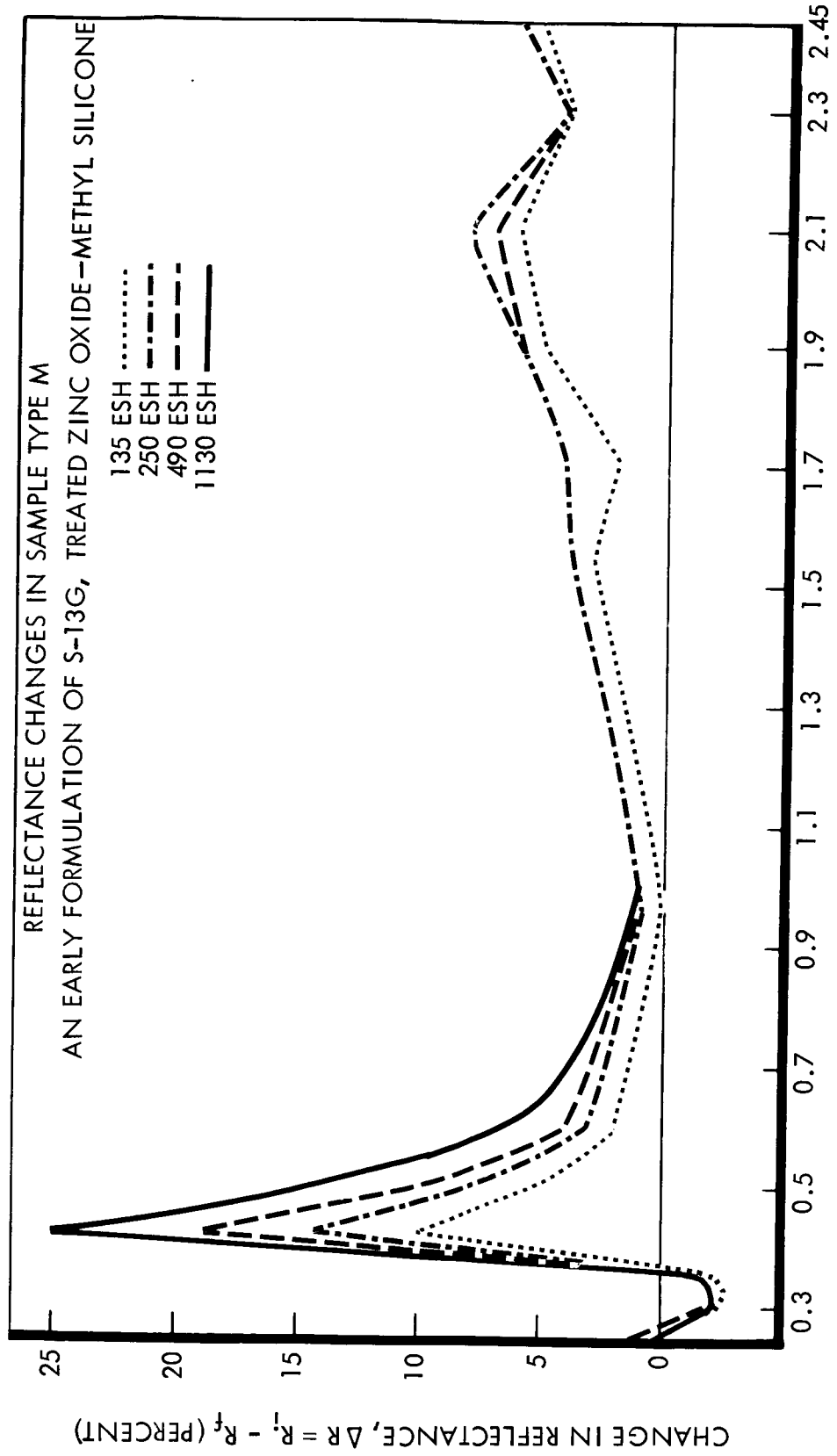

Figure 33. Spectral Reflectance Changes in an Early Formulation of S-13G, Treated Zinc Oxide–Methyl Silicone (Type M), Following Exposure to Ultraviolet Radiation

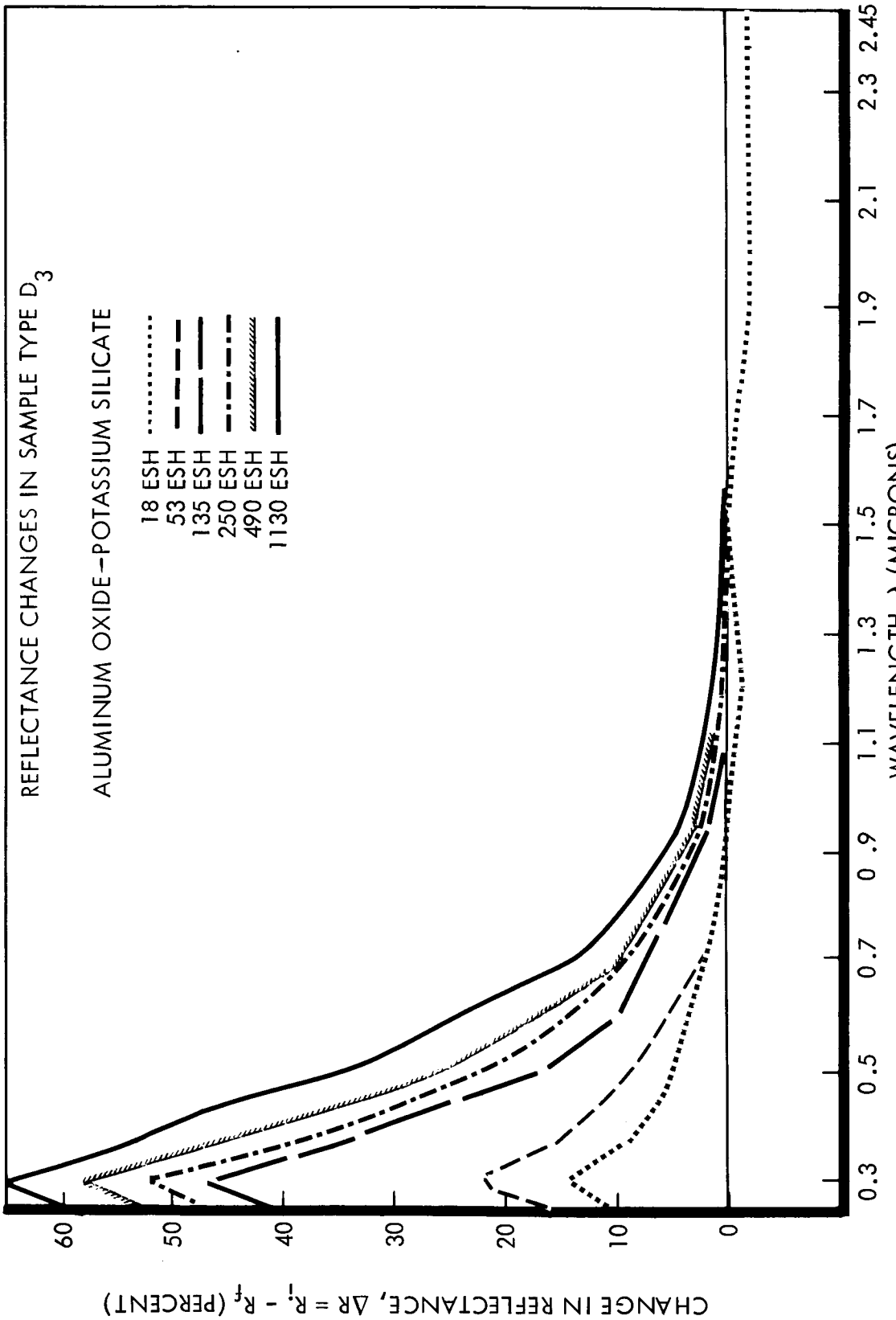

Figure 34. Spectral Reflectance Changes in Aluminum Oxide – Potassium Silicate (Type D_3), Following Exposure to Ultraviolet Radiation

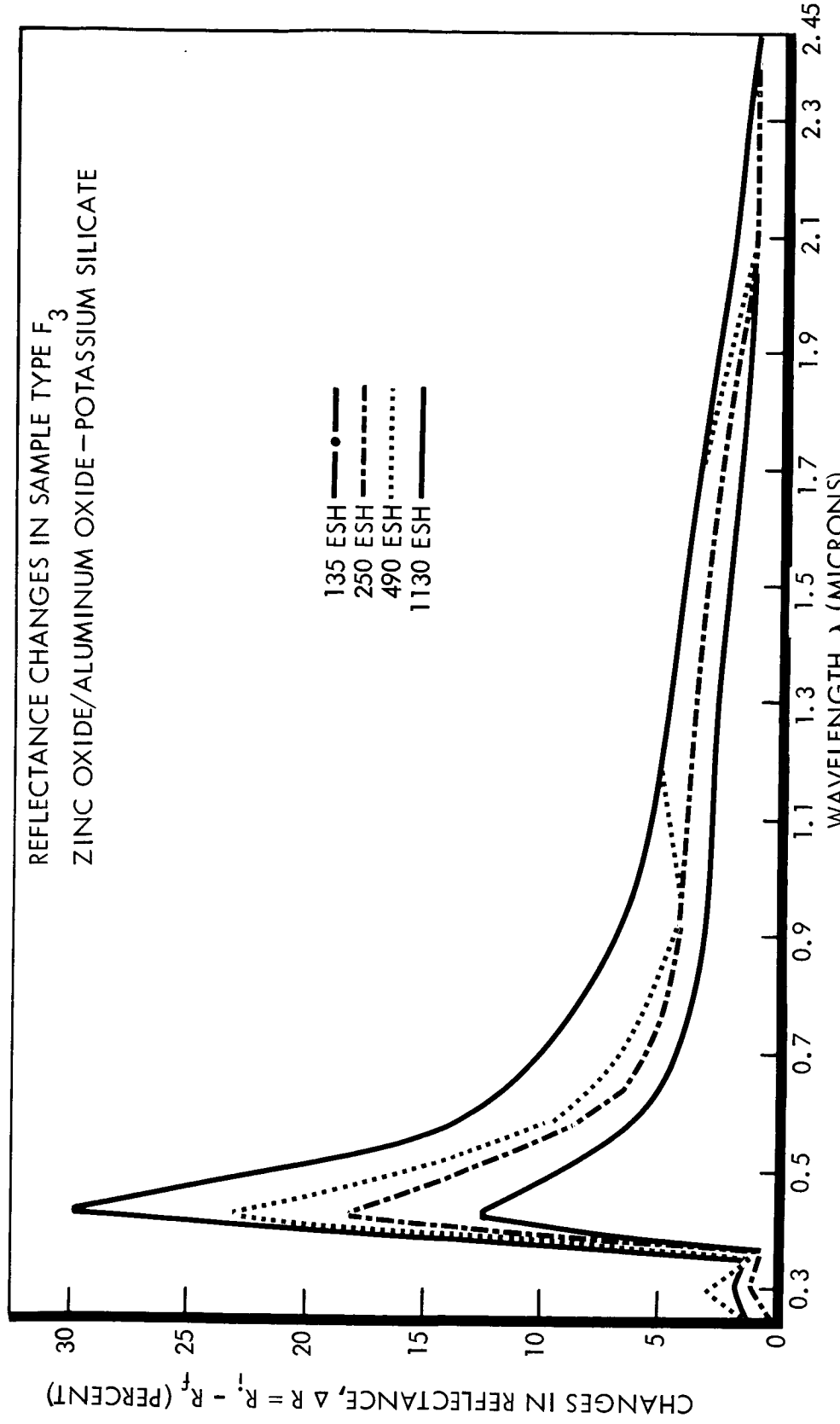

Figure 35. Spectral Reflectance Changes in Zinc Oxide/Aluminum Oxide – Potassium Silicate (Type F_3), Following Exposure to Ultraviolet Radiation

When measured in situ before exposure, type Q (mixed zinc oxide and titanium dioxide pigments in a mixed silicone-silicate vehicle) increases its reflectance by small amounts in the ultraviolet, the visible, and the 1.3 to 2.5 micron portion of the infrared, relative to in-air reflectance values measured before exposure. Due to exposure, reflectance is found to degrade moderately between 400 and 1900 millimicrons, the worst region being the short-wavelength visible. See Figure 36.

Of all paints, the largest reflectance changes occur in Pyromark, a titanium dioxide—methyl phenyl silicone coating (type Y). Losses of reflectance severe enough nearly to double Pyromark's solar absorptance at an exposure of 1130 ESH take place across the entire wavelength region measured. Figure 37 shows spectral reflectance change data for Pyromark; Table 16 indicates solar absorptance data determined for Pyromark.

Table 16. Solar Absorptance Calculations for Pyromark

Equivalent Space UV Sun Hours	0	53	135	490	1130
α_s	0.27	0.39	0.42	0.47	0.50
$\Delta\alpha_s$	-	0.12	0.15	0.20	0.23
% increase in $\alpha_s = \Delta\alpha_s/\alpha_s$	-	44%	56%	74%	85%

Solar absorptance has also been calculated for Pyromark exposed to ultraviolet radiation in a separate test at a 1.8 UV-sun rate, up to 18 ESH. Table 17 shows a comparison with data derived from tests at the 4.4 UV-sun rate. While indicative of the fact that there are no significant rate differences for Pyromark between 1.8 and 5 sun rates when exposed to 18 ESH, it is insufficient data to draw any conclusions about ultraviolet radiation rate effects in this coating at longer exposures or for much different lamp source spectra. Furthermore, the results on this sample cannot be extrapolated to other types.

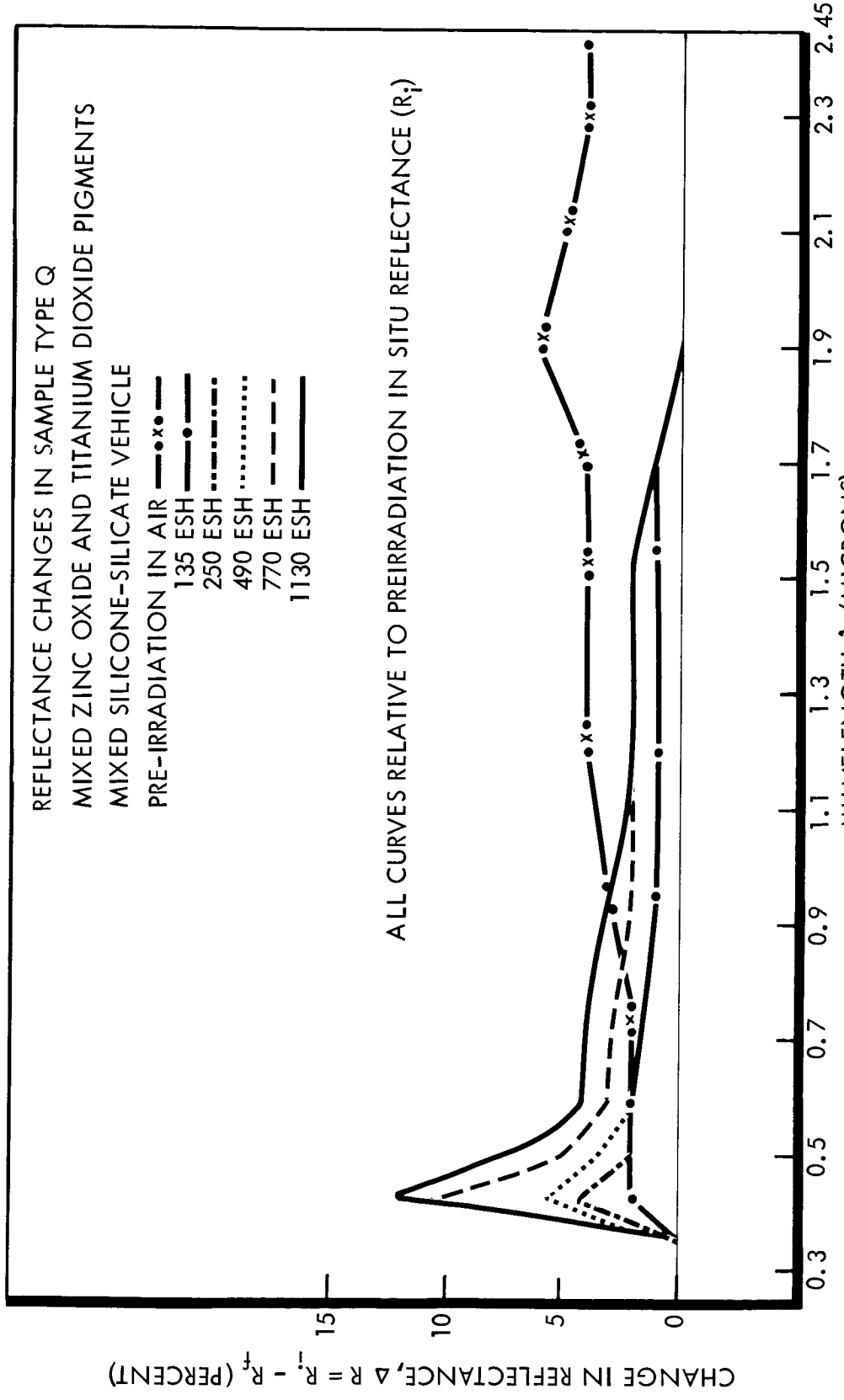

Figure 36. Spectral Reflectance Changes in Type Q, a Coating with Mixed Pigments and Mixed Vehicles, Following Exposure to Ultraviolet Radiation

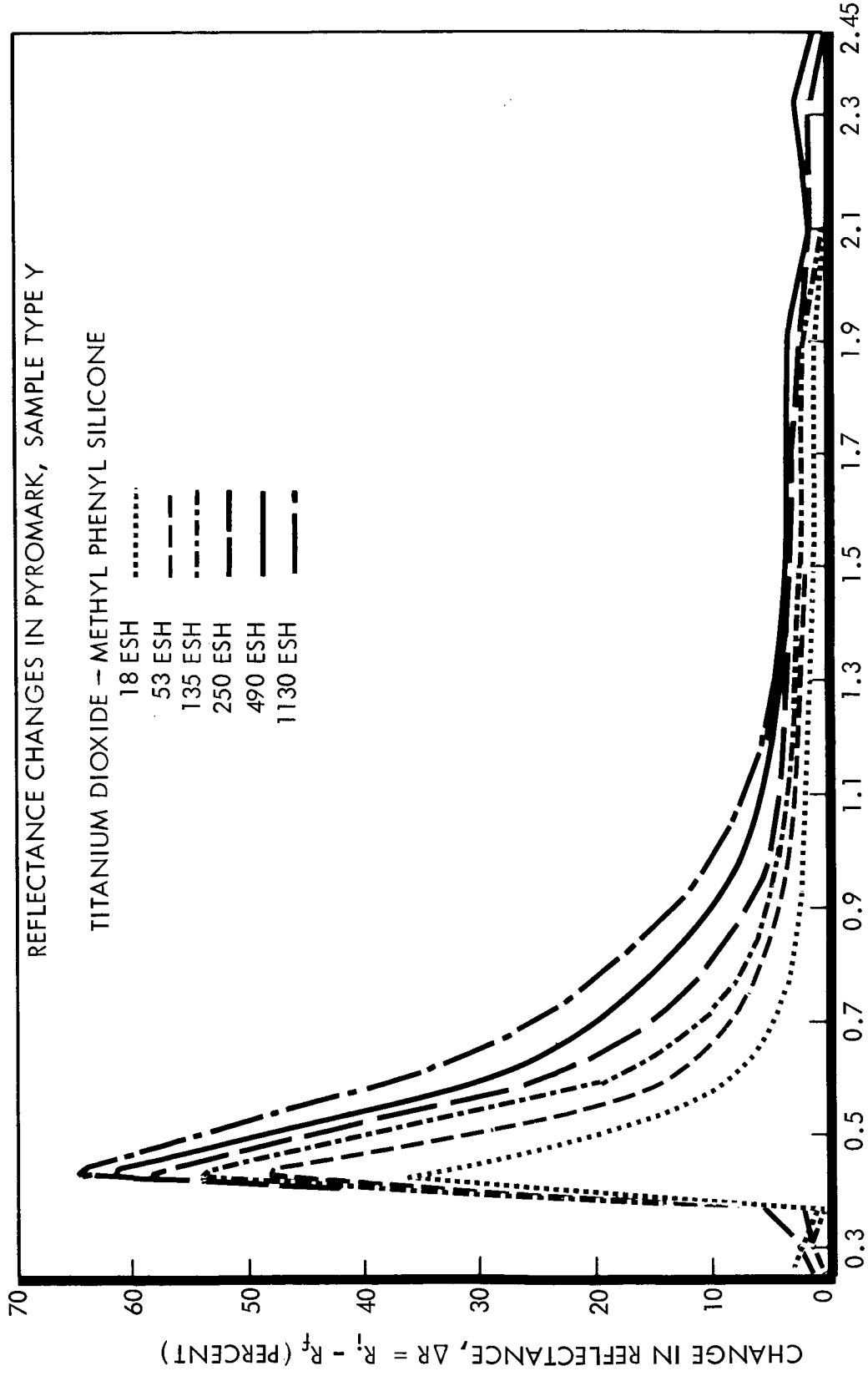

Figure 37. Spectral Reflectance Changes in Titanium Dioxide–Methyl Phenyl Silicone (Pyromark, Type Y), Following Exposure to Ultraviolet Radiation

Table 17. Comparison of Pyromark α_s at Two Sun Rates

SAMPLE SUN RATE	α_s at		$\Delta\alpha_s$ after
	0 ESH	18 ESH	18 ESH
Pyromark #8 at 1.8 UV suns	0.28	0.36	0.08
Pyromark #5 at 4.4 UV suns	0.27	0.35	0.08

Significant changes in sample reflectance resulting from mercury-arc ultraviolet exposure, as measured in situ, are summarized for selected wavelengths in Tables 18 through 31, for all sample types tested and represented by Figures 22 through 37.

Whereas control samples (shielded from the electromagnetic radiation but otherwise in situ) of most sample types show high stability as testing proceeds, L_1 and L_2 controls themselves undergo large reflectance changes. The original air cure of 24 hours for L_1 and L_2 is sufficient to account for this later instability during testing. Thus, in Tables 21 through 31, reflectance changes for L_1 and L_2 are shown in two forms: for 135 ESH through 1130 ESH, (1) "as measured" in the usual manner (relative to pre-irradiation values) and (2) with the control change at the same ESH subtracted. For 18 ESH through 120 ESH (the second set of exposures, conducted using control samples after the conclusion of the regular test at 1130 ESH), the "as measured" entries are actually the sum of (a) the reflectance change measured at 18, 53, and 120 ESH, and (b) the control change previously measured at 1130 ESH, since this change is that which the L_1 and L_2 controls "saw" prior to the second set of short exposures. For 18 ESH through 120 ESH, the second form of entries, "control change subtracted," is simply the reflectance change at 18, 53, and 120 ESH, relative to the beginning of ultraviolet exposure on the controls. Reflectance changes in Figures 29 and 30 include control changes.

Tables 28 through 31 show a similar pair of two forms of entries for sample type B at infrared wavelengths beyond 1700 millimicrons. The difference between

Table 18. Reflectance Changes at 250 Millimicrons

Sample Type	Decrease (Increase) in Reflectance at 250 mμ for Eight UV Exposures $\Delta R = R_i - R_f$ (Percent)							
	18 ESH	53 ESH	120 ESH	135 ESH	250 ESH	490 ESH	770 ESH	1130 ESH
I, leafing aluminum-silicone	-	-	(3)	10	13	17	21	24
J, vapor-deposited aluminum	-	-	-	6	13	21	25	29
K, polished aluminum	-	-	(1)	10	14	19	25	28
H, SiO_2 on polished aluminum	-	-	-	(21)	(16)	(11)	-	(7)
Alzak #26, 0.10-mil	11	17	21	-	-	-	-	-
Alzak #21, 0.29-mil	-	-	-	51	54	59	60	60
N, Kapton H-film	-	-	-	3	5	6	-	7
L_1, TiO_2-methyl silicone	0	-	0	0	0	2	-	4
L_2, TiO_2-methyl silicone	0	-	0	0	2	2	-	3
O, TiO_2-methyl silicone	-	-	-	-	(2)	(2)	-	(2)
P, TiO_2-methyl silicone	-	-	-	-	(2)	(2)	-	(1)
B, ZnO-methyl silicone (S-13)	-	-	-	(10)	(10)	(9)	-	(6)
M, ZnO-methyl silicone (S-13G)	-	-	-	(3)	(2)	(2)	-	0
D_3, Al_2O_3-K_2SiO_3	11	17	25	41	46	51	-	58
F_3, ZnO/Al_2O_3-K_2SiO_3	-	-	-	1	1	2	-	2
Q, mixed ZnO and TiO_2, mixed silicone-silicate	-	-	-	0	0	0	-	0
Y (Pyromark), TiO_2-methyl phenyl silicone	0	-	-	2	2	1	-	3

Table 19. Reflectance Changes at 300 Millimicrons

Sample Type	Decrease (Increase) in Reflectance at 300 mμ for Eight UV Exposures $\Delta R = R_i - R_f$ (Percent)							
	18 ESH	53 ESH	120 ESH	135 ESH	250 ESH	490 ESH	770 ESH	1130 ESH
I, leafing aluminum-silicone	-	-	(3)	6	7	9	11	14
J, vapor-deposited aluminum	-	-	-	1	2	6	7	11
K, polished aluminum	-	-	0	4	6	8	12	14
H, SiO_2 on polished aluminum	-	-	-	10	10	14	-	18
Alzak #26, 0.10-mil	7	13	18	-	-	-	-	-
Alzak #21, 0.29-mil	-	-	-	55	61	66	69	70
N, Kapton H-film	-	-	-	2	3	4	-	5
L_1, TiO_2-methyl silicone	0	-	-	0	0	1	-	3
L_2, TiO_2-methyl silicone	0	-	-	0	1	1	-	3
O, TiO_2-methyl silicone	-	-	-	0	0	(2)	-	(2)
P, TiO_2-methyl silicone	-	-	-	0	(1)	(1)	-	(1)
B, ZnO-methyl silicone (S-13)	-	-	-	(6)	(6)	(6)	-	(5)
M, ZnO-methyl silicone (S-13G)	-	-	-	(2)	(1)	(1)	-	(1)
D_3, Al_2O_3-K_2SiO_3	14	22	27	47	52	58	-	65
F_3, ZnO/Al_2O_3-K_2SiO_3	-	-	-	1	1	2	-	2
Q, mixed ZnO and TiO_2, mixed silicone-silicate	-	-	-	0	0	0	-	0
Y (Pyromark), TiO_2-methyl phenyl silicone	0	-	-	1	1	1	-	2

Table 20. Reflectance Changes at 360 Millimicrons

Sample Type	Decrease (Increase) in Reflectance at 360 mμ for Eight UV Exposures $\Delta R = R_i - R_f$ (Percent)							
	18 ESH	53 ESH	120 ESH	135 ESH	250 ESH	490 ESH	770 ESH	1130 ESH
I, leafing aluminum-silicone	-	-	(2)	3	4	5	6	11
J, vapor-deposited aluminum	-	-	-	1	1	1	3	4
K, polished aluminum	-	-	0	1	3	3	5	12
H, SiO_2 on polished aluminum	-	-	5	7	10	13	14	15
Alzak #26, 0.10-mil	4	8	11	-	-	-	-	-
Alzak #21, 0.29-mil	-	-	-	37	43	48	52	55
N, Kapton H-film	-	-	(2)	(1)	(1)	(1)	0	0
L_1, TiO_2-methyl silicone	(1)	0	0	(1)	1	1	-	1
L_2, TiO_2-methyl silicone	0	0	0	0	3	0	-	2
O, TiO_2-methyl silicone	-	-	-	(1)	(1)	(1)	(1)	(2)
P, TiO_2-methyl silicone	-	-	-	0	0	1	0	0
B, ZnO-methyl silicone (S-13)	-	(2)	(3)	(3)	(4)	(5)	(3)	(3)
M, ZnO-methyl silicone (S-13G)	-	-	-	(1)	(1)	(1)	0	(1)
D_3, Al_2O_3-K_2SiO_3	10	16	21	35	40	47	51	54
F_3, ZnO/Al_2O_3-K_2SiO_3	-	-	0	1	1	1	1	1
Q, mixed ZnO and TiO_2, mixed silicone-silicate	-	-	-	0	0	0	0	0
Y (Pyromark), TiO_2-methyl phenyl silicone	0	0	1	1	1	0	-	5

Table 21. Reflectance Changes at 425 Millimicrons

Sample Type	Decrease (Increase) in Reflectance at 425 mμ for Eight UV Exposures $\Delta R = R_i - R_f$ (Percent)							
	18 ESH	53 ESH	120 ESH	135 ESH	250 ESH	490 ESH	770 ESH	1130 ESH
I, leafing aluminum-silicone	-	-	-	1	1	2	3	4
J, vapor-deposited aluminum	-	-	-	1	1	1	-	2
K, polished aluminum	-	-	-	0	0	1	-	2
H, SiO_2 on polished aluminum	-	-	4	6	8	10	11	12
Alzak #26, 0.10-mil	2	4	5	-	-	-	-	-
Alzak #21, 0.29-mil	-	-	-	20	27	32	35	38
N, Kapton H-film	-	-	(2)	(2)	(2)	(2)	(2)	(2)
AS MEASURED:								
L_1, TiO_2-methyl silicone	7	8	10	12	14	17	-	20
L_2, TiO_2-methyl silicone	7	10	12	14	18	23	-	29
O, TiO_2-methyl silicone	-	-	-	5	8	14	19	25
P, TiO_2-methyl silicone	-	-	-	5	6	7	8	10
B, ZnO-methyl silicone (S-13)	-	1	2	5	8	14	20	26
M, ZnO-methyl silicone (S-13G)	-	-	-	10	14	19	23	25
D_3, Al_2O_3-K_2SiO_3	7	12	16	27	31	37	42	45
F_3, ZnO/Al_2O_3-K_2SiO_3	-	-	8	13	18	23	27	30
Q, mixed ZnO and TiO_2, mixed silicone-silicate	-	-	-	2	4	7	10	12
Y (Pyromark), TiO_2-methyl phenyl silicone	38	50	57	58	60	64	-	67
LESS CONTROL CHANGE:								
L_1	4	5	6	10	12	12	-	17
L_2	5	7	10	13	17	20	-	27

Table 22. Reflectance Changes at 500 Millimicrons

Sample Type	Decrease (Increase) in Reflectance at 500 mμ for Eight UV Exposures $\Delta R = R_i - R_f$ (Percent)							
	18 ESH	53 ESH	120 ESH	135 ESH	250 ESH	490 ESH	770 ESH	1130 ESH
I, leafing aluminum-silicone	-	-	-	0	1	1	2	1
J, vapor-deposited aluminum	-	-	-	0	0	0	-	1
K, polished aluminum	-	-	-	0	0	1	-	1
H, SiO_2 on polished aluminum	-	-	2	2	3	6	7	10
Alzak #26, 0.10-mil	1	2	2	-	-	-	-	-
Alzak #21, 0.29-mil	-	-	-	9	14	18	21	25
N, Kapton H-film	-	-	(1)	(2)	(2)	(2)	(2)	(2)
AS MEASURED:								
L_1, TiO_2-methyl silicone	10	12	13	14	14	16	-	18
L_2, TiO_2-methyl silicone	10	12	14	15	17	20	-	22
O, TiO_2-methyl silicone	-	-	-	2	3	7	10	14
P, TiO_2-methyl silicone	-	-	-	2	2	3	5	6
B, ZnO-methyl silicone (S-13)	-	1	1	2	4	7	11	14
M, ZnO-methyl silicone(S-13G)	-	-	-	5	8	10	11	14
D_3, Al_2O_3-K_2SiO_3	5	9	12	17	22	26	30	33
F_3, ZnO/Al_2O_3-K_2SiO_3	-	-	5	9	12	16	18	20
Q, mixed ZnO and TiO_2, mixed silicone-silicate	-	-	-	2	3	5	6	7
Y (Pyromark), TiO_2-methyl phenyl silicone	18	30	38	39	44	49	-	55
LESS CONTROL CHANGE:								
L_1	5	6	8	11	11	10	-	13
L_2	7	9	11	14	16	18	-	20

Table 23. Reflectance Changes at 590 Millimicrons

Sample Type	Decrease (Increase) in Reflectance at 590 mμ for Eight UV Exposures $\Delta R = R_i - R_f$ (Percent)							
	18 ESH	53 ESH	120 ESH	135 ESH	250 ESH	490 ESH	770 ESH	1130 ESH
I, leafing aluminum-silicone	-	-	-	0	0	0	1	0
J, vapor-deposited aluminum	-	-	-	0	0	0	-	0
K, polished aluminum	-	-	-	0	0	0	-	0
H, SiO_2 on polished aluminum	-	-	1	2	4	4	4	6
Alzak #26, 0.10-mil	1	1	1	-	-	-	-	-
Alzak #21, 0.29-mil	-	-	-	7	8	10	15	15
N, Kapton H-film	-	-	3	4	6	8	10	13
AS MEASURED:								
L_1, TiO_2-methyl silicone	13	16	18	18	19	20	-	21
L_2, TiO_2-methyl silicone	14	16	18	18	20	21	-	22
O, TiO_2-methyl silicone	-	-	-	1	2	4	5	7
P, TiO_2-methyl silicone	-	-	-	1	2	3	3	4
B, ZnO-methyl silicone (S-13)	-	1	1	2	2	3	6	6
M, ZnO-methyl silicone (S-13G)	-	-	-	2	3	4	6	6
D_3, Al_2O_3-K_2SiO_3	4	6	9	10	15	19	20	25
F_3, ZnO/Al_2O_3-K_2SiO_3	-	-	4	7	9	11	12	14
Q, mixed ZnO and TiO_2, mixed silicone-silicate	-	-	-	2	2	3	4	4
Y (Pyromark), TiO_2-methyl phenyl silicone	8	13	19	20	26	30	-	37
LESS CONTROL CHANGE:								
L_1	7	9	11	13	15	13	-	14
L_2	9	11	13	16	17	18	-	18

Table 24. Reflectance Changes at 950 Millimicrons

Sample Type	Decrease (Increase) in Reflectance at 950 mμ for Eight UV Exposures $\Delta R = R_i - R_f$ (Percent)							
	18 ESH	53 ESH	120 ESH	135 ESH	250 ESH	490 ESH	770 ESH	1130 ESH
I, leafing aluminum-silicone	-	-	-	(1)	0	1	-	0
J, vapor-deposited aluminum	-	-	-	(1)	1	1	-	1
K, polished aluminum	-	-	-	(1)	1	1	-	0
H, SiO_2 on polished aluminum	-	-	-	0	2	3	2	4
Alzak #26, 0.10-mil	1	1	0	-	-	-	-	-
Alzak #21, 0.29-mil	-	-	-	0	1	2	-	3
N, Kapton H-film	-	-	-	0	2	2	2	3
AS MEASURED:								
L_1, TiO_2-methyl silicone	18	21	22	22	25	26	-	27
L_2, TiO_2-methyl silicone	19	22	24	25	26	28	-	28
O, TiO_2-methyl silicone	-	-	-	1	2	2	3	3
P, TiO_2-methyl silicone	-	-	-	2	2	3	3	3
B, ZnO-methyl silicone (S-13)	2	3	3	4	5	5	-	7
M, ZnO-methyl silicone (S-13G)	-	-	-	0	1	1	1	1
D_3, Al_2O_3-K_2SiO_3	-	(1)	0	(1)	2	3	-	4
F_3, ZnO/Al_2O_3-K_2SiO_3	-	-	-	3	5	5	-	6
Q, mixed ZnO and TiO_2, mixed silicone-silicate	-	-	-	1	1	2	3	3
Y (Pyromark), TiO_2-methyl phenyl silicone	3	4	5	5	7	9	-	11
LESS CONTROL CHANGE:								
L_1	8	11	13	17	18	17	-	17
L_2	12	14	17	21	22	24	-	20

Table 25. Reflectance Changes at 1200 Millimicrons

Sample Type	Decrease (Increase) in Reflectance at 1200 mμ for Eight UV Exposures $\Delta R = R_i - R_f$ (Percent)							
	18 ESH	53 ESH	120 ESH	135 ESH	250 ESH	490 ESH	770 ESH	1130 ESH
I, leafing aluminum-silicone	-	-	-	(1)	0	1	-	1
J, vapor-deposited aluminum	-	-	-	(1)	1	1	-	1
K, polished aluminum	-	-	-	(1)	1	1	-	0
H, SiO_2 on polished aluminum	-	-	-	(1)	1	2	1	2
Alzak #26, 0.10-mil	1	1	(1)	-	-	-	-	-
Alzak #21, 0.29-mil	-	-	-	0	1	2	2	2
N, Kapton H-film	-	-	-	(1)	1	2	2	2
AS MEASURED:								
L_1, TiO_2-methyl silicone	23	26	28	28	30	30	-	32
L_2, TiO_2-methyl silicone	24	27	29	30	32	33	-	34
O, TiO_2-methyl silicone	-	-	-	1	2	2	2	3
P, TiO_2-methyl silicone	-	-	-	1	2	2	2	2
B, ZnO-methyl silicone (S-13)	4	5	6	7	9	10	-	11
M, ZnO-methyl silicone (S-13G)	-	-	-	1	2	2	2	2
D_3, Al_2O_3-K_2SiO_3	0	(1)	(1)	0	1	1	-	2
F_3, ZnO/Al_2O_3-K_2SiO_3	-	-	-	3	4	5	-	5
Q, mixed ZnO and TiO_2, mixed silicone-silicate	-	-	-	1	1	1	2	2
Y (Pyromark), TiO_2-methyl phenyl silicone	3	3	3	4	4	5	-	6
LESS CONTROL CHANGE:								
L_1	10	13	15	21	21	20	-	19
L_2	14	17	19	26	27	27	-	24

Table 26. Reflectance Changes at 1550 Millimicrons

Sample Type	Decrease (Increase) in Reflectance at 1550 mμ for Eight UV Exposures $\Delta R = R_i - R_f$ (Percent)							
	18 ESH	53 ESH	120 ESH	135 ESH	250 ESH	490 ESH	770 ESH	1130 ESH
I, leafing aluminum-silicone	-	-	-	(1)	0	1	-	1
J, vapor-deposited aluminum	-	-	-	(1)	1	1	-	1
K, polished aluminum	-	-	-	(1)	1	1	-	1
H, SiO_2 on polished aluminum	-	-	-	(2)	1	1	0	1
Alzak #26, 0.10-mil	1	0	(1)	-	-	-	-	-
Alzak #21, 0.29-mil	-	-	-	0	1	2	-	2
N, Kapton H-film	-	-	-	(1)	1	1	0	1
AS MEASURED:								
L_1, TiO_2-methyl silicone	27	31	32	32	35	36	-	38
L_2, TiO_2-methyl silicone	28	32	33	35	37	39	-	40
O, TiO_2-methyl silicone	-	-	-	1	1	1	1	1
P, TiO_2-methyl silicone	-	-	-	1	1	1	1	1
B, ZnO-methyl silicone (S-13)	8	11	13	15	17	19	-	21
M, ZnO-methyl silicone (S-13G)	-	-	-	3	4	4	4	4
D_3, Al_2O_3-K_2SiO_3	0	(1)	(1)	(1)	0	0	-	(1)
F_3, ZnO/Al_2O_3-K_2SiO_3	-	-	-	2	3	4	-	4
Q, mixed ZnO and TiO_2, mixed silicone-silicate	-	-	-	1	1	1	1	2
Y (Pyromark), TiO_2-methyl phenyl silicone	1	2	2	2	3	3	-	4
LESS CONTROL CHANGE:								
L_1	11	15	16	23	24	24	-	22
L_2	17	21	22	30	30	32	-	29

Table 27. Reflectance Changes at 1700 Millimicrons

Sample Type	Decrease (Increase) in Reflectance at 1700 mμ for Eight UV Exposures $\Delta R = R_i - R_f$ (Percent)							
	18 ESH	53 ESH	120 ESH	135 ESH	250 ESH	490 ESH	770 ESH	1130 ESH
Alzak #26, 0.10-mil	1	1	(1)	-	-	-	-	-
Alzak #21, 0.29-mil	-	-	-	0	1	1	0	1
N, Kapton H-film	-	-	-	(2)	2	2	(1)	1
AS MEASURED:								
L_1, TiO_2-methyl silicone	22	25	26	26	29	31	-	31
L_2, TiO_2-methyl silicone	23	26	29	28	30	33	-	33
O, TiO_2-methyl silicone	-	-	-	0	1	1	1	1
P, TiO_2-methyl silicone	-	-	-	0	0	1	0	0
B, ZnO-methyl silicone (S-13)	7	9	10	11	14	16	-	17
M, ZnO-methyl silicone (S-13G)	-	-	-	2	4	3	3	3
D_3, Al_2O_3-K_2SiO_3	(1)	(1)	(1)	(1)	(1)	0	-	0
Q, mixed ZnO and TiO_2, mixed silicone-silicate	-	-	-	1	1	1	1	1
Pyromark, TiO_2- methyl phenyl silicone	1	1	1	2	3	3	-	3
LESS CONTROL CHANGE:								
L_1	10	12	14	-	-	-	-	19
L_2	14	17	19	-	-	-	-	23

Table 28. Reflectance Changes at 1900 Millimicrons

Sample Type	Decrease (Increase) in Reflectance at 1900 mu for Eight UV Exposures $\Delta R = R_i - R_f$ (Percent)							
	18 ESH	53 ESH	120 ESH	135 ESH	250 ESH	490 ESH	770 ESH	1130 ESH
Alzak #26, 0.10-mil	1	0	(2)	-	-	-	-	-
Alzak #21, 0.29-mil	-	-	-	5	1	1	0	1
N, Kapton H-film	-	-	-	(2)	2	2	(1)	1
AS MEASURED:								
L_1, TiO_2-methyl silicone	31	35	37	37	39	42	-	45
L_2, TiO_2-methyl silicone	33	36	39	41	43	45	-	46
O, TiO_2-methyl silicone	-	-	-	0	0	1	(1)	(1)
P, TiO_2-methyl silicone	-	-	-	0	1	0	0	1
B, ZnO-methyl silicons (S-13)	18	22	25	25	28	31	-	35
M, ZnO-methyl silicone (S-13G)	-	-	-	5	6	6	4	4
D_3, Al_2O_3-K_2SiO_3	0	(1)	(2)	(1)	(1)	0	-	0
Q, mixed ZnO and TiO_2, mixed silicone-silicate	-	-	-	0	0	0	(1)	(1)
Pyromark, TiO_2 - methyl phenyl silicone	1	1	1	2	2	3	-	3
LESS CONTROL CHANGE:								
L_1	13	17	19	-	-	-	-	27
L_2	20	24	26	-	-	-	-	33
B	14	18	21	25	27	29	-	31

Table 29. Reflectance Changes at 2100 Millimicrons

Sample Type	Decrease (Increase) in Reflectance at 2100 mμ for Eight UV Exposures $\Delta R = R_i - R_f$ (Percent)							
	18 ESH	53 ESH	120 ESH	135 ESH	250 ESH	490 ESH	770 ESH	1130 ESH
I, leafing aluminum-silicone	-	-	-	(2)	1	1	-	1
J, vapor-deposited aluminum	-	-	-	(2)	1	2	-	1
K, polished aluminum	-	-	-	(1)	2	2	-	0
H, SiO_2 on polished aluminum	-	-	-	(4)	1	1	(1)	2
Alzak #26, 0.10-mil	1	0	(2)	-	-	-	-	-
Alzak #21, 0.29-mil	-	-	-	(1)	1	1	-	1
N, Kapton H-film	-	-	-	(2)	2	2	0	1
AS MEASURED:								
L_1, TiO_2-methyl silicone	30	34	37	35	38	41	-	42
L_2, TiO_2-methyl silicone	31	35	39	40	42	44	-	46
O, TiO_2-methyl silicone	-	-	-	0	1	1	1	1
P, TiO_2-methyl silicone	-	-	-	0	0	1	1	1
B, ZnO-methyl silicone (S-13)	21	27	30	30	34	37	-	40
M, ZnO-methyl silicone (S-13G)	-	-	-	6	8	8	7	6
D_3, Al_2O_3-K_2SiO_3	(1)	(1)	(1)	(1)	(1)	(1)	-	0
F_3, ZnO/Al_2O_3-K_2SiO_3	-	-	-	1	1	2	-	2
Q, mixed ZnO and TiO_2, mixed silicone-silicate	-	-	-	0	0	0	0	0
Y (Pyromark), TiO_2-methyl phenyl silicone	0	0	0	1	1	1	-	2
LESS CONTROL CHANGE:								
L_1	13	17	19	26	25	27	-	25
L_2	19	23	27	34	35	33	-	34
B	17	22	25	30	33	34	-	36

Table 30. Reflectance Changes at 2300 Millimicrons

Sample Type	Decrease (Increase) in Reflectance at 2300 mu for Eight UV Exposures $\Delta R = R_i - R_f$ (Percent)							
	18 ESH	53 ESH	120 ESH	135 ESH	250 ESH	490 ESH	770 ESH	1130 ESH
Alzak #26, 0.10-mil	1	0	(3)	-	-	-	-	-
Alzak #21, 0.29-mil	-	-	-	(2)	2	2	-	1
N, Kapton H-film	-	-	-	(2)	2	3	(1)	1
AS MEASURED:								
L_1, TiO_2-methyl silicone	20	23	25	23	25	27	-	28
L_2, TiO_2-methyl silicone	20	23	25	25	27	29	-	30
O, TiO_2-methyl silicone	-	-	-	0	1	1	1	1
P, TiO_2-methyl silicone	-	-	-	0	0	0	0	0
B, ZnO-methyl silicone (S-13)	10	13	14	14	16	18	-	20
M, ZnO-methyl silicone (S-13G)	-	-	-	4	4	4	4	4
D_3, Al_2O_3-K_2SiO_3	(0)	(1)	(2)	(1)	(1)	(1)	-	(1)
Q, mixed ZnO and TiO_2, mixed silicone-silicate	-	-	-	0	0	0	0	0
Pyromark, TiO_2 - methyl phenyl silicone	0	0	0	0	1	3	-	1
LESS CONTROL CHANGE:								
L_1	8	11	13	-	-	-	-	17
L_2	12	15	17	-	-	-	-	22
B	8	11	13	14	16	17	-	17

Table 31. Reflectance Changes at 2500 Millimicrons

Sample Type	Decrease (Increase) in Reflectance at 2500 m for Eight UV Exposures $\Delta R = R_i - R_f$ (Percent)							
	18 ESH	53 ESH	120 ESH	135 ESH	250 ESH	490 ESH	770 ESH	1130 ESH
I, leafing aluminum-silicone	-	-	-	(2)	1	2	-	1
J, vapor-deposited aluminum	-	-	-	(3)	3	3	-	3
K, polished aluminum	-	-	-	(2)	2	2	-	2
H, SiO_2 on polished aluminum	-	-	-	(4)	1	3	0	2
Alzak #26, 0.10-mil	1	0	(3)	-	-	-	-	-
Alzak #21, 0.29-mil	-	-	-	(1)	1	1	-	1
N, Kapton H-film	-	-	-	(2)	3	3	0	1
AS MEASURED:								
L_1, TiO_2-methyl silicone	22	26	28	27	29	32	-	32
L_2, TiO_2-methyl silicone	23	27	30	31	32	35	-	34
O, TiO_2-methyl silicone	-	-	-	1	1	1	1	1
P, TiO_2-methyl silicone	-	-	-	0	0	0	0	1
B, ZnO-methyl silicone (S-13)	13	17	19	19	23	24	-	24
M, ZnO-methyl silicone (S-13G)	-	-	-	5	6	5	5	4
D_3, Al_2O_3-K_2SiO_3	(1)	(2)	(2)	(1)	(1)	(1)	-	(2)
F_3, ZnO/Al_2O_3-K_2SiO_3	-	-	-	1	1	1	-	1
Q, mixed ZnO and TiO_2, mixed silicone-silicate	-	-	-	0	0	0	(1)	0
Pyromark, TiO_2 - methyl phenyl silicone	0	0	(1)	0	0	1	-	1
LESS CONTROL CHANGE:								
L_1	10	13	15	21	18	22	-	20
L_2	14	18	21	27	27	28	-	25
B	12	15	17	19	22	22	-	22

entries in this case again is equal to a reflectance change in the type B control in the infrared, which occurred as exposure of the test sample progressed. The primer for type B evidently received only one hour of air drying.

The CRETC was backfilled with dry air at the conclusion of the ultraviolet exposures. Several types of coatings were measured during the backfilling, and over a period of six days following it. A complete set of post-irradiation, in-air reflectance measurements was then made on all types of samples some seven days after backfilling, a sufficient time to expect in-air recovery to have stabilized.

Backfilling the CRETC with dry air was accomplished in stages, to determine the effects of a partial atmosphere upon sample recovery. The backfill schedule and levels of pressure used are listed in Tables 32 and 33.

Table 32. Schedule of Chamber Backfill Following Ultraviolet Tests

Pressure Level Reached	Time After Start of Chamber Backfill
35μ	0 minutes
42μ	13
67μ	26
175μ	42
350μ	52
430μ	84
750μ	97

The chamber pressure was maintained at 750μ for 18 hours, whereupon the backfill schedule given in Table 33 was begun.

At this point (54.1 hours since the start of backfill) a second cycling of pump-down and backfill with room air was done, with the chamber being held at 10^{-4} torr between about 57 and 78 hours after the first backfill. Beyond the 78-hour point, the chamber was at one atmosphere.

Table 33. Schedule of Chamber Backfill Following Ultraviolet Tests

Pressure Level Held	Time After Start of Chamber Backfill
10 mm Hg	from 19.7 to 22.9 hours
138 mm Hg	from 23.0 to 24.0 hours
225 mm Hg	from 24.0 to 24.2 hours
427 mm Hg	from 24.3 to 24.6 hours
595 mm Hg	from 24.6 to 24.8 hours
760 mm Hg	from 24.8 to 54.1 hours

This sequence of events was prompted by data being obtained hour by hour from measurements at the various partial atmospheric pressures. Sample types B, D_3, M, Pyromark, and Alzak were monitored to determine reflectance changes during the first six days following backfill with dry air. In general, recovery toward reflectance values obtained before the ultraviolet exposures began was found to be much slower than recovery following exposures to 50-keV electrons. In addition, reflectance changes were found to be small during the period of time when the chamber was at partial atmospheric pressures. An exception to the slow recovery was the nearly complete recovery of type B (9 mils of S-13) in the infrared region before the first measurement was taken.

In contrast to B, type M (which is 10-12 mils of S-13G, and which had undergone only small changes in the infrared due to exposure) exhibited little recovery, even after seven days. In the visible region, M showed no recovery and B underwent only slow, partial recovery. Reflectance change data for B during recovery is shown in Figure 38 as a function of time and in Figure 39 as a function of wavelength.

The slight recovery of Pyromark was nearly complete when the first post-irradiation in-air measurements at one atmosphere pressure were taken, as Figure 40 indicates. Figure 41 shows that some recovery took place at virtually all wavelengths measured. The largest reflectance gains following reexposure to air are seen to be in the near infrared.

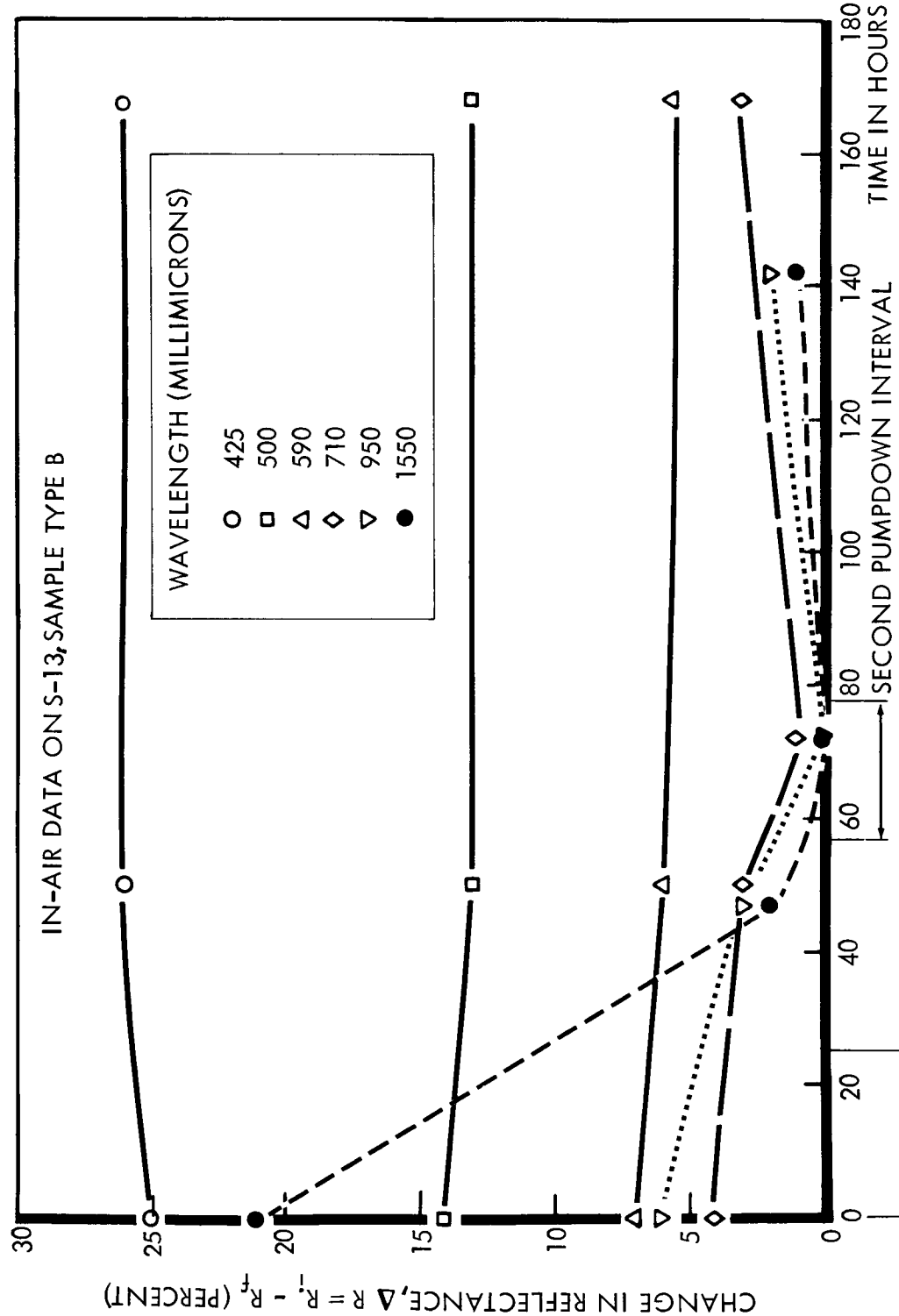

Figure 38. Reflectance Recovery of S-13 With Respect to Time in Air, Following Exposure to Ultraviolet Radiation. Presentation at Selected Wavelengths

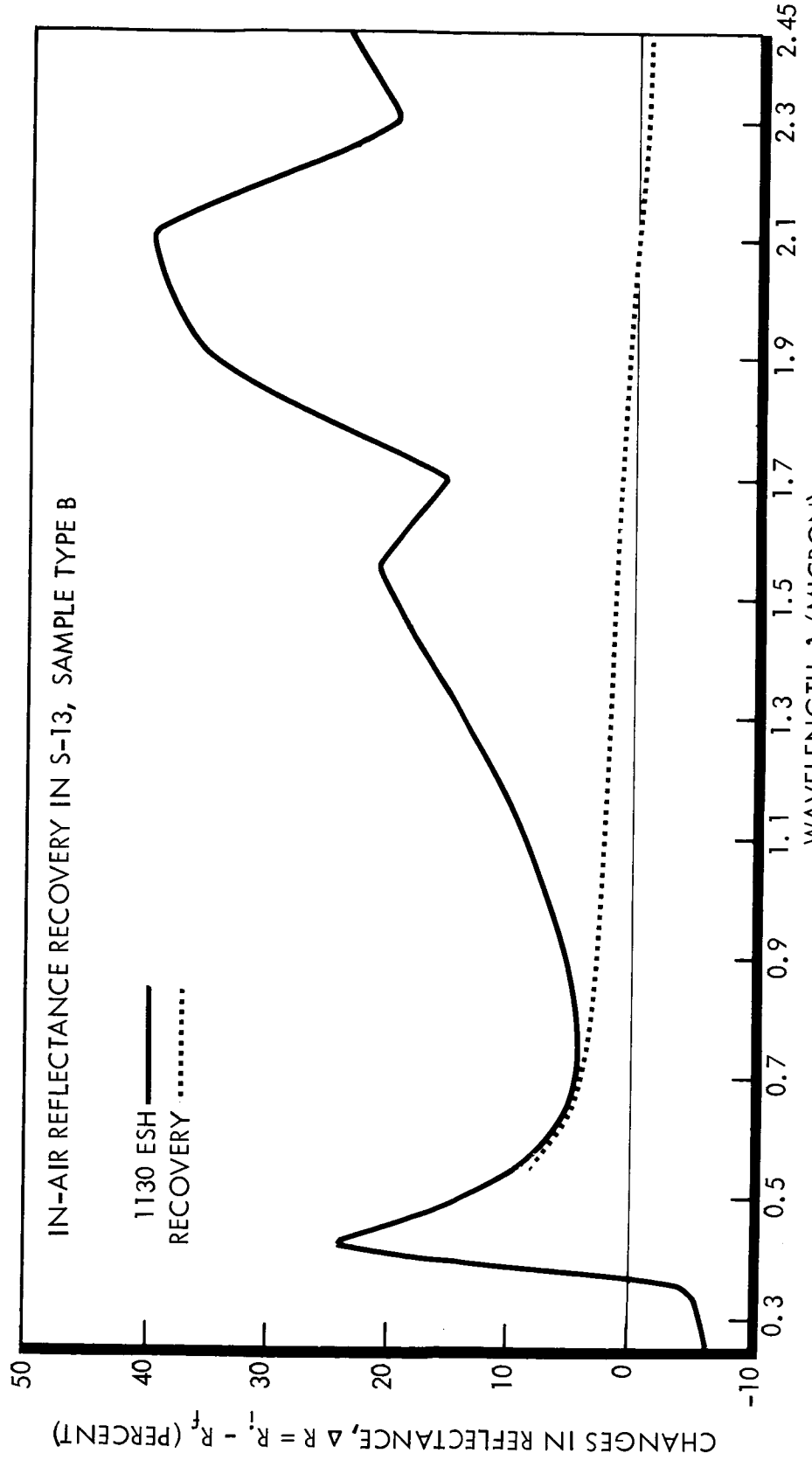

Figure 39. Reflectance Recovery of S-13 in Air, as a Function of Wavelength, Following Exposure to Ultraviolet Radiation

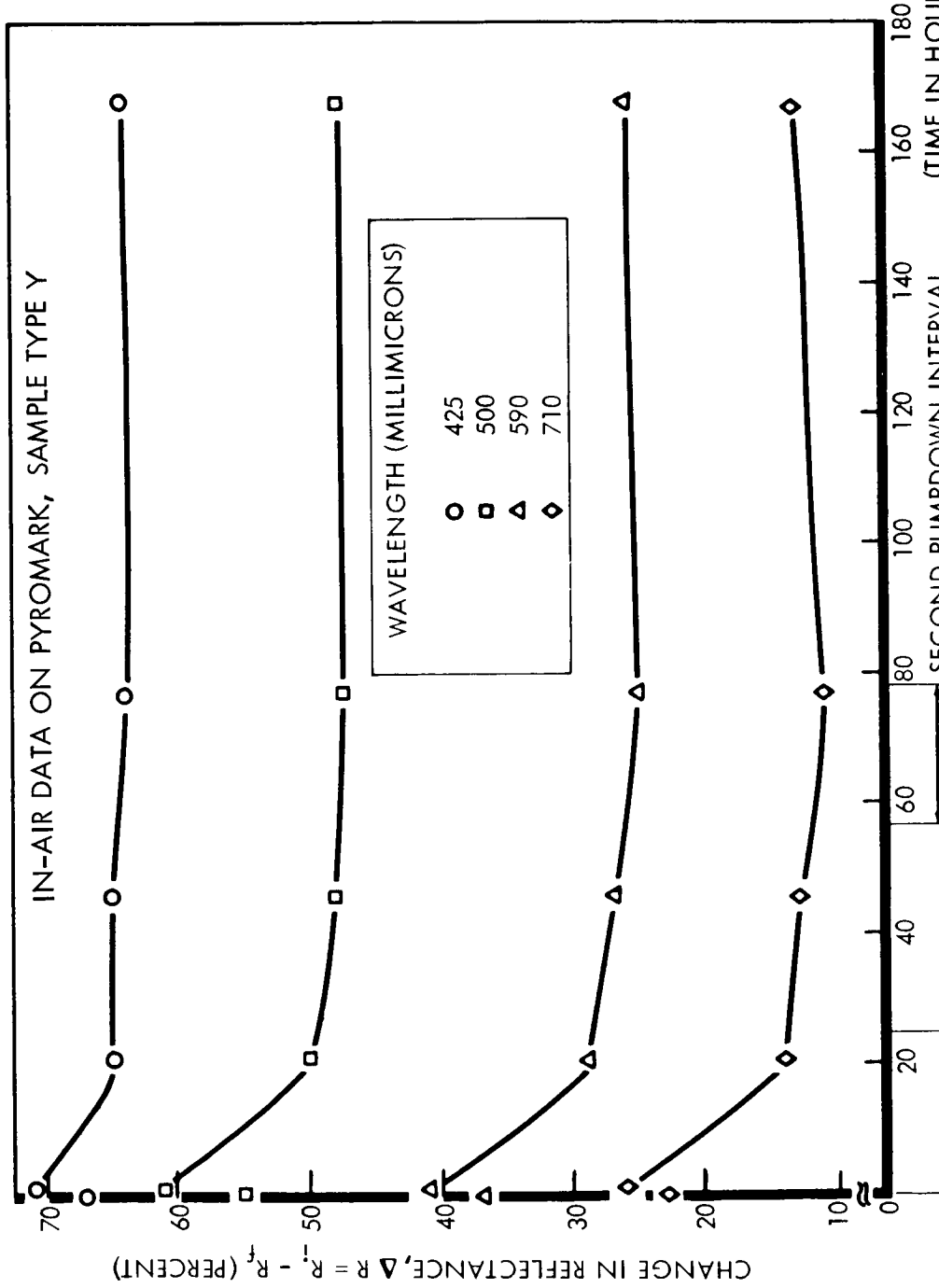

Figure 40. Reflectance Recovery of Pyromark With Respect to Time in Air, Following Exposure to Ultraviolet Radiation. Presentation at Selected Wavelengths

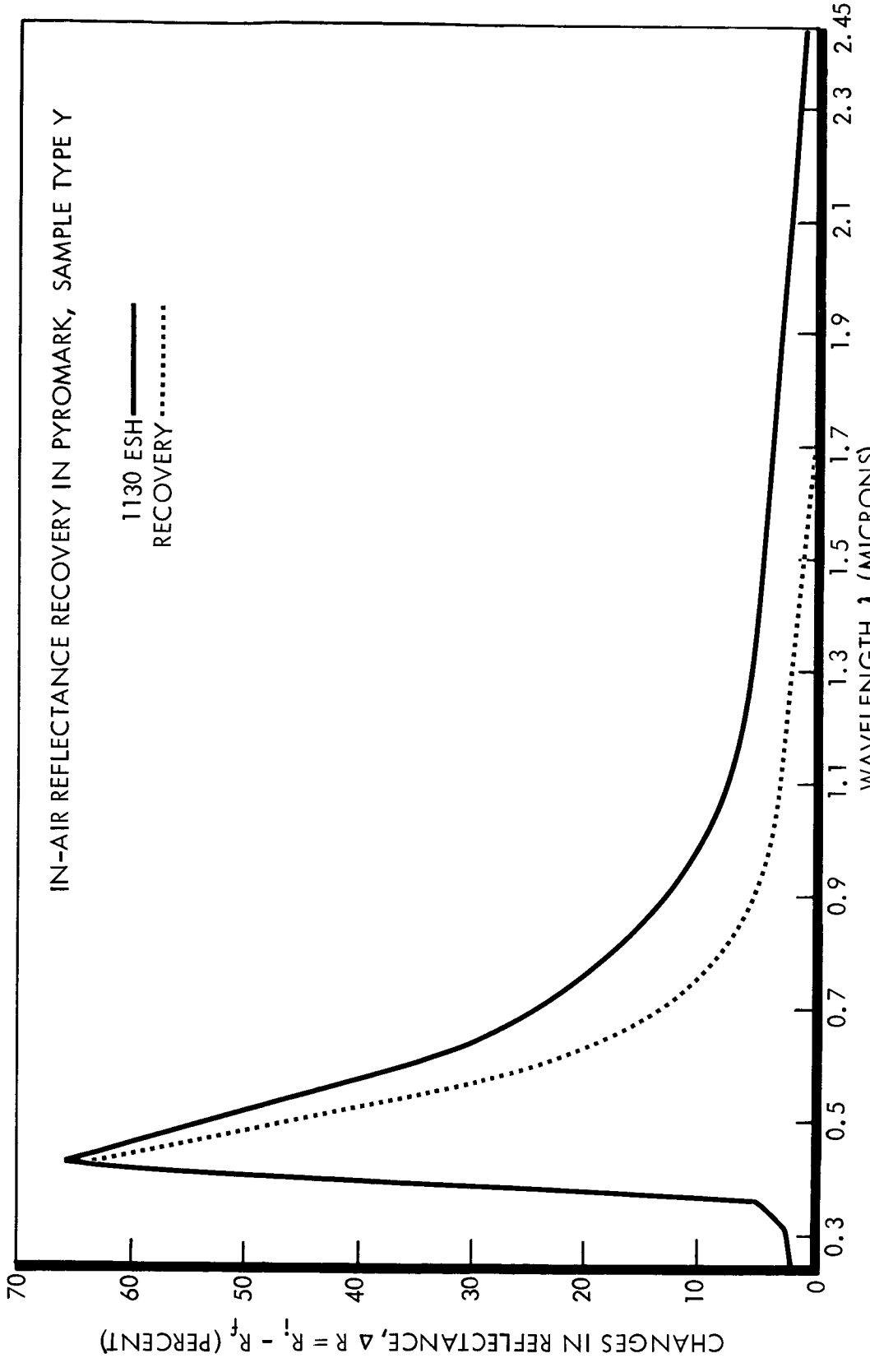

Figure 41. Reflectance Recovery of Pyromark in Air, as a Function of Wavelength, Following Exposure to Ultraviolet Radiation

Alzak (specimen #21, 0.29-mil) exhibited overall recovery which was greatest at the longer wavelengths. Figure 42 indicates the fact that reflectance recovered to values exceeding initial pre-exposure levels at wavelengths greater than about one micron. Figure 43 shows that recovery was rapid for wavelengths less than 1.55 microns and became progressively slower at longer wavelengths.

Type D_3 (aluminum oxide—potassium silicate) exhibited very little recovery, as Figure 44 indicates. Reflectance even decreased at wavelengths longer than about 0.9 micron.

The remaining eleven types of samples were measured for reflectance some seven days after backfill, to determine the extent of in-air recovery.

Type F_3 (zinc oxide/aluminum oxide—potassium silicate) underwent partial recovery in the visible and near infrared wavelength regions, but beyond 1.7 microns had small reflectance losses in air, as shown in Figure 45.

Type Q (a mixture of zinc oxide and titanium dioxide pigments in a mixed silicone-silicate vehicle), which had increased reflectance in going from air to vacuum before irradiation, and then had seen only small reflectance losses due to UV exposure, exhibited no recovery upon re-exposure to air, and even degraded further in the infrared beyond about 1.8 microns, to preirradiation, in-air reflectance values.

Types L_1 and L_2 (titanium dioxide—methyl silicone) recovered part of their large reflectance losses when re-exposed to air, as Figure 46 indicates.

Types O and P (also titanium dioxide—methyl silicone) exhibited only small reflectance changes during recovery. A partial recovery took place in the visible region, and a slight reflectance loss occurred in the 2-micron wavelength region.

Kapton H-film (type N) remained essentially unchanged in air in the wavelength region between 240 and 340 $m\mu$. Partial recovery was seen in the visible region, and in-air reflectance values equal to or greater than preirradiation values in situ were established in the infrared region, as Figure 47 indicates.

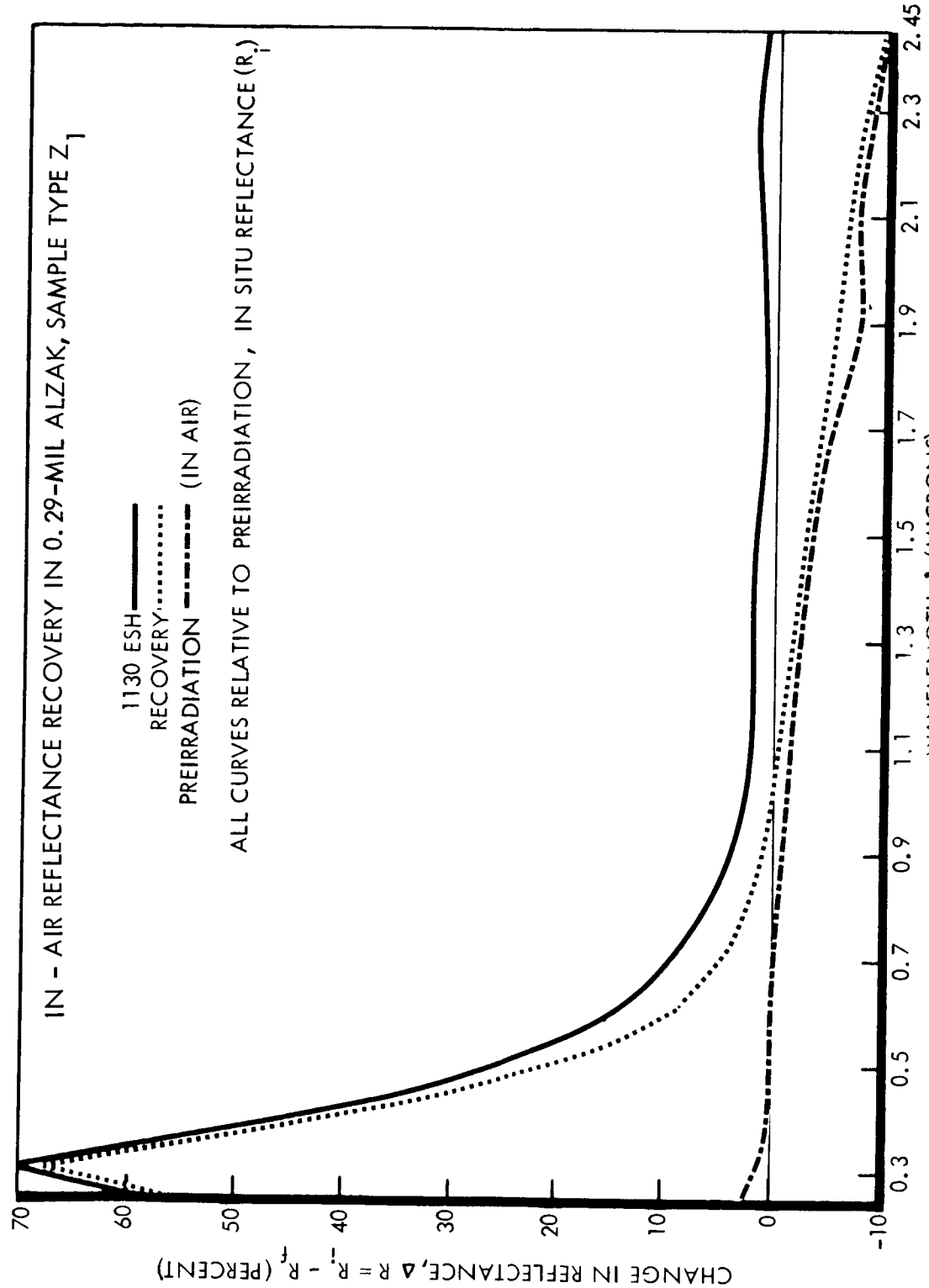

Figure 42. Reflectance Recovery of Alzak in Air, as a Function of Wavelength, Following Exposure to Ultraviolet Radiation

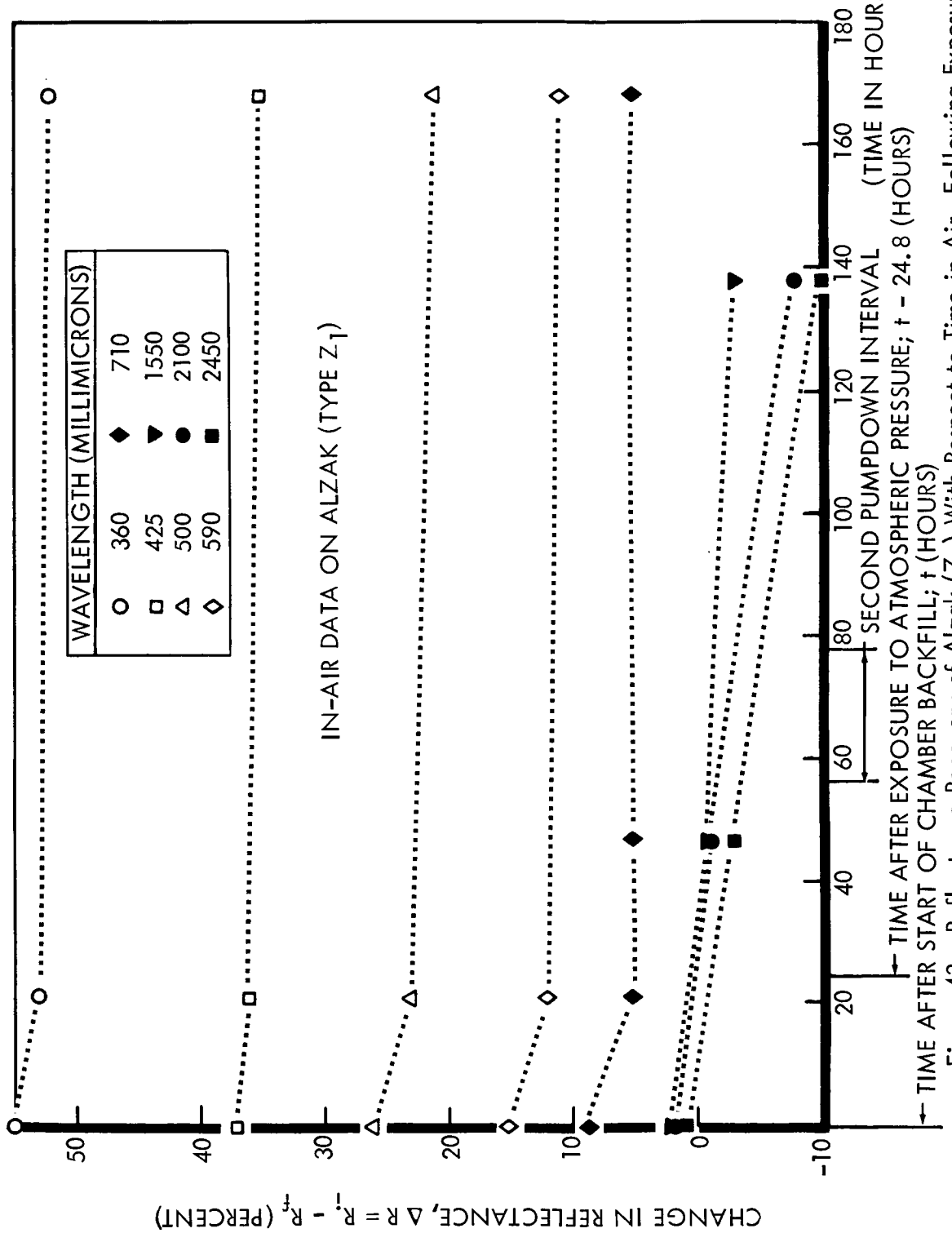

Figure 43. Reflectance Recovery of Alzak (Z_1) With Respect to Time in Air, Following Exposure to Ultraviolet Radiation. Presentation at Selected Wavelengths

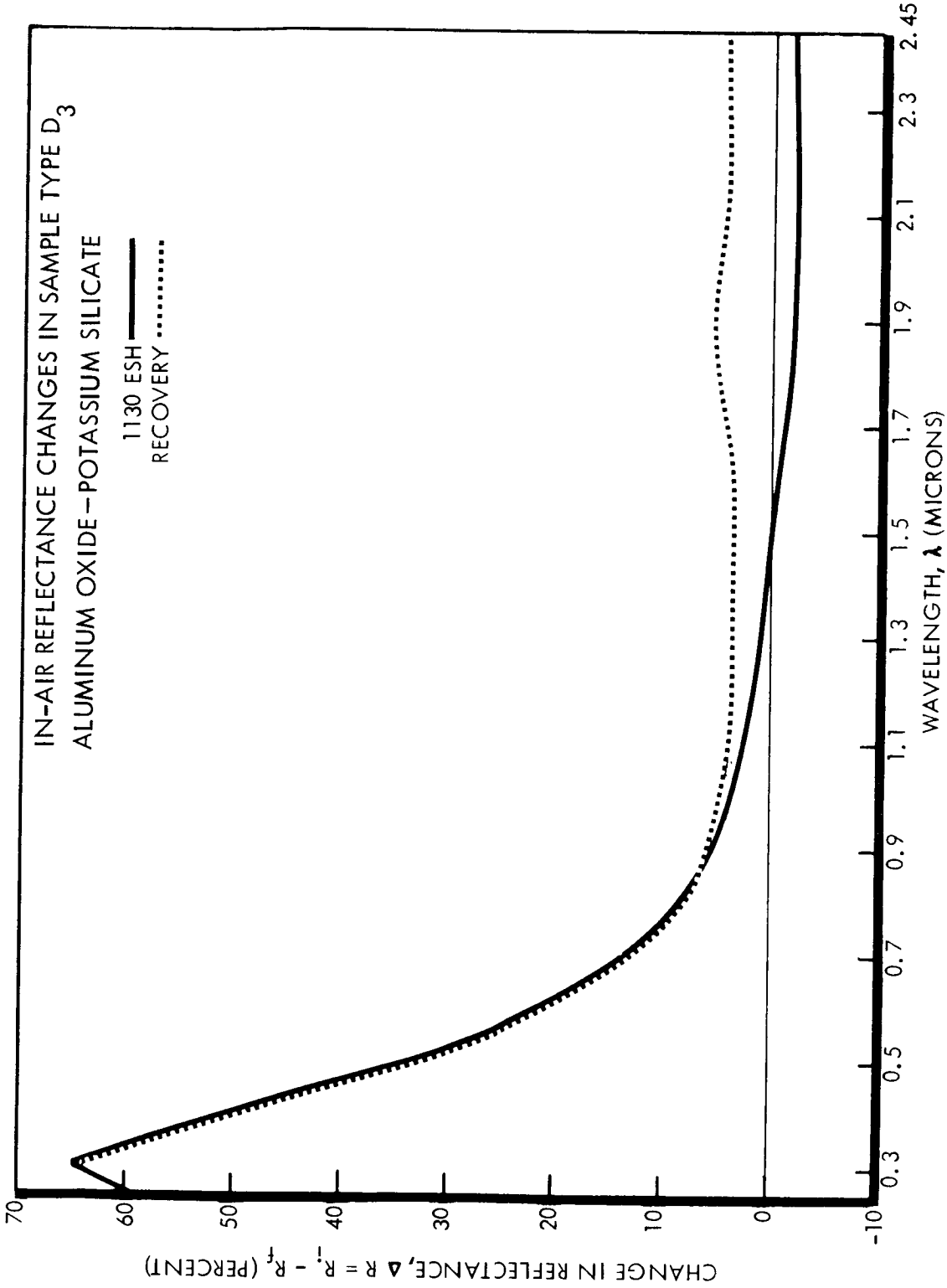

Figure 44. Reflectance Recovery of Type D_3 in Air, as a Function of Wavelength, Following Exposure to Ultraviolet Radiation

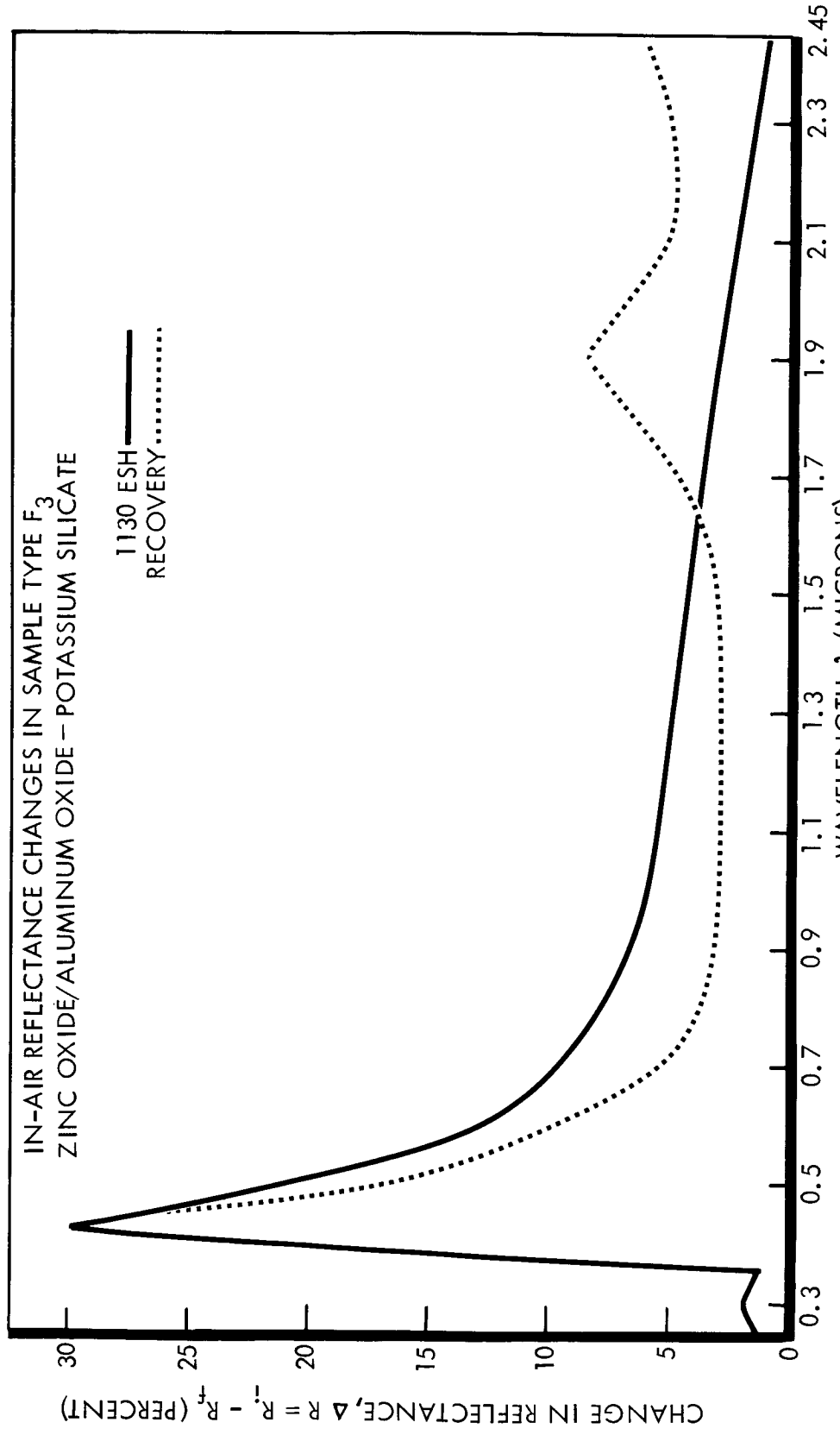

Figure 45. Reflectance Recovery of Type F_3 in Air, as a Function of Wavelength, Following Exposure to Ultraviolet Radiation

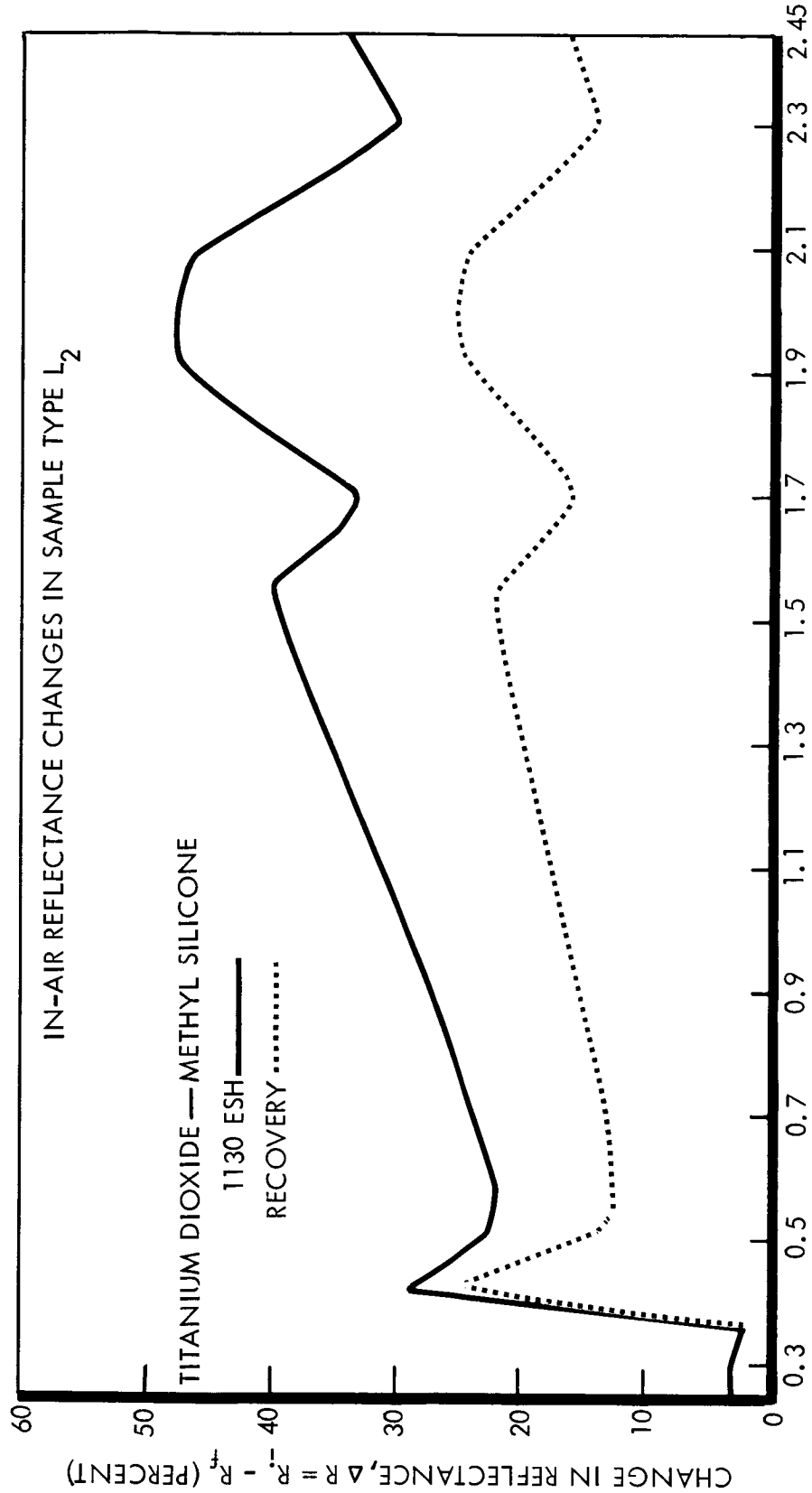

Figure 46. Reflectance Recovery of Type L_2 in Air, as a Function of Wavelength, Following Exposure to Ultraviolet Radiation

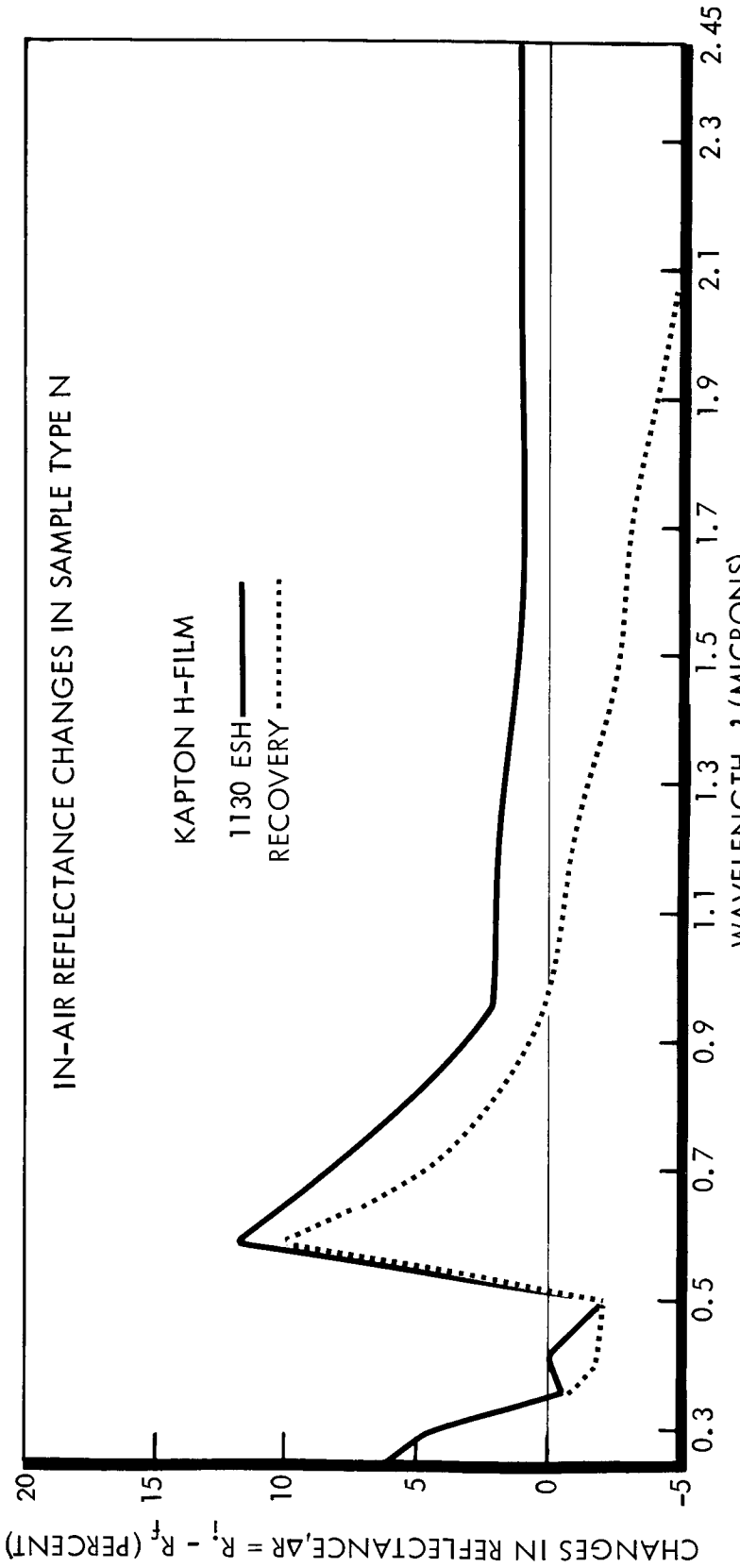

Figure 47. Reflectance Recovery in Kapton H-Film (Type N) in Air, as a Function of Wavelength, Following Exposure to Ultraviolet Radiation

Type H (SiO_2 on polished aluminum) showed some reflectance improvement across most of the wavelength region measured. In-air reflectance values exceeded pre-irradiation values in the infrared wavelength region.

Type I (leafing aluminum in phenylated silicone) exhibited only small changes during recovery. Beyond one micron, though, such changes as occurred resulted in reflectance greater than both post-exposure and pre-exposure in vacuum.

Type J (aluminum vapor-deposited on a lacquered substrate) and type K (buffed aluminum) showed little recovery in the ultraviolet and visible wavelength regions. As with type I, recovery in the infrared increased the reflectance of types J (Figure 48) and K to values greater than those measured in vacuum, either before or after exposure.

2.3.2 Ultraviolet Source Comparison Using Xenon-Arc Lamps

Separate tests to determine the degradation in selected coatings due to continuum ultraviolet from long-arc xenon lamps have been conducted, and the results compared with data from line-emitting, low-pressure, mercury-arc sources (Section 2.3.1). Both types of sources were water-cooled in jackets, for attenuation of infrared output energy. Using the CRETC in situ spectral ultraviolet source monitor, the low-pressure mercury arc has been found not to have excessive line emission relative to the sun at 2537 Å. Indeed, using the in situ spectral monitor it has been possible to ascertain that low-pressure UA-11 mercury-arc sources emit energy in a fairly orderly series of spectral lines (Figure 6).

The in situ spectral monitor has also been used to determine the spectral output of the long-arc xenon sources. Figure 49 indicates the output relative to that of the sun between 0.25 and 0.70 microns. The xenon curve has been corrected for variations in the sensitivity function of the RCA 7200 far UV photomultiplier across the same wavelength region. The use of far UV silica for lenses and magnesium-fluoride-overcoated first-surface aluminum for mirrors would not be expected to attenuate various wavelengths between 0.25 and 0.70 microns selectively. Therefore, the curve has not been corrected for variations (with

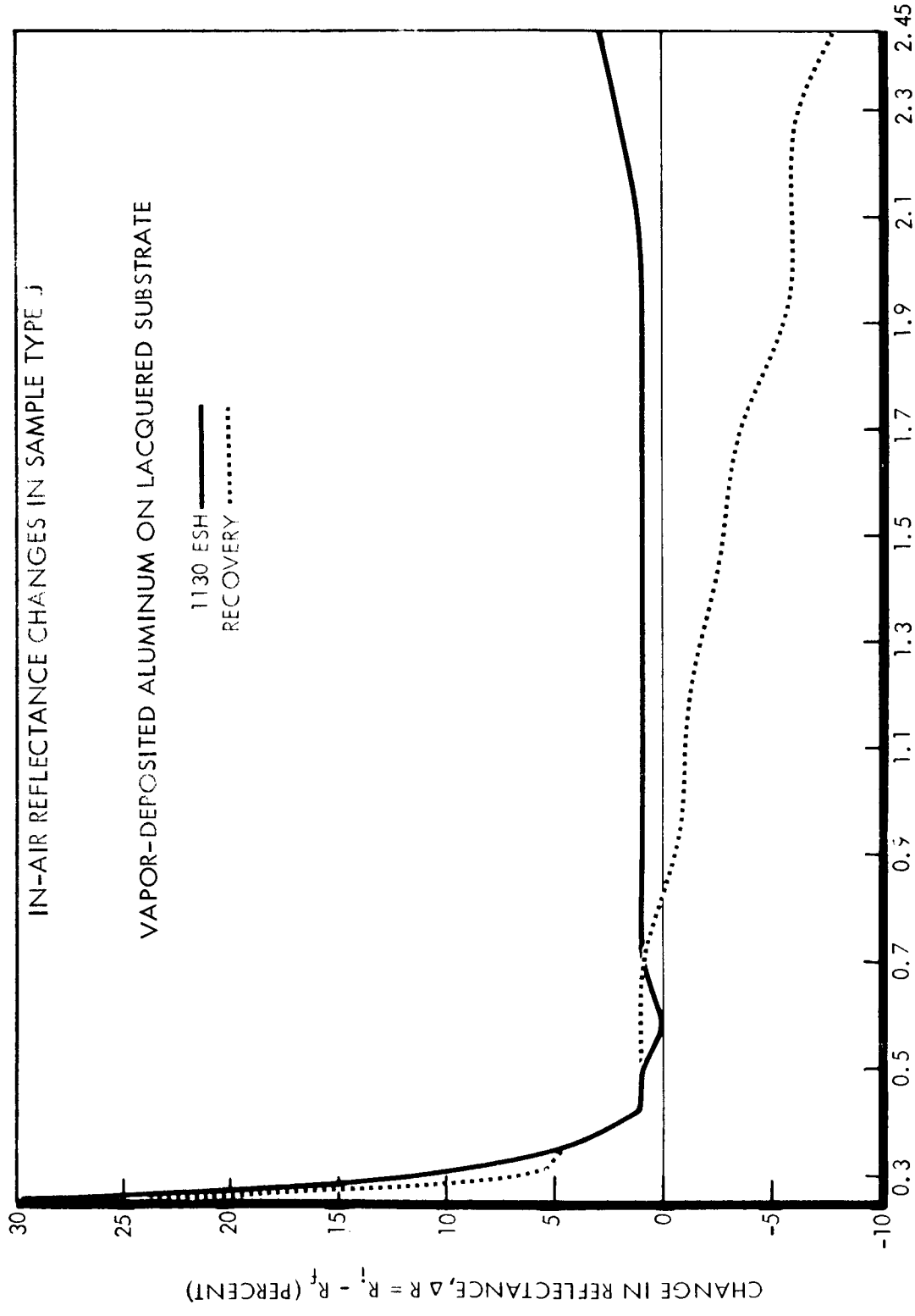

Figure 48. Reflectance Recovery of Type J in Air, as a Function of Wavelength, Following Exposure to Ultraviolet Radiation

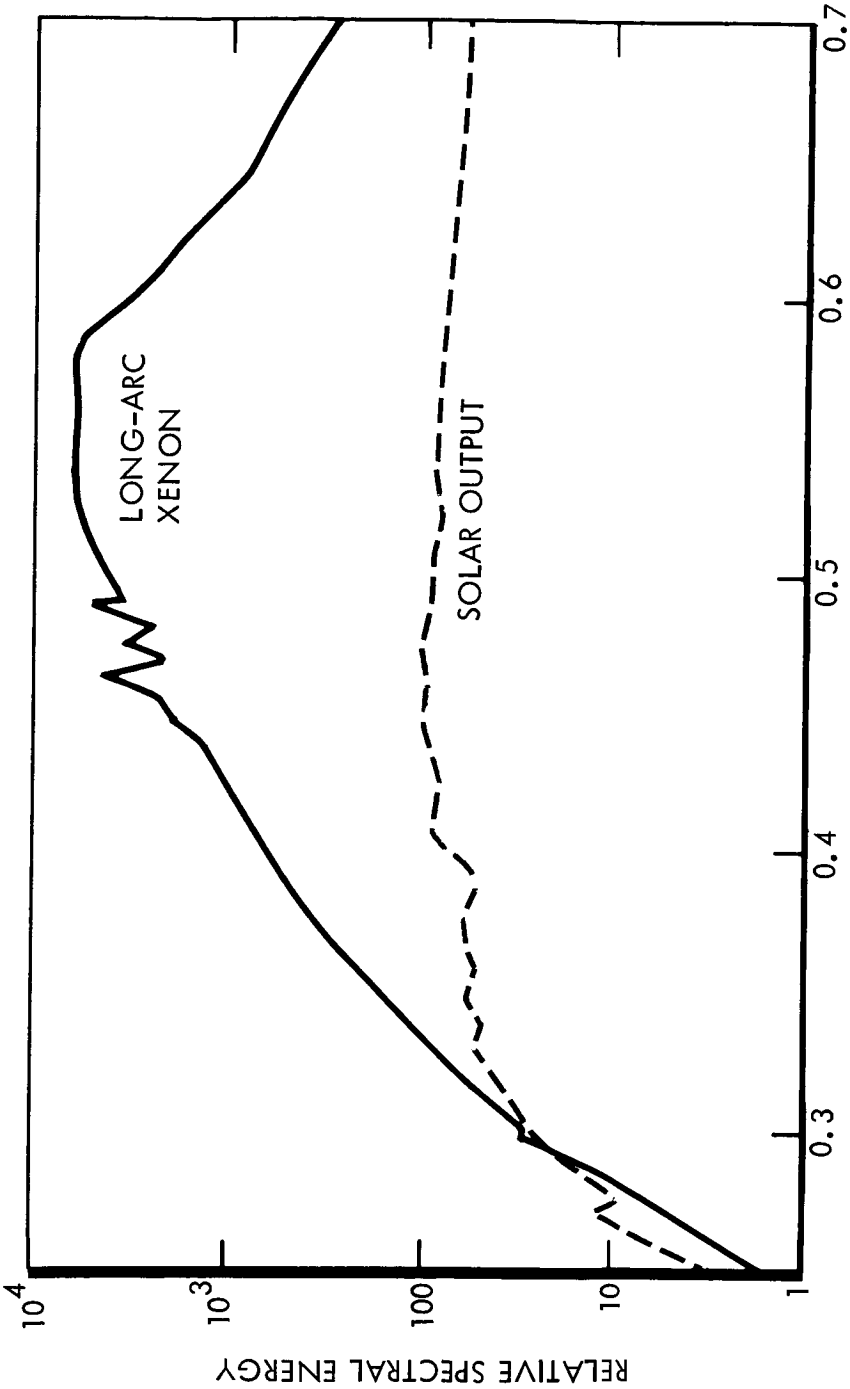

Figure 49. Relative Spectral Output of Long-Arc Xenon UV Source and Space Sun—Ultraviolet and Visible Wavelength Regions

respect to wavelength) of transmittance of lenses, or reflectance of mirrors along the monitor's optical train (Figure 5). The strong output of a Penray lamp at 2537 Å has been used to ascertain that the in situ monitor's optical train transmits energy in that wavelength region. Original energy-mode DK-2A charts also show xenon lamp spectral energy to 1650 Å.

The tests comparing the relative effectiveness of mercury and xenon sources were each conducted with a higher-than-one-sun rate in the ultraviolet wavelength region between 0.2 and 0.4 micron. Different specimens of selected types of coatings (anatase TiO_2 in methyl silicone, ZnO in methyl silicone (S-13), and Al_2O_3 in potassium silicate) received equivalent ultraviolet sun hour exposures from each type of source.

In the case of anatase—silicone (type L_1), the xenon-arc source is relatively more effective in producing degradation of reflectance below 1.9 microns wavelength. As shown in Figure 50, a 50 ESH exposure from the xenon source causes greater decrease in reflectance than 120 ESH from the mercury source, in the visible and near infrared. Beyond 1.9 microns the two sources of ultraviolet-rich electromagnetic radiation are about equally effective, at least for exposures of about 50 ESH.

In type B coating (S-13), as Figure 51 indicates, the xenon source after 85 ESH causes as much or more damage than 135 ESH from UA series mercury-arc lamps, at nearly all wavelengths of interest. Only between 0.4 and 0.5 micron does damage build up to greater values from the 135 ESH mercury exposure.

Reflectance degradation in aluminum oxide—potassium silicate (type D_3) is seen from Figure 52 to proceed at comparable rates from both types of ultraviolet sources. Also, the spectral character of the buildup of damage is observed to be substantially the same for both types of sources.

The data presented in Figures 50, 51, and 52 confirm that UA series mercury-arc lamps do not produce excessively severe degradation, as has been charged to high-pressure mercury-arc sources such as AH-6 and BH-6 lamps. The data also

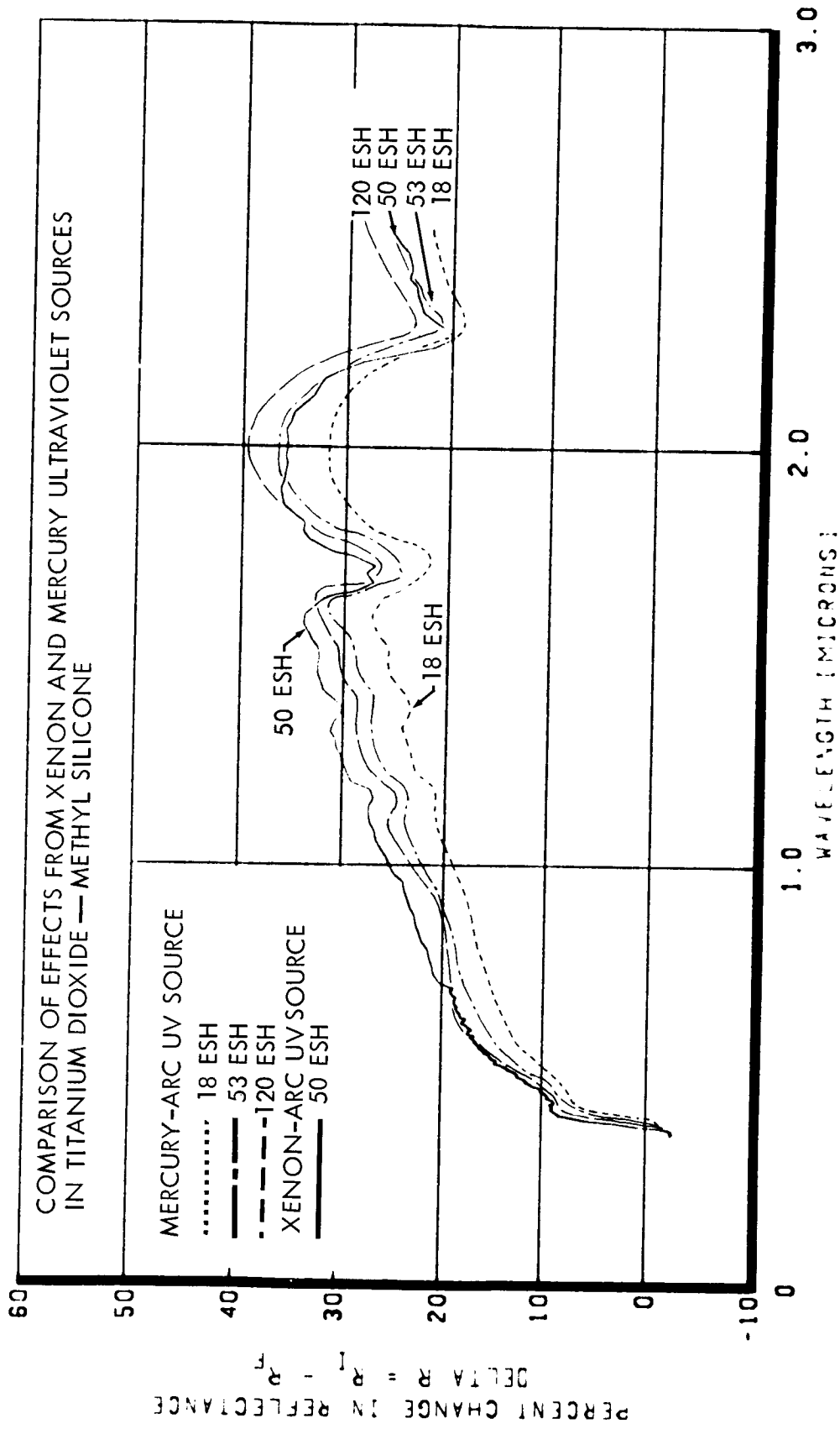

Figure 50. Relative Effectiveness of Mercury-Arc and Xenon-Arc Ultraviolet Sources for Producing Reflectance Degradation in Coating Type L_1

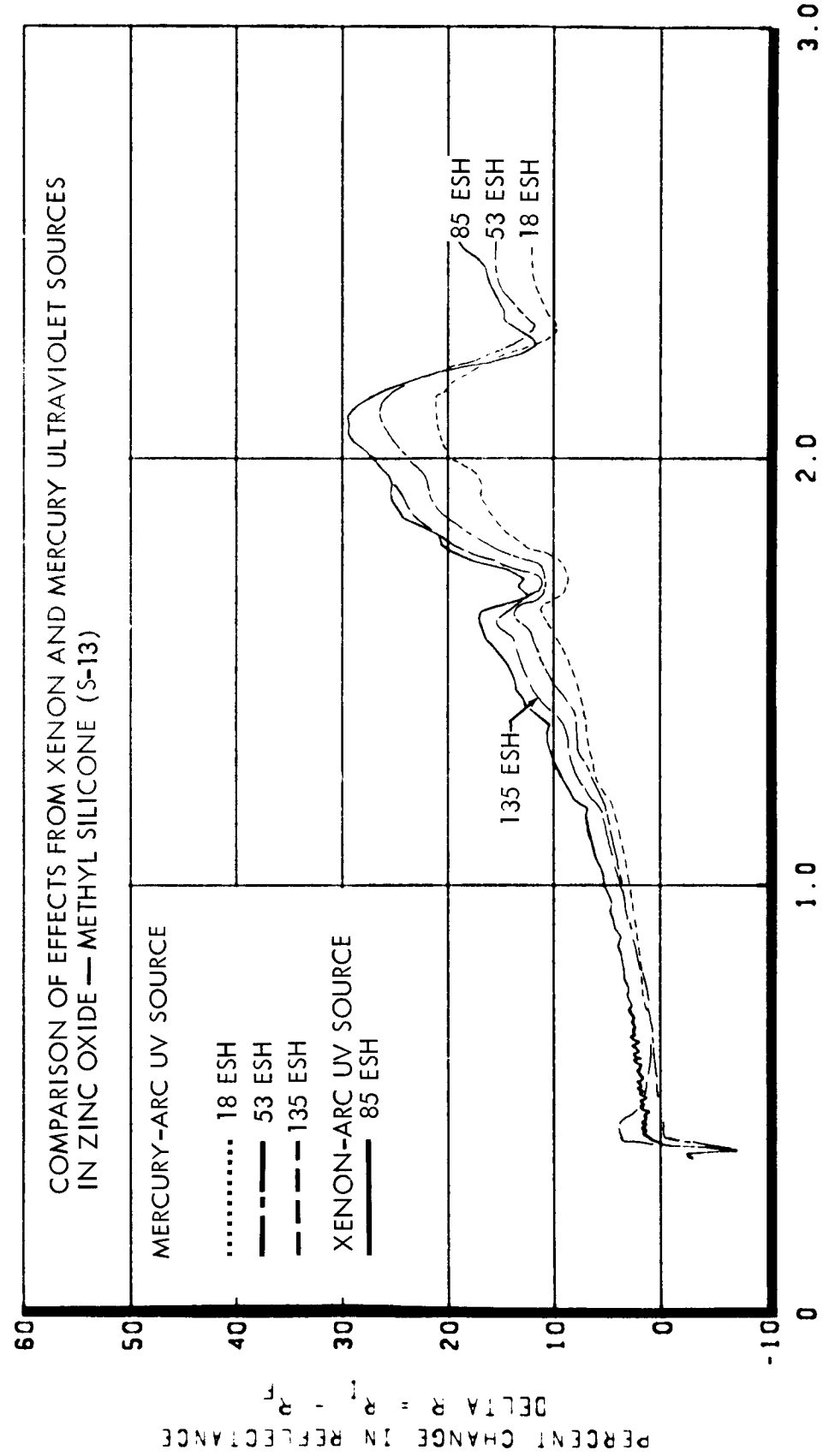

Figure 51. Relative Effectiveness of Mercury-Arc and Xenon-Arc Ultraviolet Sources for Producing Reflectance Degradation in Coating Type B

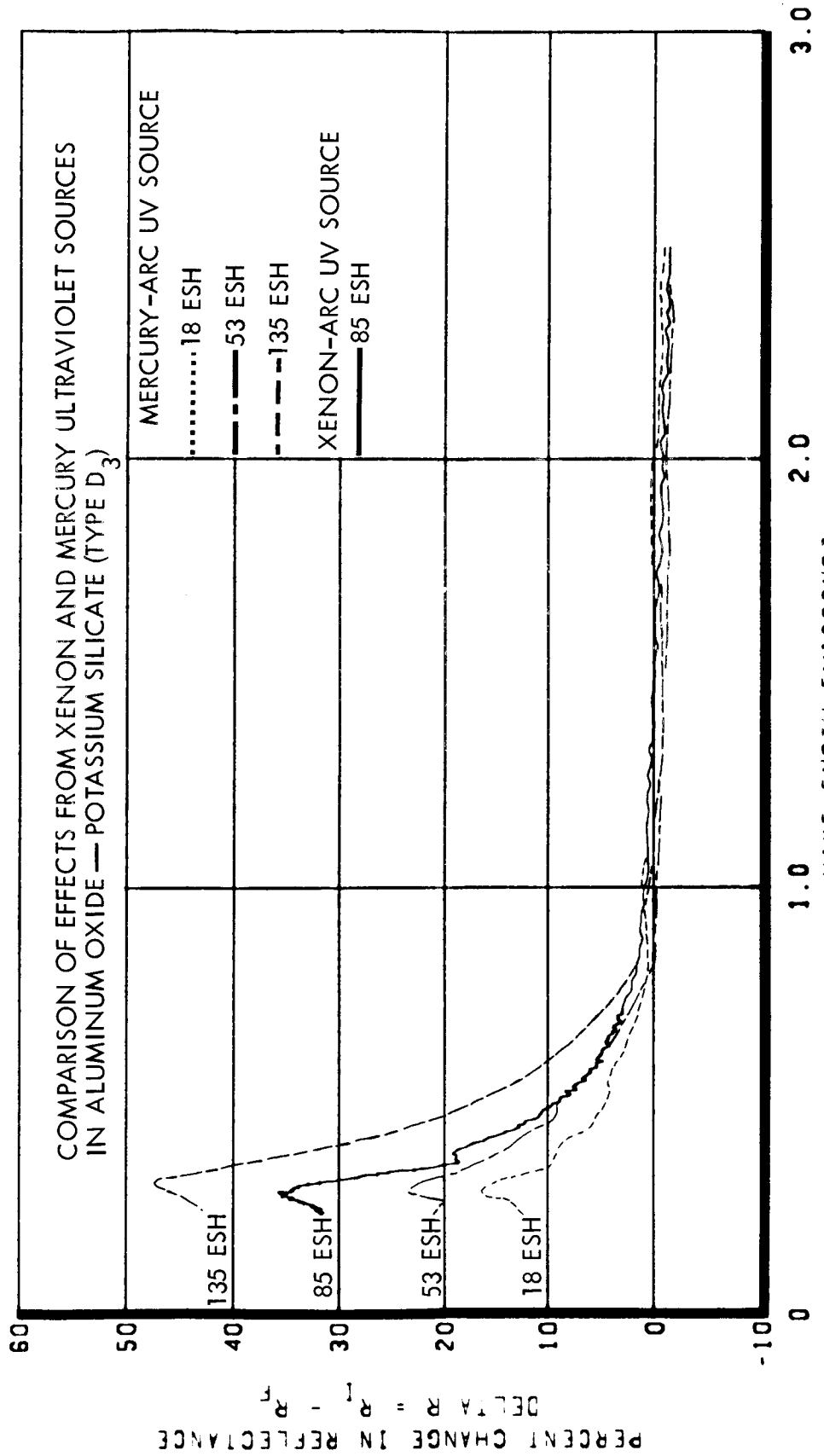

Figure 52. Relative Effectiveness of Mercury-Arc and Xenon-Arc Ultraviolet Sources for Producing Reflectance Degradation in Coating Type D_3

points out the shortcomings resulting from using on an unweighted basis (1) the 0.2- to 0.4-micron wavelength region, and (2) the relative emitted radiant flux in the ultraviolet, visible, and infrared wavelength regions, for determining equivalent space sun exposure rates.

The effects observed from in situ reflectance measurement following exposure using the xenon-arc source have also been determined for relatively low ESH values in the following types of coatings: type R (Figure 53), type M (Figure 54), type E_3 (Figures 55 and 56), type F_3 (Figure 57), type K (Figure 58), and type Y (Figure 59). In type Y (Pyromark), the spectral character and rate of buildup of reflectance damage is seen from a comparison of Figures 59 and 37 to differ markedly for the two cases of exposure to mercury and xenon ultraviolet sources.

2.4 COMBINED ELECTRON-ULTRAVIOLET RADIATION EXPOSURES

Building on results obtained from separate electron and ultraviolet irradiations, selected coating types were exposed to the combined influence of simultaneous and sequenced electron and ultraviolet radiation. Significant differences in sample damage were observed during a series of exposures that saw as the test variable the sequence in which electrons and ultraviolet irradiated the coatings.

Table 34 shows spectral reflectance changes in S-13 (zinc oxide—methyl silicone) after four types of exposure: ultraviolet only, electrons only, ultraviolet followed by electron, and simultaneous ultraviolet and electron exposure. All ultraviolet exposures were 18 ESH and all electron exposures were 5×10^{14} electrons/cm^2. Samples receiving sequential exposure remained in situ between exposures. All reflectance measurements were made in situ. Deviations from the arithmetic sum of reflectance changes due to separate exposures demonstrate the presence of nonadditive synergistic effects during combined exposures. Note that initial ultraviolet exposure preconditions S-13 so that later electron exposure leaves it less degraded in reflectance (due to both exposures) than an electron-only exposure does.

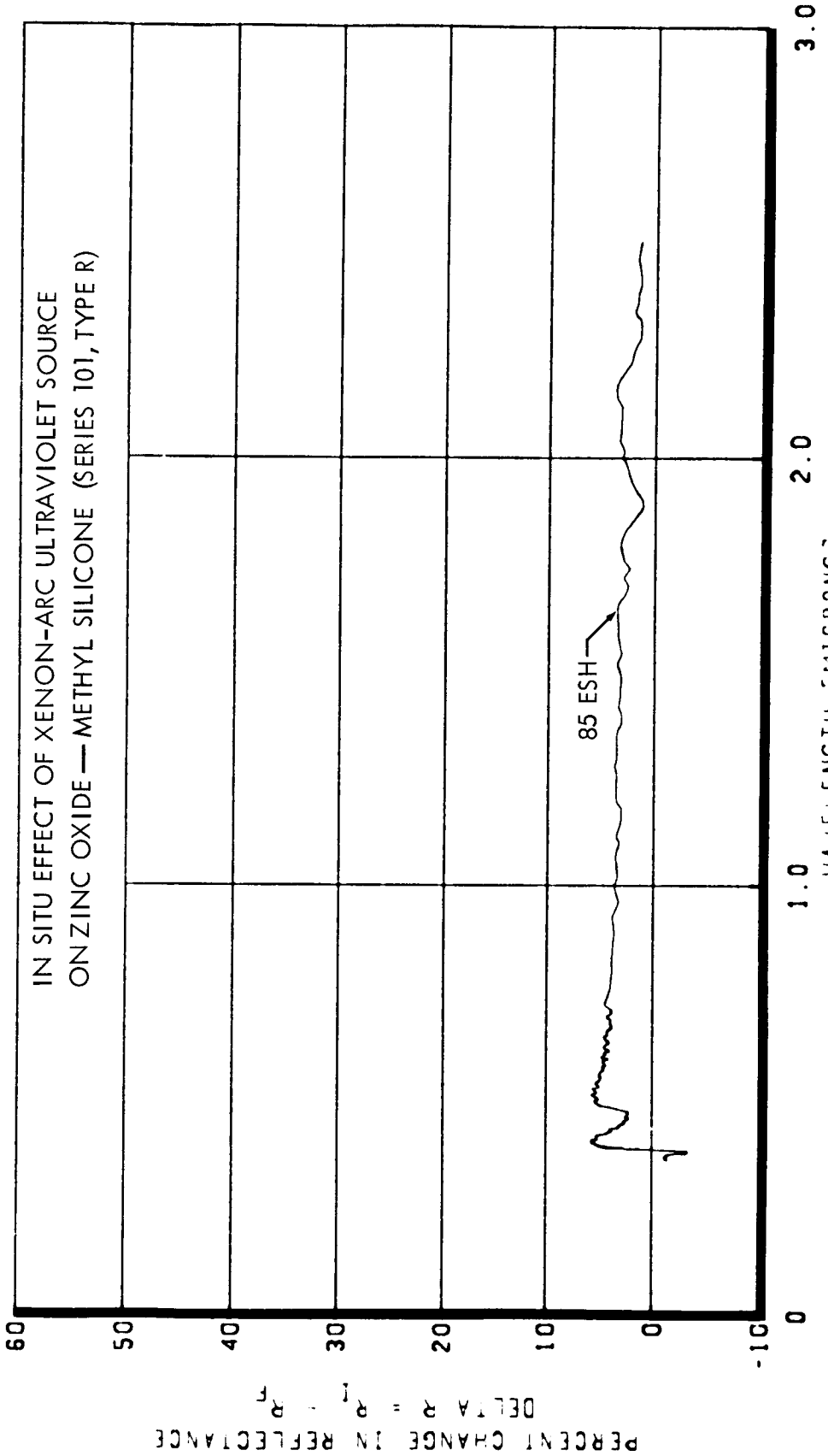

Figure 53. Changes in Spectral Reflectance of Type R, Series 101 Zinc Oxide–Methyl Silicone, Following Exposure to 85 ESH Ultraviolet Radiation From Long-Arc Xenon Source

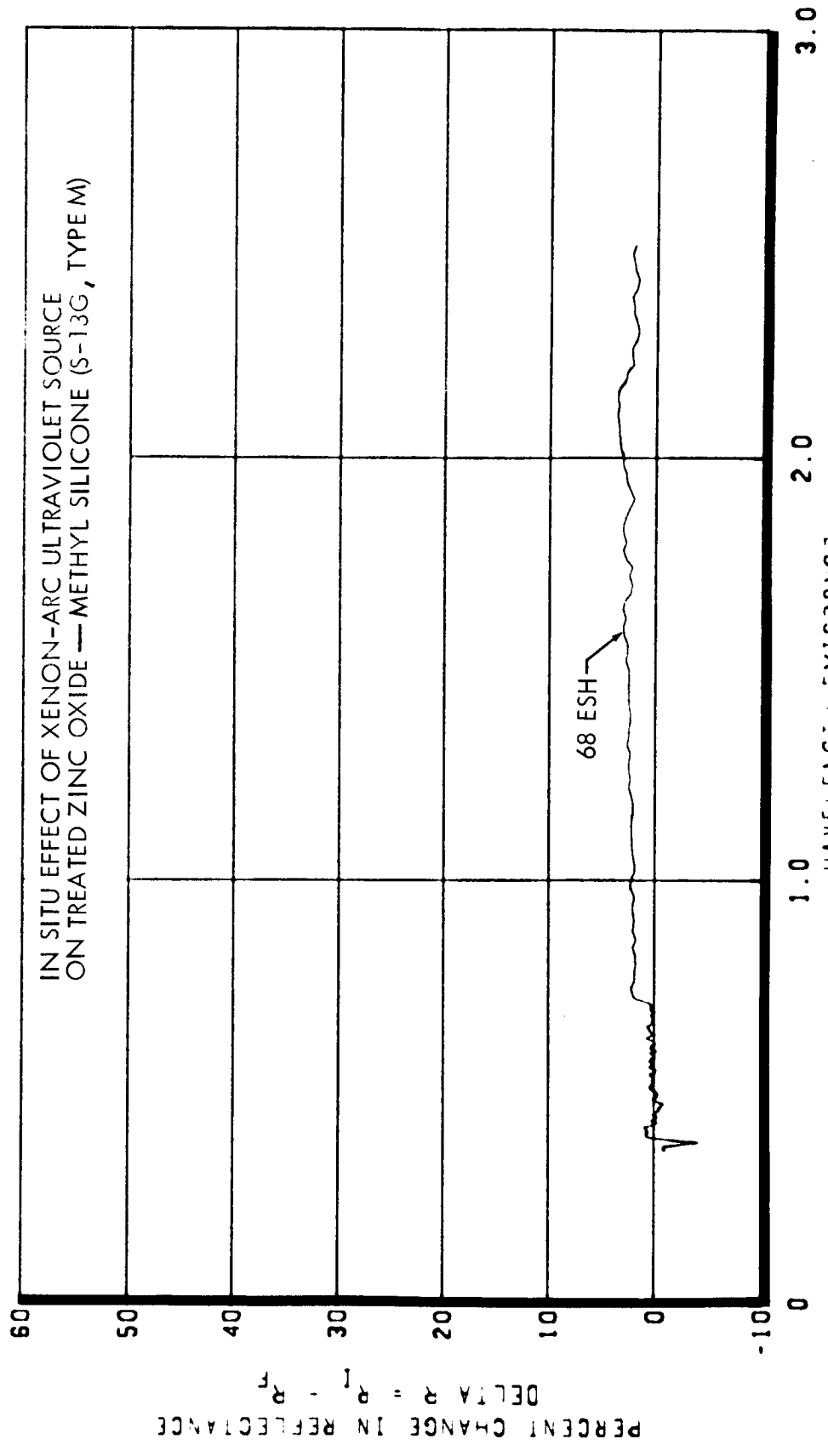

Figure 54. Changes in Spectral Reflectance of Type M, S-13G Treated Zinc Oxide–Methyl Silicone, Following Exposure to 68 ESH Ultraviolet Radiation From Long-Arc Xenon Source

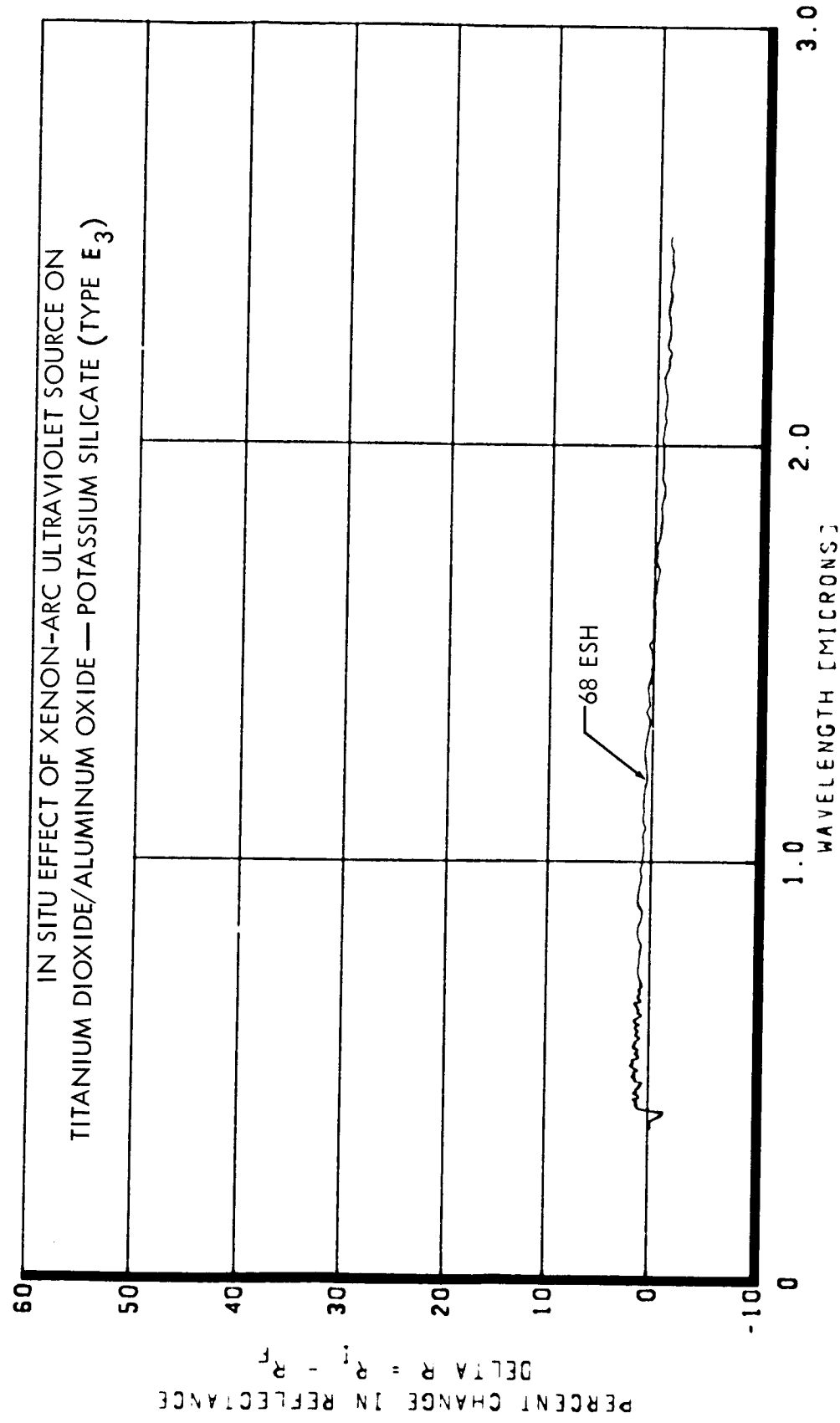

Figure 55. Changes in Spectral Reflectance of Type E_3, Titanium Dioxide/Aluminum Oxide—Potassium Silicate, Following Exposure to 68 ESH Ultraviolet Radiation From Long-Arc Xenon Source

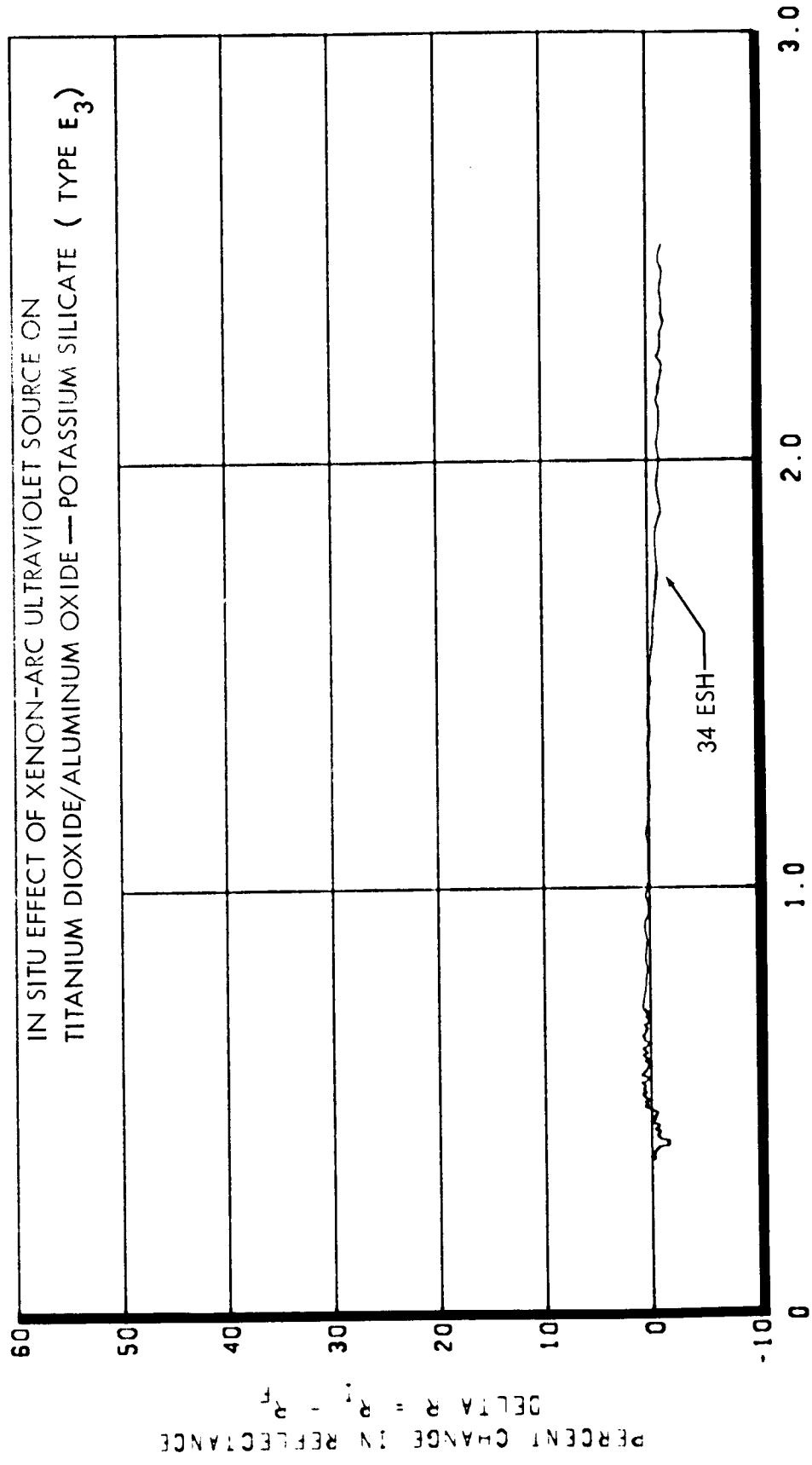

Figure 56. Changes in Spectral Reflectance of Type E_3, Following Exposure to 34 ESH Ultraviolet Radiation.

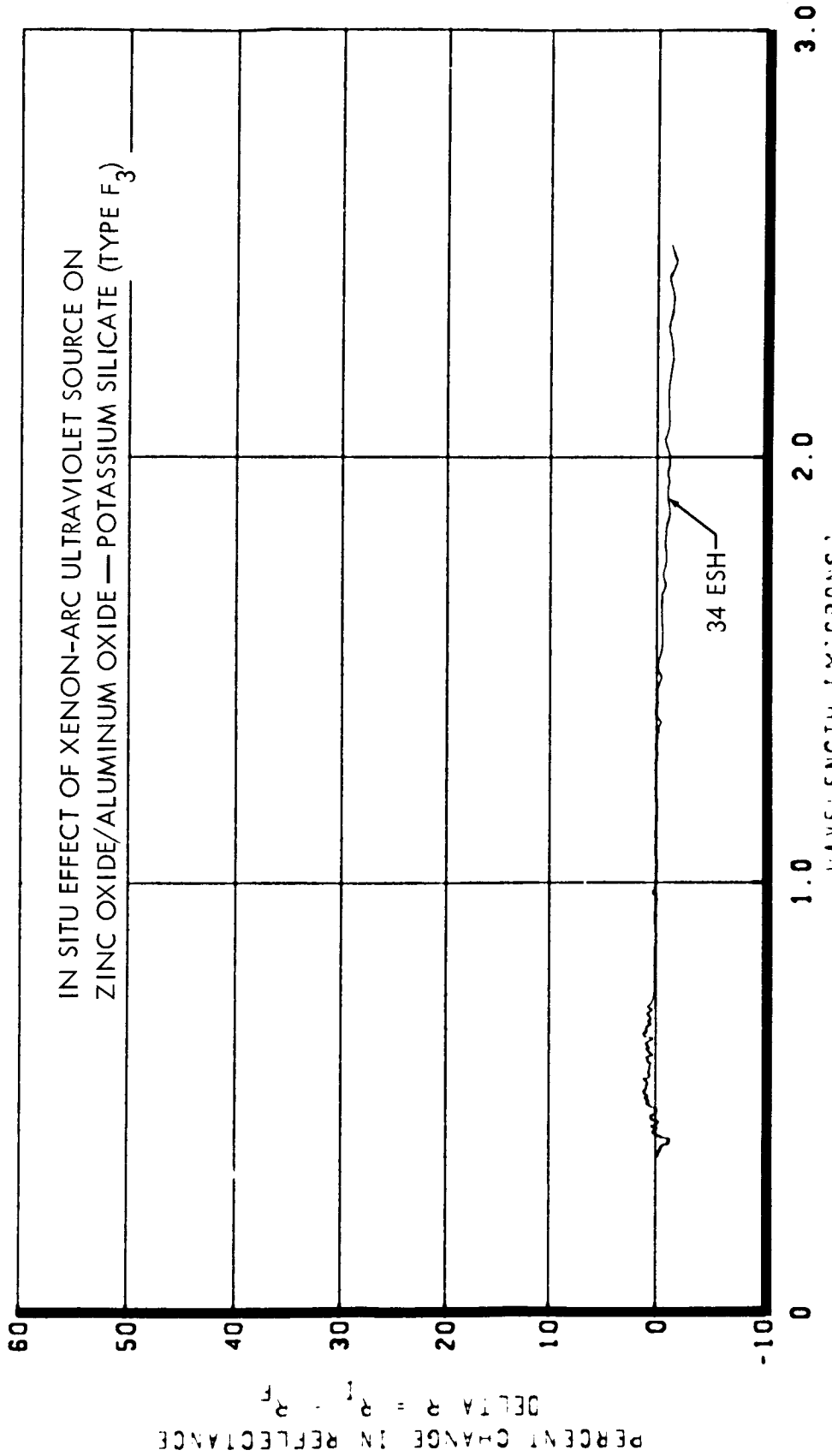

Figure 57. Changes in Spectral Reflectance of Type F_3, Zinc Oxide/Aluminum Oxide – Potassium Silicate, Following Exposure to 34 ESH Ultraviolet Radiation From Long-Arc Xenon Source

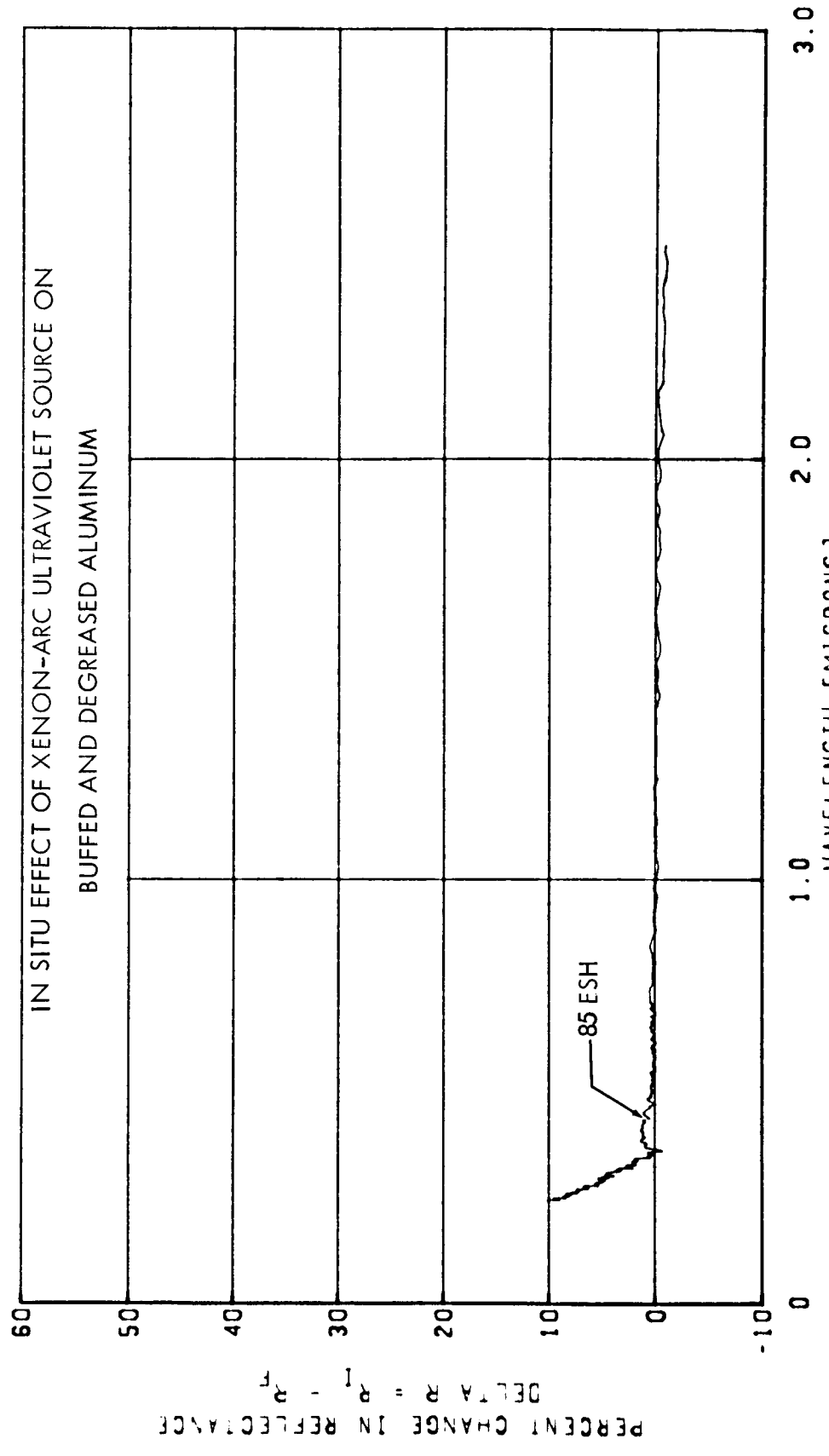

Figure 58. Changes in Spectral Reflectance of Type K, Buffed and Degreased Aluminum, Following Exposure to 85 ESH Ultraviolet Radiation From Long-Arc Xenon Source

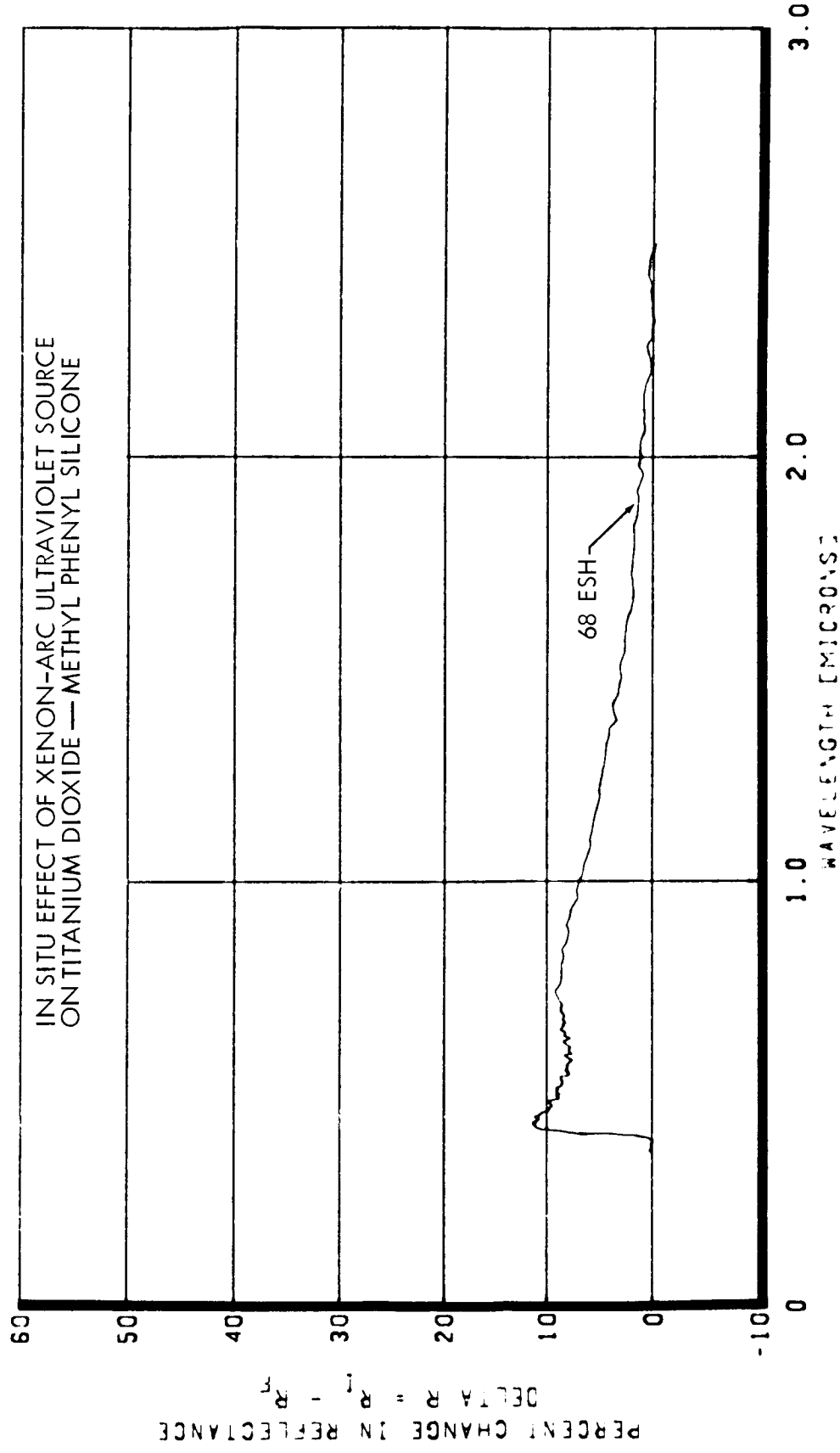

Figure 59. Changes in Spectral Reflectance of Type Y (Pyromark), Titanium Dioxide–Methyl Phenyl Silicone, Following Exposure to 68 ESH Ultraviolet Radiation From Long-Arc Xenon Source

Table 34. Decrease in Reflectance in S-13 (Type B)

Measured After Exposure to:	$\Delta R = R_i - R_f$ (%) at Selected Wavelengths						
	425 mμ	590 mμ	950 mμ	1,200 mμ	1,550 mμ	2,100 mμ	2,500 mμ
UV only	1	1	3	6	10	22	14
Electrons only	0	2	6	11	20	37	26
ARITHMETIC SUM OF ABOVE	1	3	9	17	30	59	40
Consecutive exposure to UV, then to electrons	0	2	4	7	15	30	19
Simultaneous UV-electron exposure	0	2	7	12	24	43	30

Table 35. Decrease in Reflectance in TiO_2—Methyl Phenyl Silicone (Type Y)

Measured After Exposure to:	$\Delta R = R_i - R_f$ (%) at Selected Wavelengths							
	425 mμ	500 mμ	590 mμ	950 mμ	1,200 mμ	1,550 mμ	2,100 mμ	2,500 mμ
UV only	36	17	8	4	3	2	2	2
Electrons only	9	10	12	18	19	17	12	6
ARITHMETIC SUM OF ABOVE	45	27	20	22	22	19	14	8
Consecutive exposure to UV then to electrons	36	19	9	5	4	3	2	1
Simultaneous UV-electron exposure	40	22	15	16	16	14	13	6

Table 35 gives similar results for TiO_2—methyl phenyl silicone (type Y). Reflectance changes from combined exposures are again less than additive, with consecutive exposure (to ultraviolet followed by electrons) causing significantly less damage than simultaneous exposure. Note that over much of the wavelength region measured, simultaneous exposure results in less degradation than electron-only exposure.

The ordering of combined-environment exposures significantly affects measured reflectance changes in other ways as well. The influence of sample exposure to ultraviolet radiation following exposure to electron radiation is seen from data in Figures 60, 61, and 62. Mixed ZnO/TiO_2—silicone/silicate (type Q), and Al_2O_3—potassium silicate (type D), recover part of their electron-induced reflectance losses when exposed later to ultraviolet-rich electromagnetic radiation. Figures 60 and 61 indicate the extent of reflectance recovery, which in type Q occurs across the entire wavelength region measured, and which in type D happens at wavelengths greater than 480 millimicrons. Both figures show reflectance measured in situ before exposure. The other curves result from exposure to 5×10^{14} electrons/cm^2, and exposure to 18 ESH ultraviolet radiation following the electron exposure.

S-13 exposed to this same sequence of exposures (electrons, then ultraviolet) does not recover (Figure 62). However, the 18 ESH of ultraviolet exposure has little additional effect on S-13 reflectance beyond the losses already sustained due to electron exposure.

The extent of degradation also appears to depend on the ratio of exposure rates of electron and ultraviolet radiation. Selected coatings have been exposed to 18 ESH at a 4.4 ultraviolet-sun rate (total exposure time 4.1 hours). Simultaneously, the samples received a fluence of 5×10^{14} electrons/cm^2, programmed so that about 90% occurred during the first hour of ultraviolet exposure, and the remaining 10% during the final 3.1 hours of ultraviolet exposure. Measurements were made after the first hour (see "partial exposure" curves in Figures 63, 64, and 65). Based

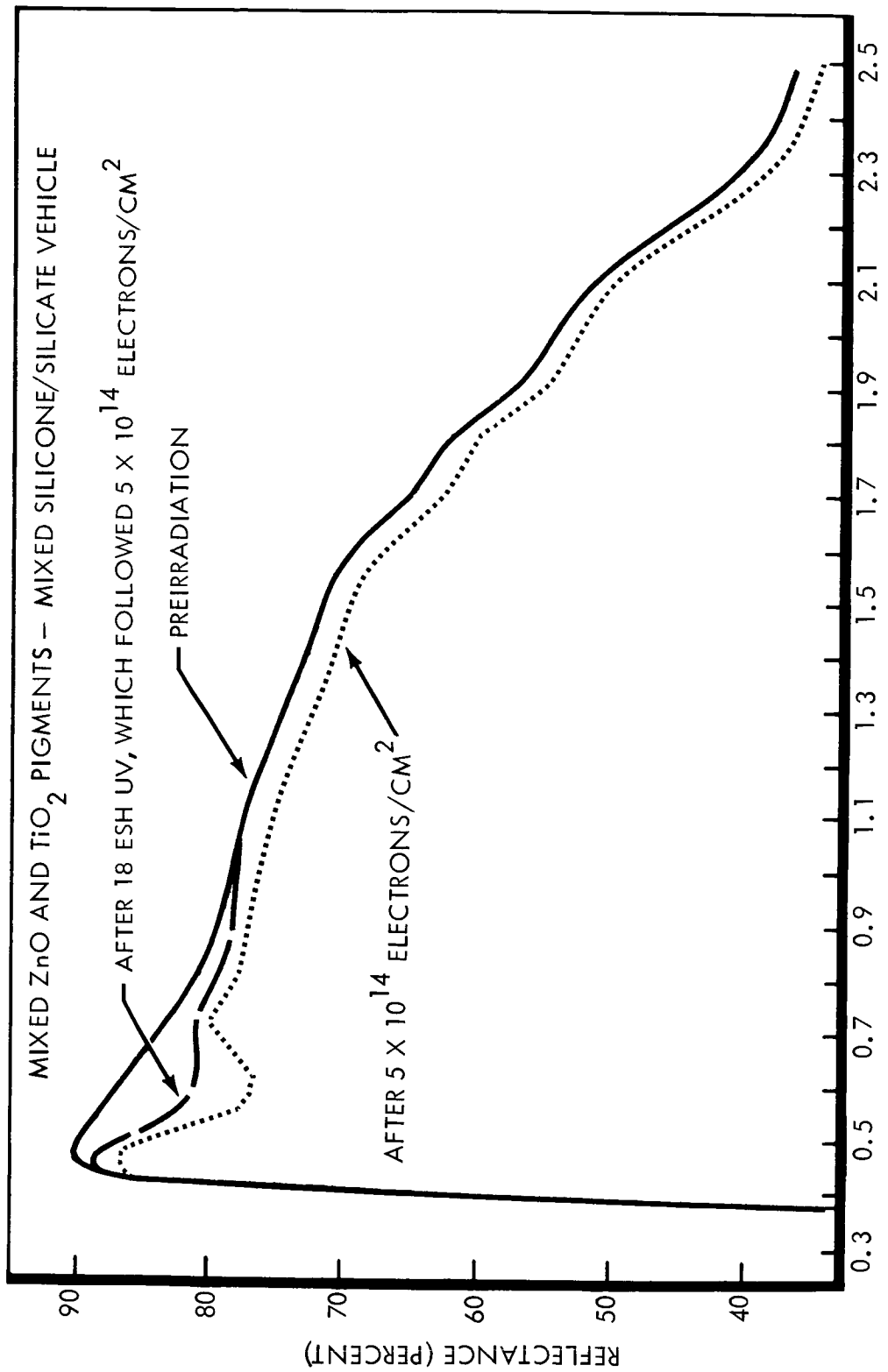

Figure 60. Spectral Reflectance of Type Q Following Consecutive Exposure to 50-keV Electrons, Then to Ultraviolet Radiation

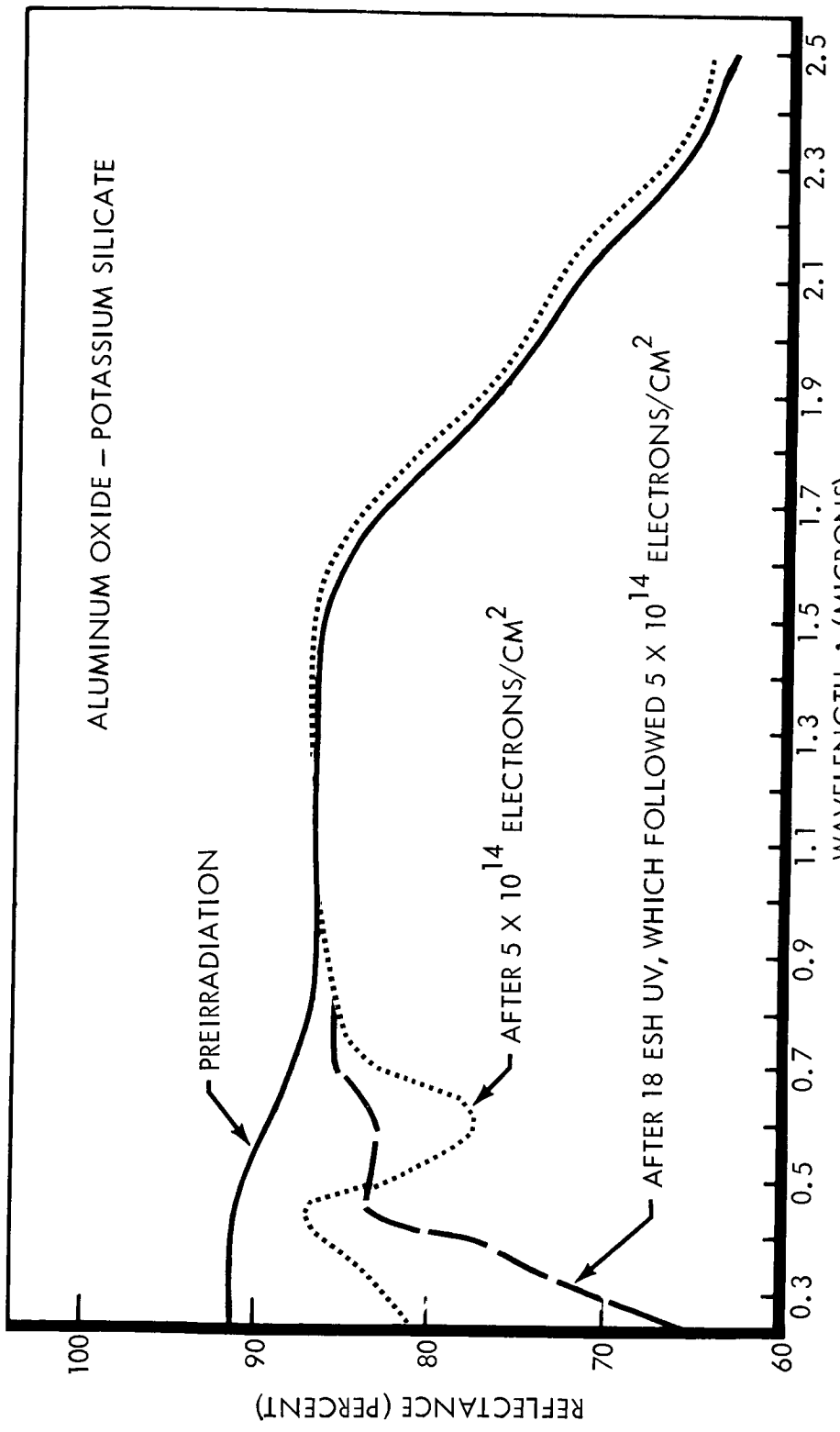

Figure 61. Spectral Reflectance of Type D Following Consecutive Exposure to 50-keV Electrons, Then to Ultraviolet Radiation

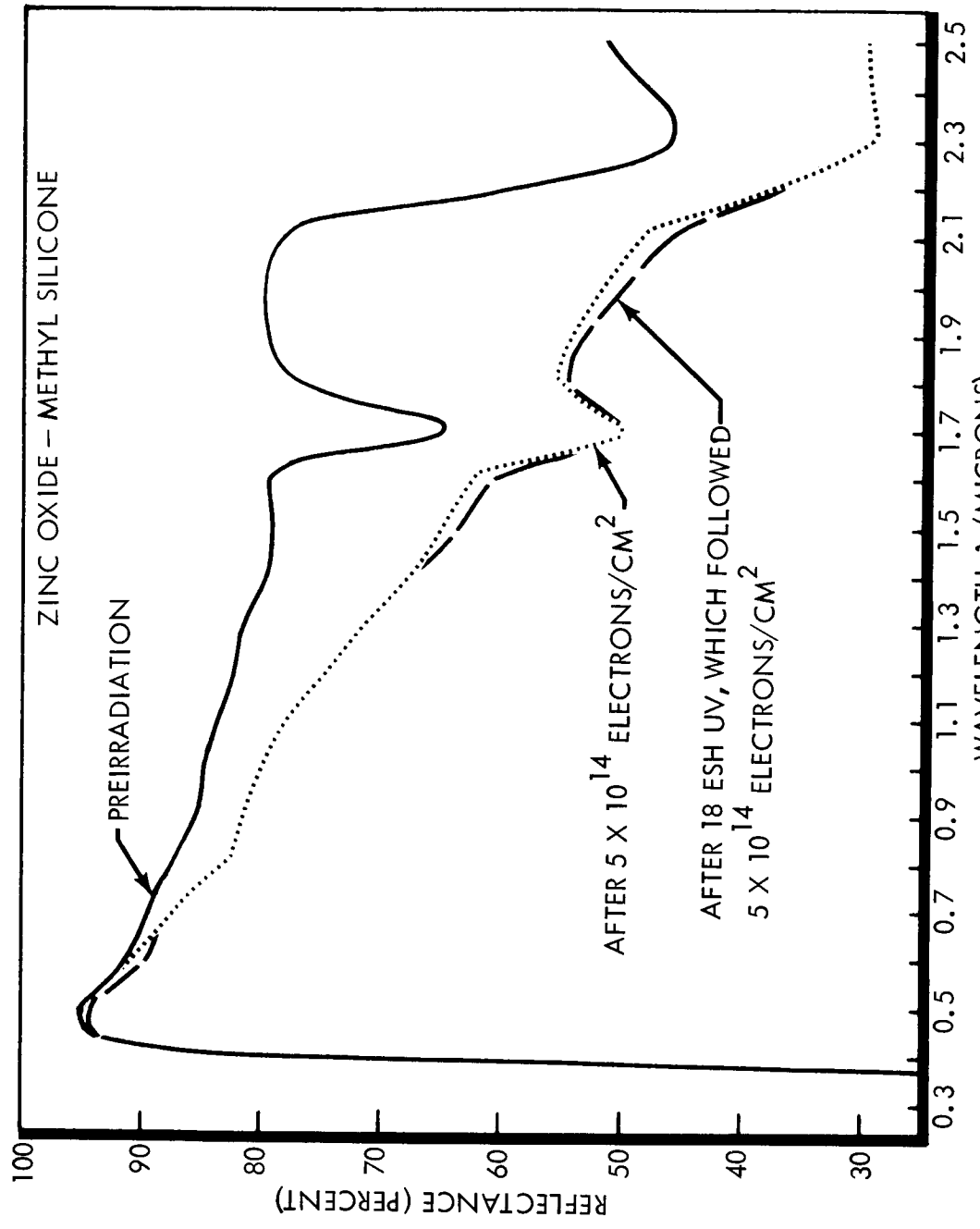

Figure 62. Spectral Reflectance of Type B (S-13) Following Consecutive Exposure to 50-keV Electrons, Then to Ultraviolet Radiation

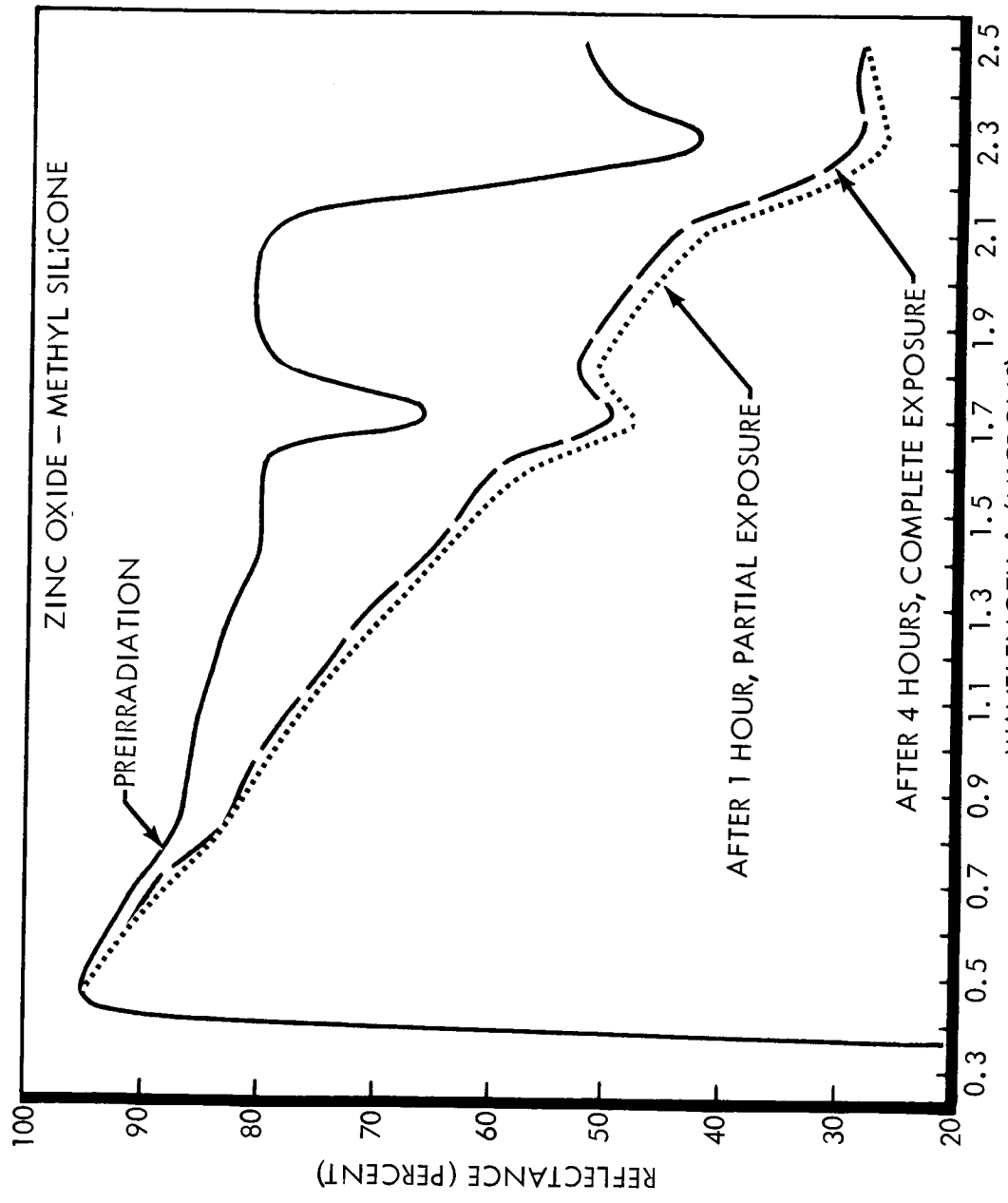

Figure 63. Spectral Reflectance of Type B (S-13) and Effects of Changing the **Electron**/Ultraviolet Exposure Ratio Midway Through Test

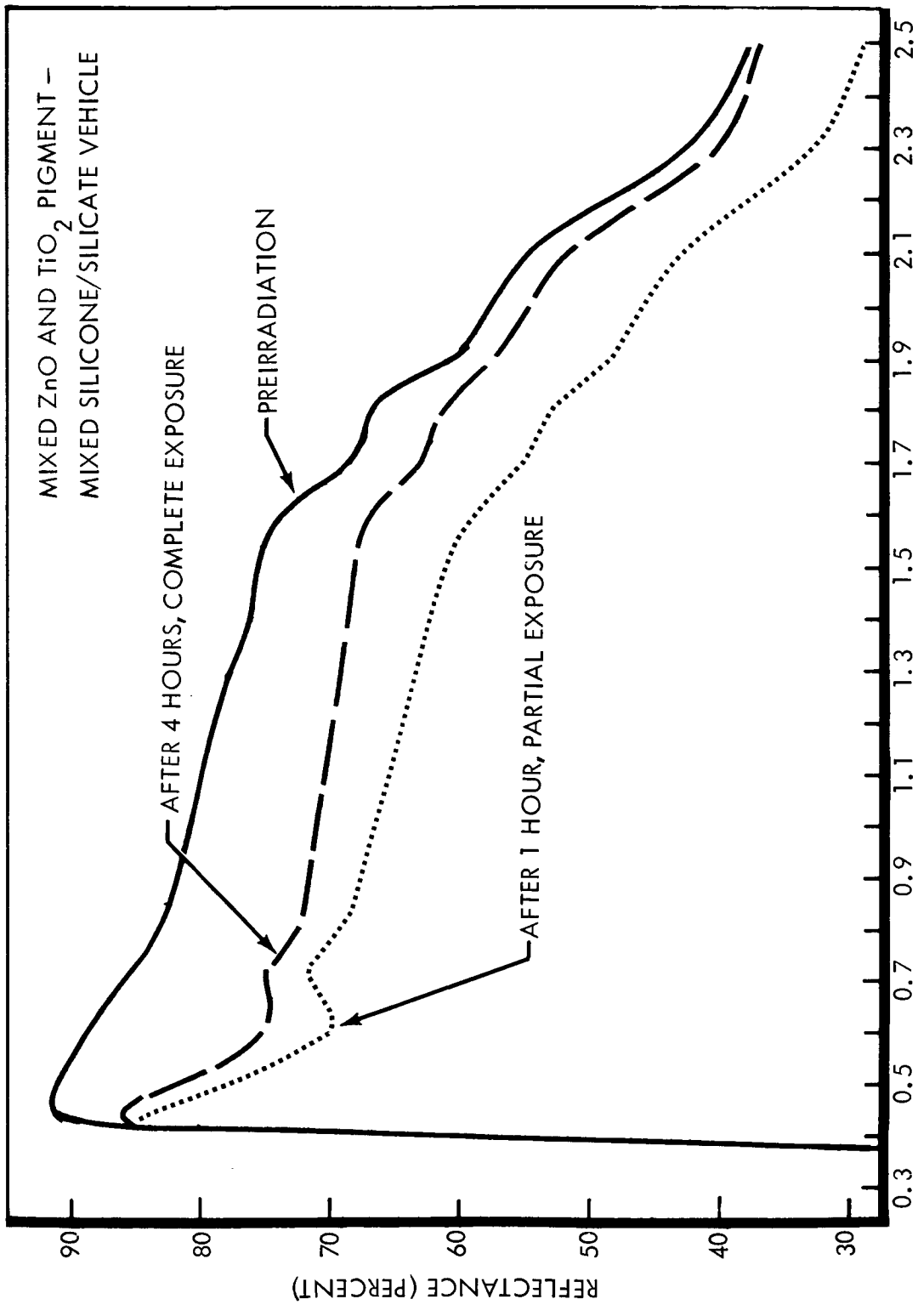

Figure 64. Spectral Reflectance of Type Q and Effects of Changing the Electron/Ultraviolet Exposure Ratio Midway Through Test

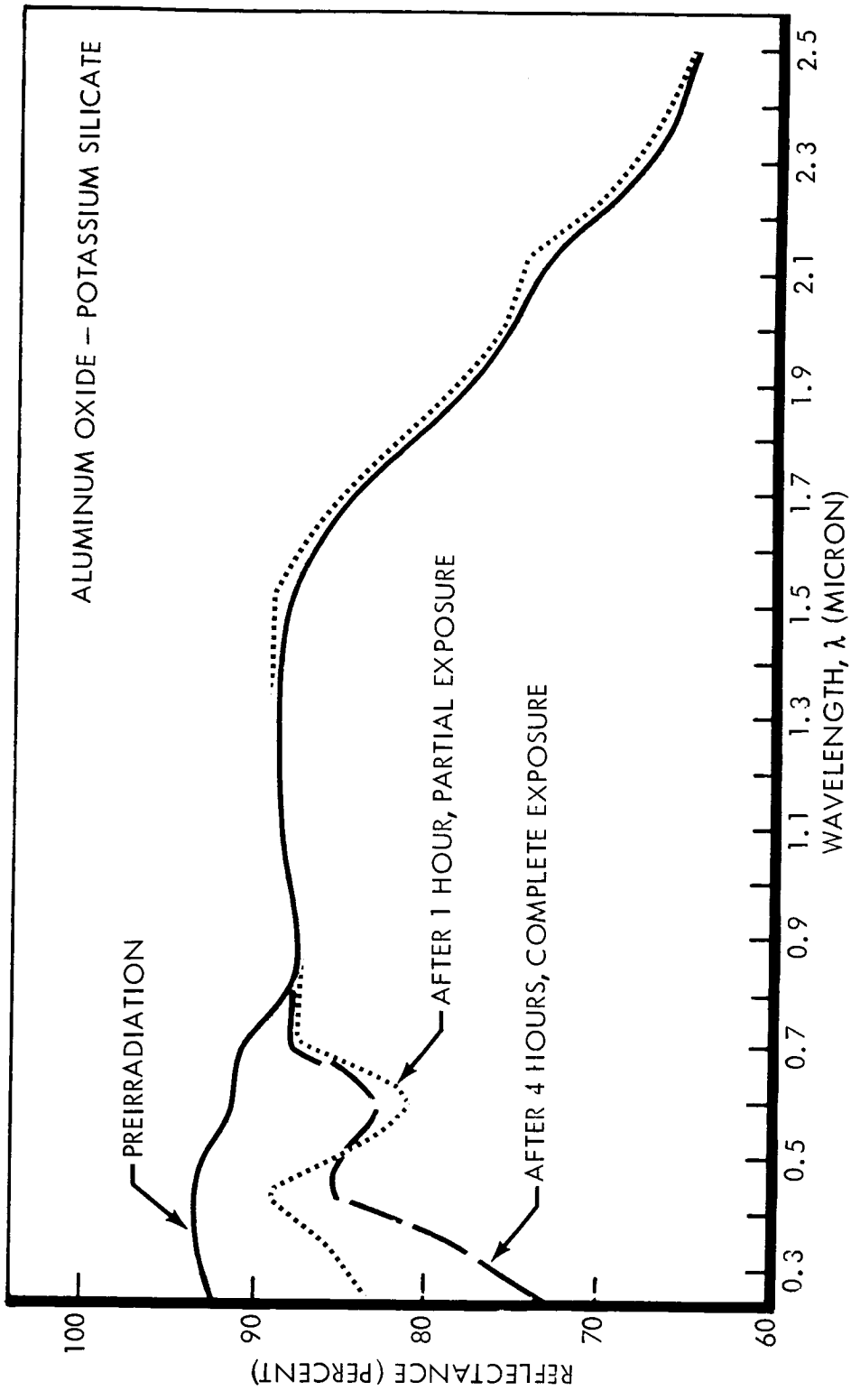

Figure 65. Spectral Reflectance of Type D and Effects of Changing the **Electron**/Ultraviolet Exposure Ratio Midway Through Test

on reflectance measurements made at the end of the complete exposure (4.1 hours), there is evidence of reflectance recovery in all three coatings tested, S-13, mixed ZnO/TiO_2—silicone/silicate, and Al_2O_3—potassium silicate.

2.5 PROTON EFFECTS SURVEY

A survey of the reflectance-degrading effects of 20-keV protons was conducted on seven types of thermal control coatings—three diffuse coatings and four specular surfaces—all currently being developed or considered for use, or in use in space thermal control applications.

All four types of specular surfaces (types G, H, J, and K) were found to be resistant to changes in reflectance from 20-keV protons. Only small changes in spectral reflectance were observed, even after exposure to 10^{17} protons/cm^2, and all specimens retained a high degree of specularity. Two white coatings tested (Pyromark and S-13G) sustained severe degradation of reflectance after exposure to 10^{16} protons/cm^2. However, threshold for damage was in the 10^{14} protons/cm^2 range, and even at 10^{15} protons/cm^2 the reflectance degradation was moderate. The buildup of damage, and the extent of reflectance recovery in air following exposure and in situ measurements, are shown in Figures 66 and 67. Note from the figures the contrasting spectral character of the measured damage in Pyromark and S-13G.

The third diffuse coating, leafing aluminum in phenylated silicone, like the specular surfaces was hard to 20-keV protons. Even at a fluence of 10^{17} protons/cm^2, in situ reflectance losses were moderate, and were confined to wavelengths shorter than 0.7 micron. On the other hand, reflectance as measured in situ increased at wavelengths longer than 0.7 micron, as shown in Figure 68. Thus a determination of solar absorptance would show little change due to proton exposure.

2.6 PHYSICAL CHANGES DUE TO RADIATION EXPOSURE

Significant changes were observed in the physical properties of many specimens when they were removed from the chamber after exposure and in situ measurement of reflectance. Many of the samples exposed to 8×10^{15} electrons/cm^2 exhibited

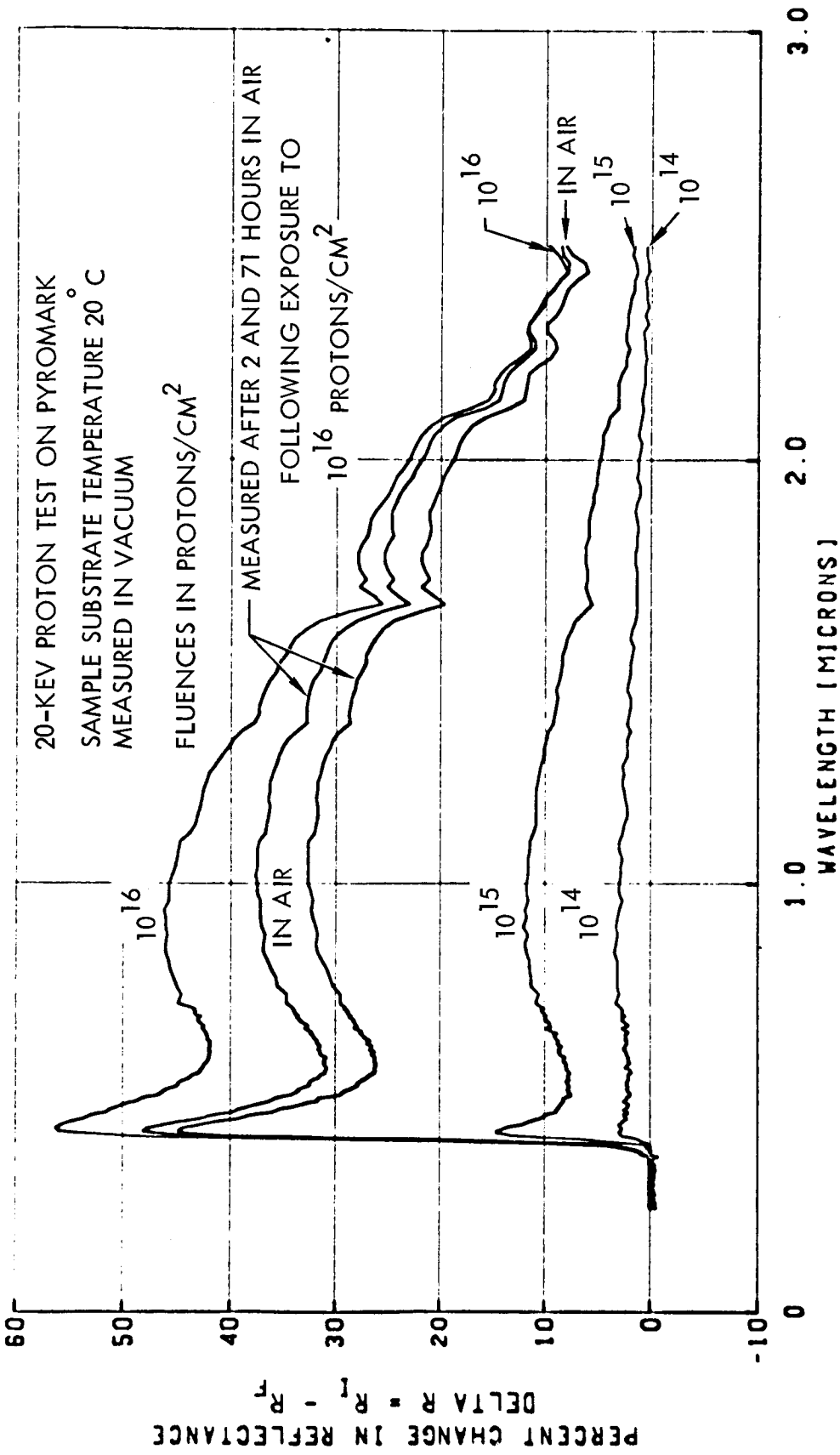

Figure 66. Buildup of 20-keV Proton Damage in Type Y (Pyromark)

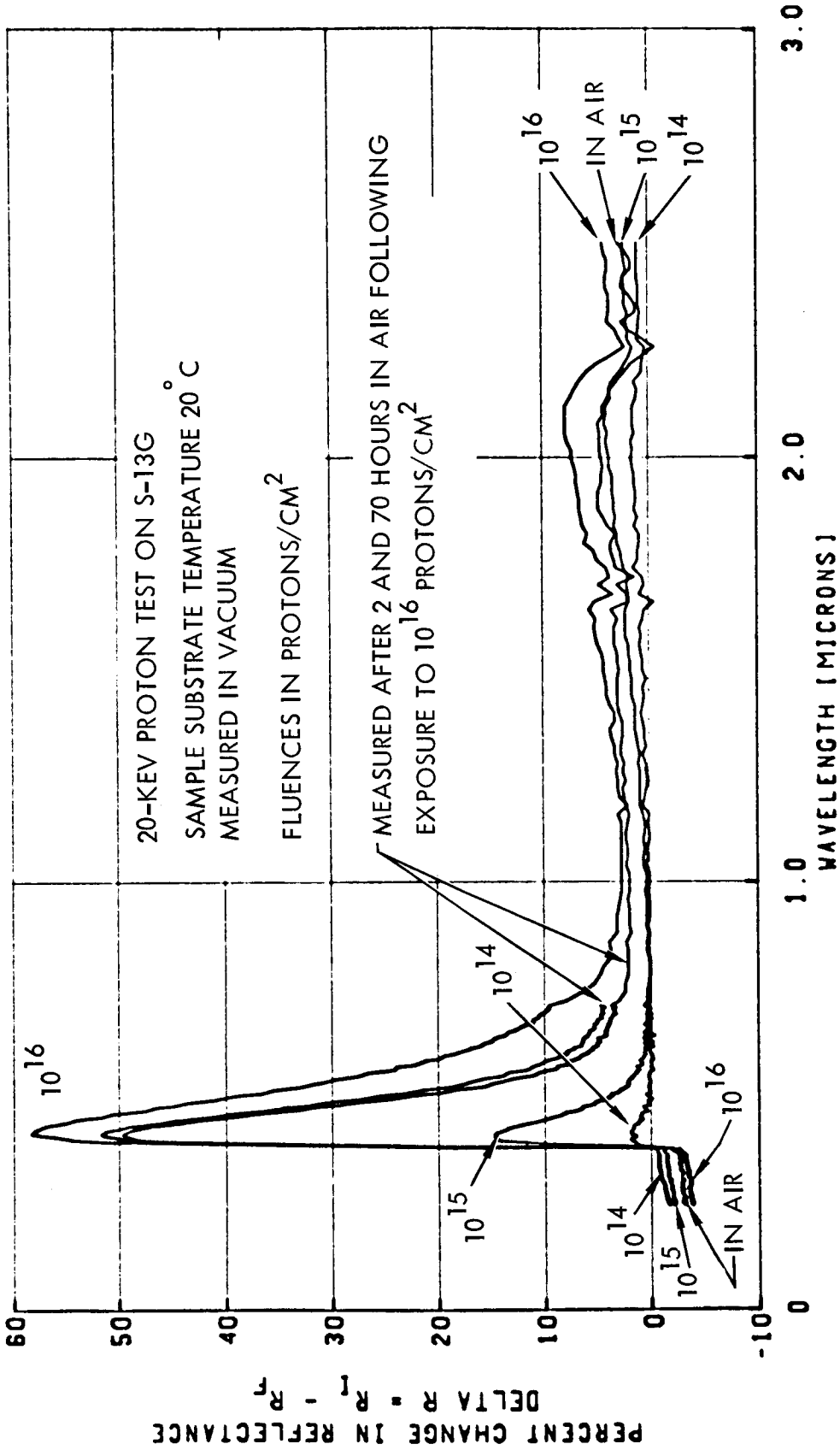

Figure 67. Buildup of 20-keV Proton Damage in Type M (S-13G)

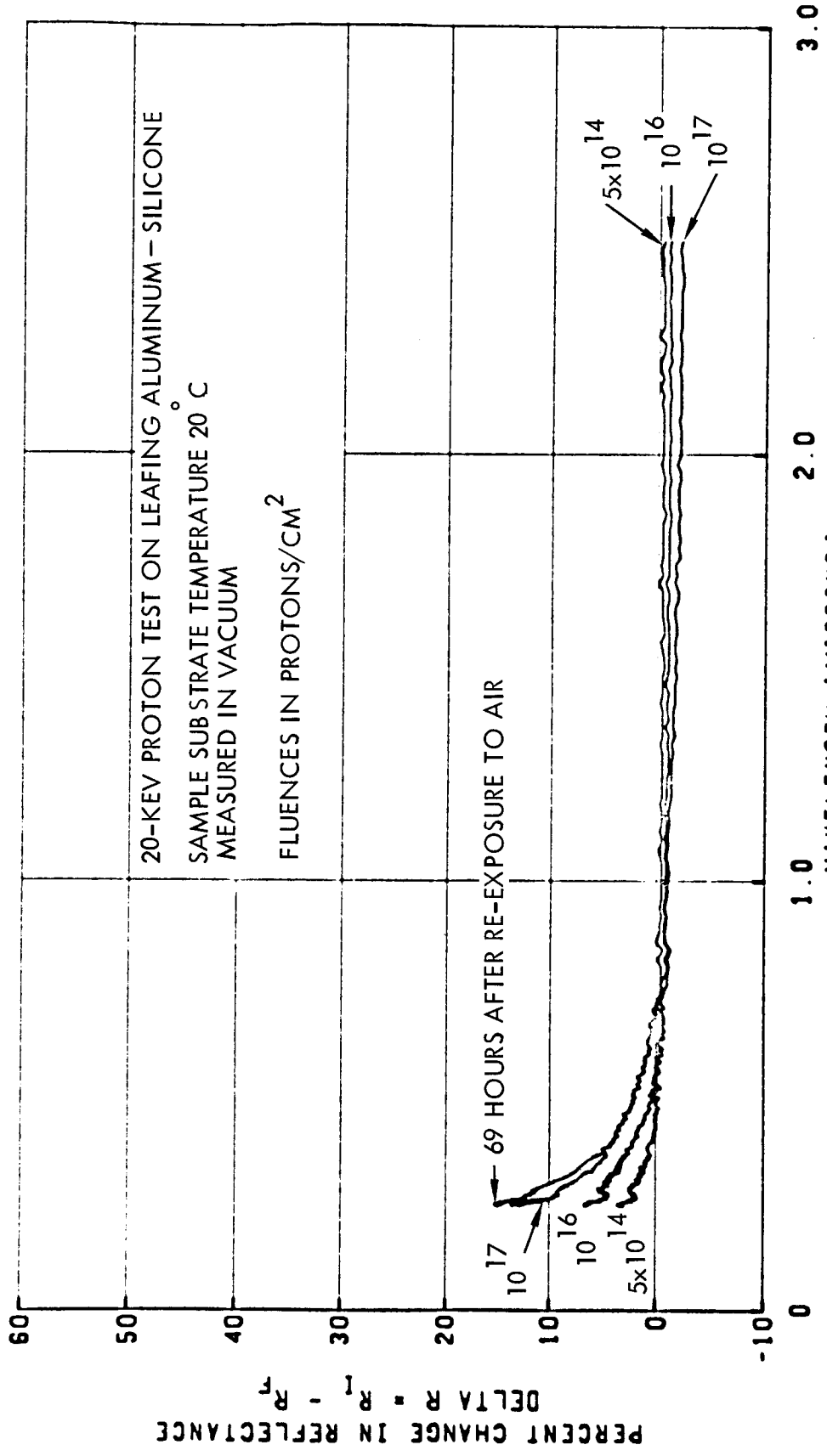

Figure 68. Buildup of 20-keV Proton Damage in Type I

a discernible graying as a result of exposure. Certain Pyromark, type M (S-13G), and type O samples exposed to ultraviolet radiation or to protons acquired a yellow or yellow-brown cast. One type O specimen, exposed to approximately 10^{15} protons/cm^2 in a dosimetry array, upon examination was found to have a crazed appearance. This specimen has been examined by optical and electron microscopy with the following results:

Crazing begins and ceases abruptly at boundaries between exposed and protected areas (Figure 69). (As used here, "protected" refers to the annular-shaped rim around the edge of each mounted sample.)

Occasional craze patterns appear to merge, diffuse, or blend with the uncrazed surface; examples are seen at center left and right in Figure 70. This blending occurs at the locations of various agglomerated particles.

The agglomerates are evident also in unexposed areas of this specimen, which was tested in vacuum (Figure 69), and in another type O sample neither pumped down to vacuum nor tested (Figure 71). As shown in this document, Figures 69, 70, and 71 are all magnified 225 times the size of the type O sample.

To study the exposed type O sample by electron microscope, a polyvinyl alcohol replica was taken from a portion of the specimen covering both areas that were exposed to protons, and areas that were unexposed. The replica was shadowed with vapor-deposited germanium at an angle of 25°, then backed with a vapor-deposited layer of carbon, deposited normal to the surface. A section of the replica comprised of approximately 50% exposed and 50% unexposed areas was cut out and placed in distilled water to dissolve the polyvinyl alcohol. The replica was then picked up on a copper grid having 75 x 300-micron openings. After drying, the grid was placed in the electron microscope for viewing.

Four electron micrographs were taken of the replica. Figure 72 shows the boundary between the exposed and unexposed areas, at 6,750X. Extensive micropitting can be seen in the exposed region, which is the upper portion of Figure 72.

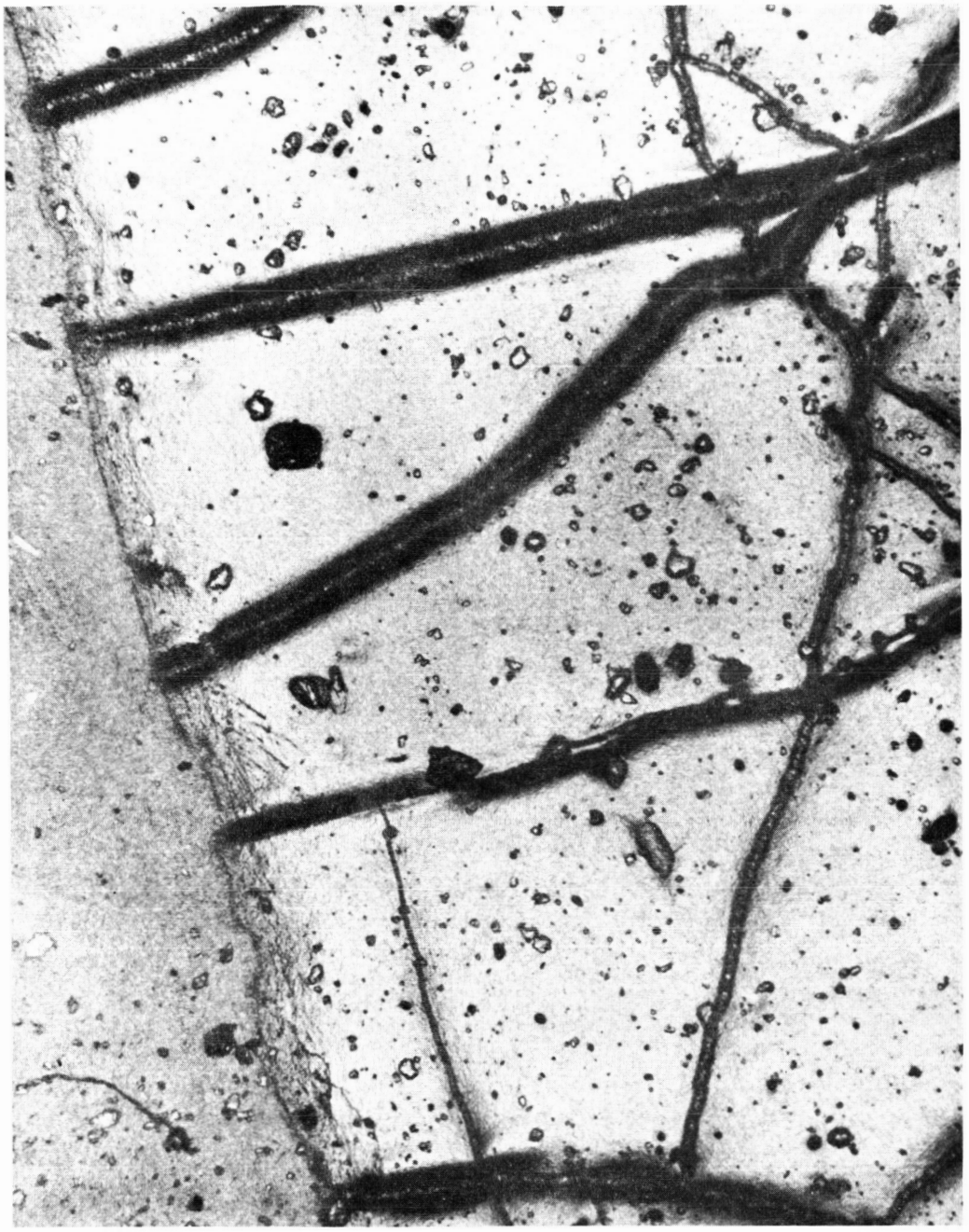

Figure 69. 225X Bright-Field Photomicrograph of Type O Sample Exposed to 20-keV Protons, Showing Boundary Between Exposed and Protected Regions, and Crazing in Exposed Region.

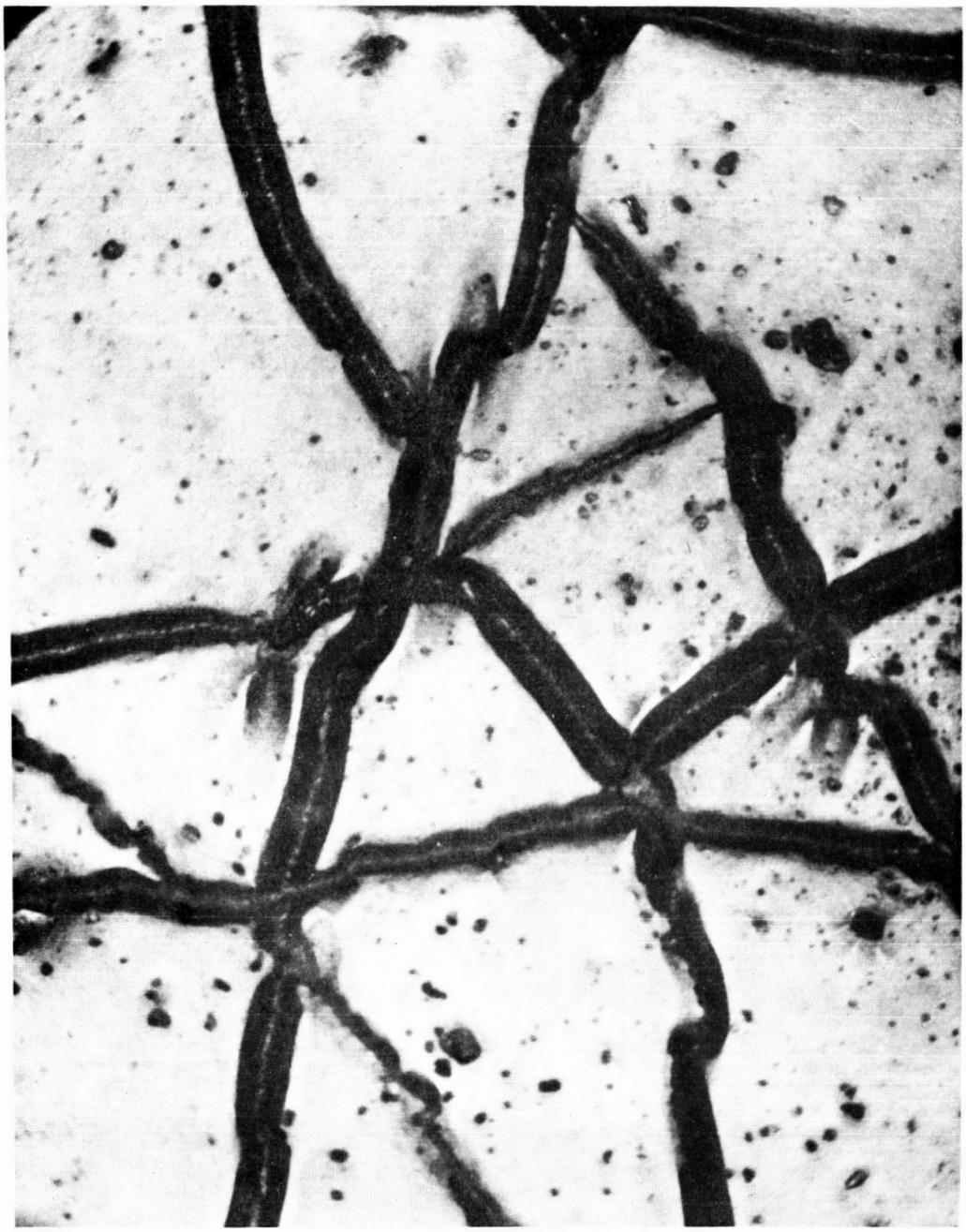

Figure 70. Patterns of Surface Crazing in Exposed Region of an O Type Sample, Including Blending of Craze Marks With the Surface at Locations of Agglomerated Particles.

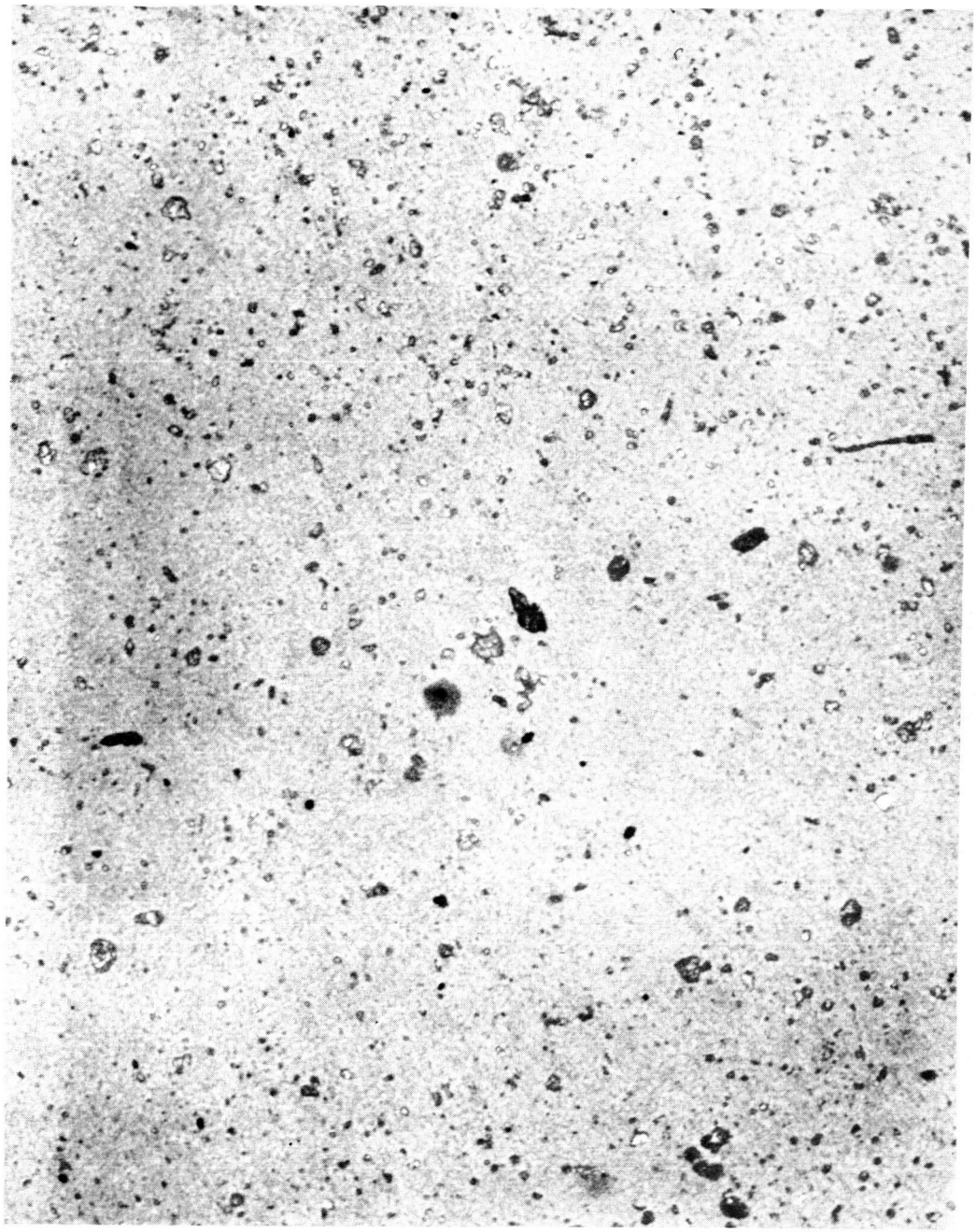

Figure 71. 225X Photomicrograph Showing Agglomerated Particles in a Sample of Coating Type O. This Sample was Neither Subjected to Vacuum nor Exposed to Radiation.

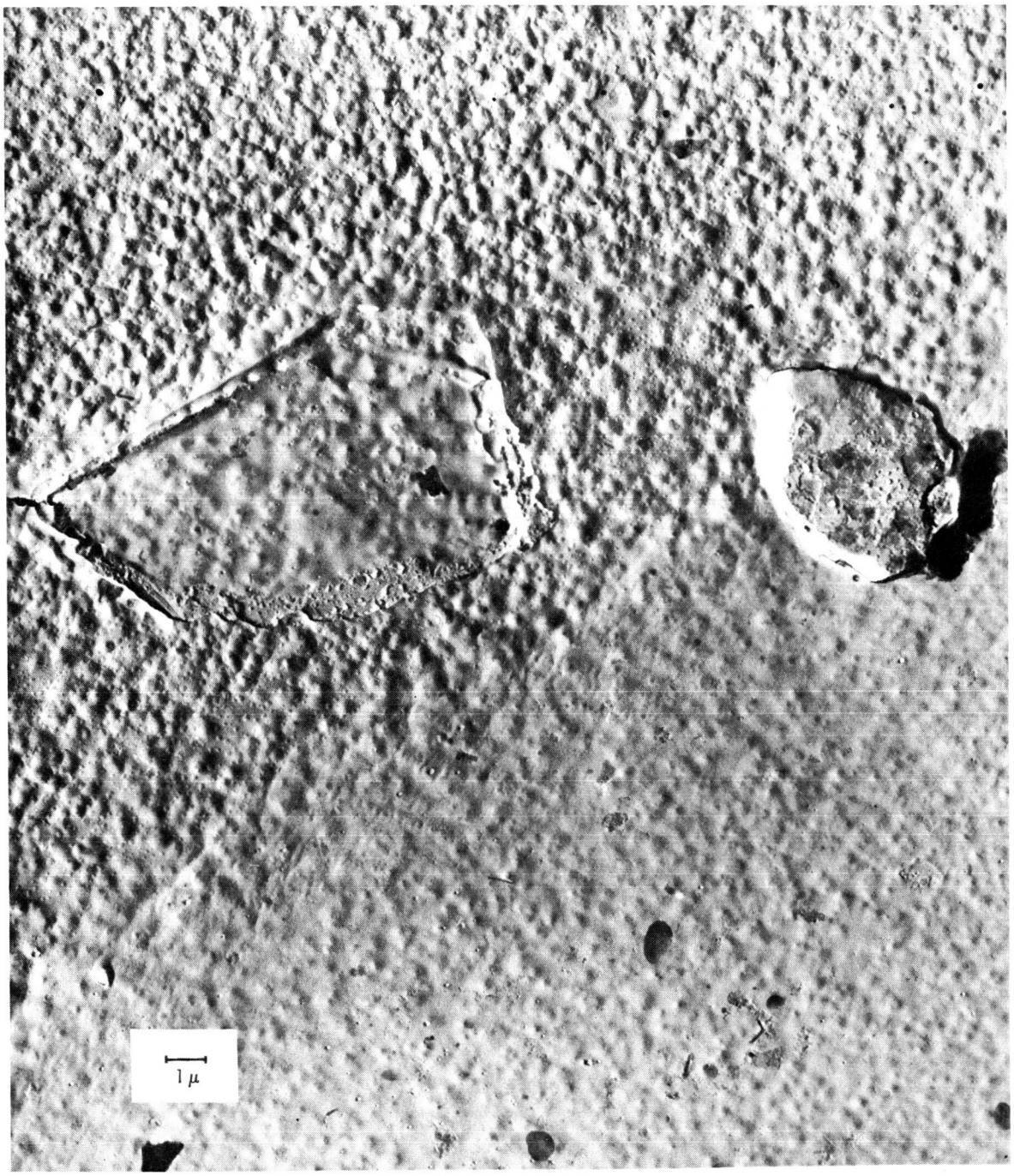

Figure 72. 6,750X Electron Micrograph of Both Proton-Exposed and Unexposed Regions of a Type O Sample

The size of the micro-pits is seen to be on the order of 0.1 micron (approximately 1000 Å). In Figure 72 there is evidence of greater hardness against pitting, in the area of the surface occupied by the 10-micron agglomerate particle. In fact, the appearance of this area is strikingly like the appearance of the unexposed area (lower portion of Figure 72).

Figure 73 establishes the shadowing direction as being from left to right. Since the polyvinyl alcohol replica is a negative impression of the original titanium dioxide—methyl silicone surface, this determination of the direction of shadowing indicates that the crazing marks are depressions in the surface of the type O sample, rather than elevations above the surface. Figure 73 shows also the contrasting pitting characteristics of the majority of the surface area, and of the agglomerate at center left.

Figures 74 and 75 explore further detail of the depressed craze marks. Easily seen is the fine structure within each depression. Figure 74 also shows a characteristic appearance noted in this surface at locations where a depression meets an agglomerated particle. Figure 75 includes an intersection of two depressions and the consequent overlapping of fine structural characteristics.

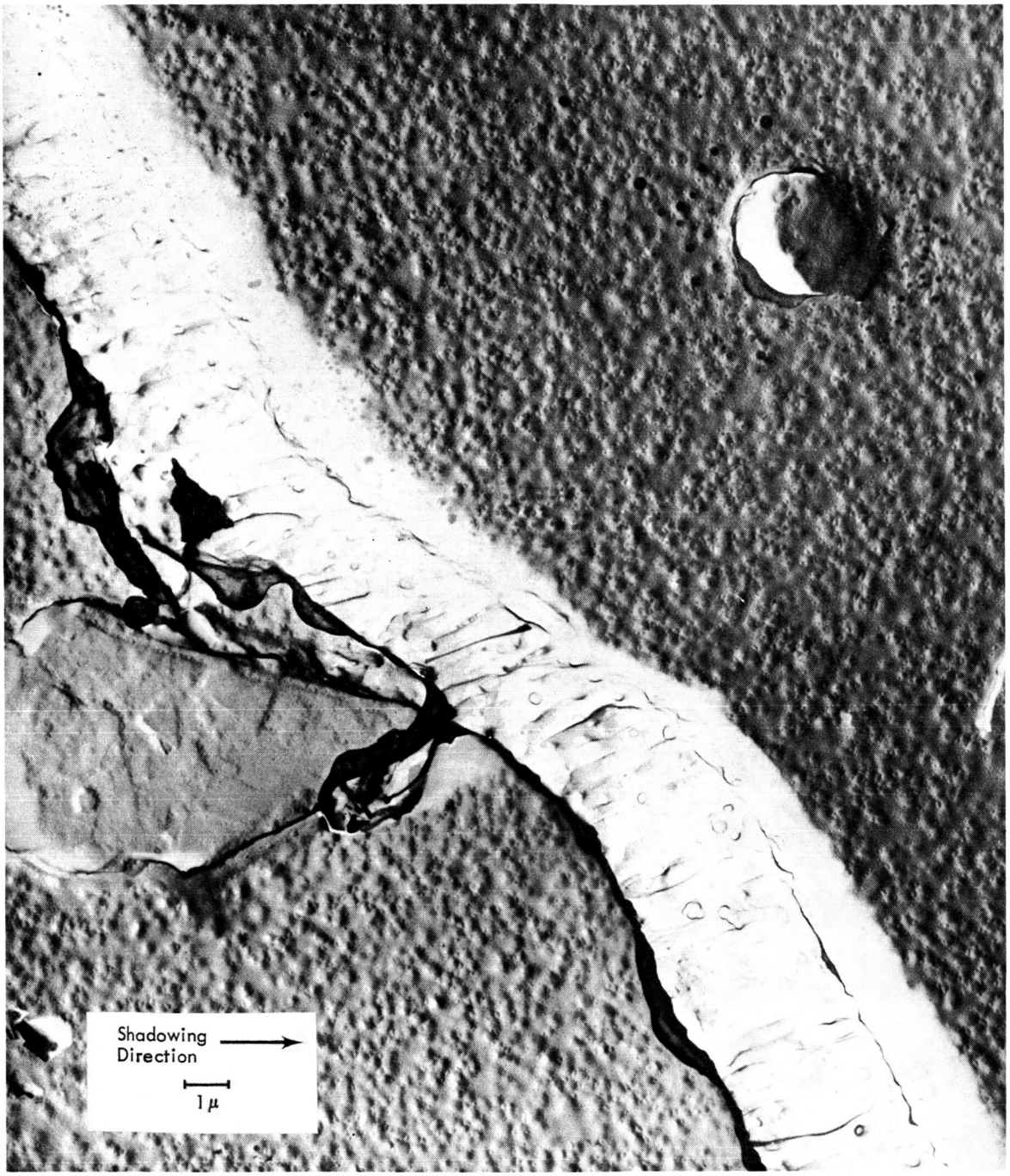

Figure 73. 6,750X Electron Micrograph Establishing the Shadowing Direction in a Proton-Exposed Type O Coating, Including a Crazing Depression.

Figure 74. 6750X Electron Micrograph of a Portion of Proton-Exposed Type O Coating, Including an Intersection of a Craze Depression With an Agglomerate Particle.

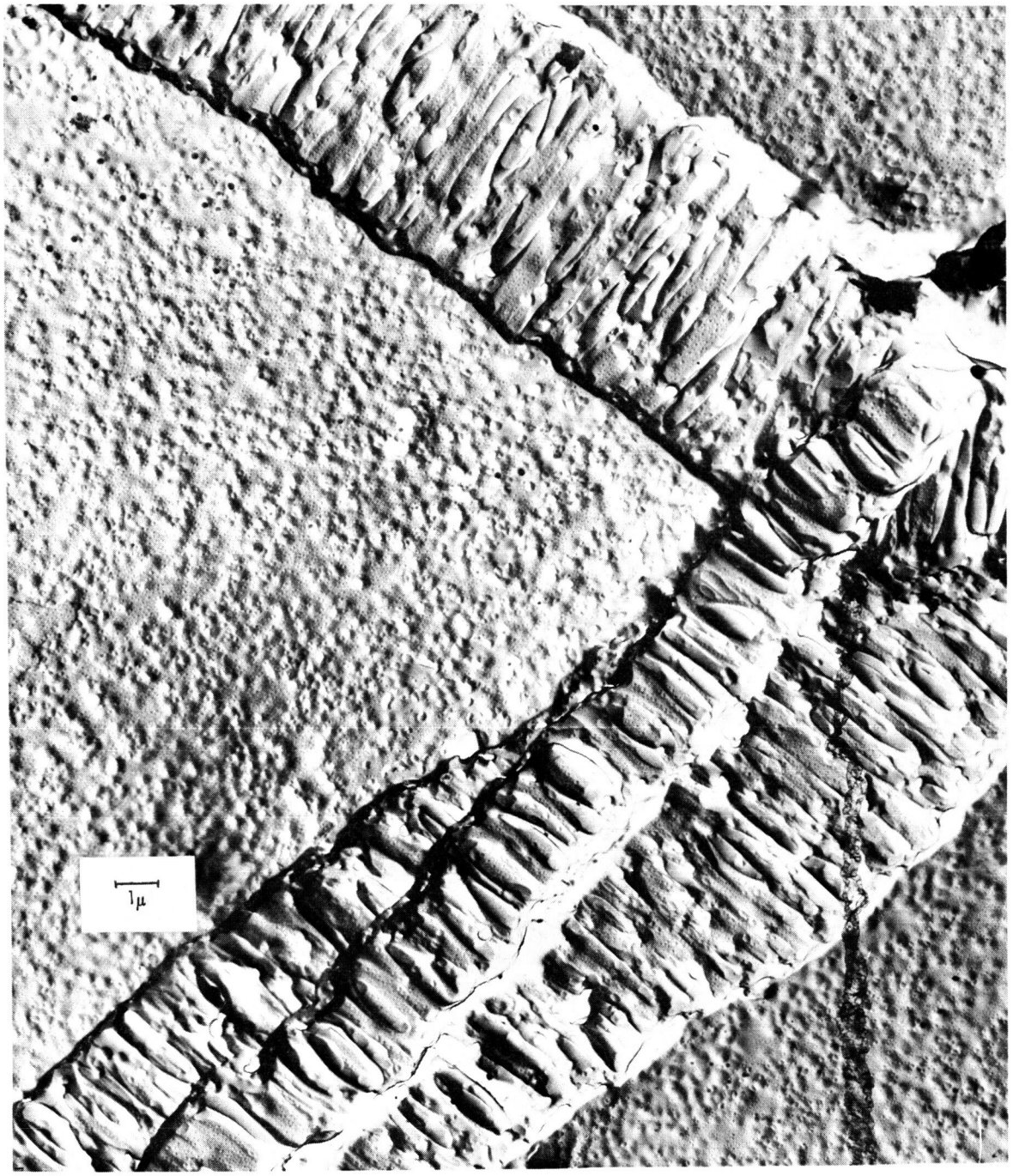

Figure 75. 6750X Electron Micrograph of a Portion of Proton-Exposed Type O Coating, Including the Intersection of Two Craze Depressions.

3.0 NEW TECHNOLOGY

The research performed on this contract has been reviewed for the purpose of uncovering potential reportable New Technology items. The review activities have considered both the results of each test in turn, and the correlation of those results to determine the overall performance of each thermal control coating. To the best of our knowledge, there is no New Technology to report.

4.0 CONCLUSIONS AND RECOMMENDATIONS

4.1 CONCLUSIONS

From the electron exposure tests we conclude that:

(1) The specular surfaces tested and the type I diffuse coating tested are relatively "hard" to reflectance degradation under 50-keV electron exposure.

(2) Excepting type I, the diffuse coatings or paints tested are subject to severe, in-air recoverable degradation in the infrared wavelength region, and to substantial visible-region reflectance losses which are less recoverable or "bleachable" upon re-exposure of test samples to air.

(3) Coatings employing methyl silicone binders sustain the greatest degree of reflectance degradation in the infrared wavelength region. Coatings using potassium silicate binders suffer the largest electron-induced reflectance losses in the visible region.

(4) Over the wide range of fluxes and fluences used (4×10^8 to 1.7×10^{12} electrons/cm^2/sec, and 10^{13} to 8×10^{15} electrons/cm^2) no irradiation rate effects from 50-keV electrons are evident from in situ measurements of hemispherical spectral reflectance obtained with an integrating sphere reflectometer. Thus, to an acceleration factor of 10^3 or so, laboratory exposures of the tested coatings to 50-keV electrons at rates greater than those in space are valid.

From the "ultraviolet" exposure tests we conclude that:

(5) The specular surfaces and type I are resistant to reflectance change in the infrared wavelength region, but undergo substantial, permanent reflectance losses in the visible and ultraviolet wavelength regions.

(6) The diffuse coatings tested are subject to reflectance degradation over much or all of the measured 0.24- to 2.5-micron wavelength region.

(7) Damage thresholds and rates of damage buildup vary widely among the classes and types of coatings tested. Within their class, titanium dioxide—methyl silicone sample types show the widest variation in effects, of all classes of samples tested. One TiO_2—methyl silicone coating type was the most resistant of the diffuse samples to reflectance changes.

(8) Upon re-exposure to air following exposure to ultraviolet-rich electromagnetic radiation, only a few types of tested coatings (B, F_3, L, O, P, and Y) recover fairly close to their respective preirradiation reflectance values. In the majority of coatings exposed to ultraviolet, there is little evidence of increased reflectance in air when compared to postirradiation in situ reflectance values.

(9) Separate tests show that UA-series long-arc mercury, and Pek long-arc xenon, ultraviolet sources are about equally effective for inducing reflectance losses in selected thermal control coatings.

From the proton exposure test we conclude that:

(10) The specular surfaces and type I are quite resistant to reflectance changes across the 0.24- to 2.5-micron wavelength region.

(11) S-13G and Pyromark exhibit severe reflectance losses in the visible wavelength region. Only partial recovery of reflectance occurs in air.

From the combined electron-ultraviolet tests we conclude that:

(12) Reflectance changes resulting from coating exposure to a combined electron-ultraviolet environment are less than additive, whether the combined irradiation occurs simultaneously or sequentially.

(13) Increasing the ultraviolet-to-electron intensity ratio during an exposure, or having ultraviolet exposure follow exposure to electrons causes partial restoration of reflectance in some types of coatings. Exposure to ultraviolet before electron exposure favorably preconditions come coatings to resist later changes due to the presence of the electron flux. This suggests

the possibility of pre-exposing properly configured thermal control coatings on the ground, in order to obtain reduced degradation later in space.

From the overall testing program we conclude that:

(14) Optimum formulation of coatings in a given class (e.g., TiO_2—methyl silicone) must be determined by iterative steps, since radiation-induced degradation is strongly dependent upon seemingly minor variations in such parameters as coating thickness, ratio of pigment to binder, and (for samples with mixed constituents) relative amounts of pigment or binder components.

(15) Wavelength regions in which the largest reflectance changes occur are substantially different for the three cases of electron, proton, and ultraviolet radiation. Exposure to 50-keV electrons causes the greatest reflectance losses in most diffuse coatings to occur in the infrared. Ultraviolet radiation and proton radiation result in more damage at shorter wavelengths, particularly at any existing ultraviolet absorption edge. Degradation from protons is more likely to extend as one band to longer wavelengths in a given type of coating, while separate bands of increased absorptance are more likely to result from incident ultraviolet radiation.

(16) Reflectance recovery phenomena following electron, proton, and ultraviolet exposure are likewise diverse. This diversity of both reflectance loss and reflectance recovery phenomena indicates that more than one damage mechanism may be operating in the types of coatings tested.

(17) The sequencing of combined environment exposures affects significantly the degradation that results. Except for simulating missions actually encountering a sequence of ultraviolet and electrons in space, test standardization on simultaneous exposure to electrons and ultraviolet is essential to prevent drawing false conclusions about performance of coatings in the existing, multiconstituent space environment. Future selection of coatings for space use should be even more strongly mission-dependent and based upon the

anticipated relative intensities of constituents in the space environment.

(18) The results of these tests on thermal control coatings tie together (a) the results of early in-air tests in which specimens exposed to high fluences evidenced lasting effects mainly in the visible region, and (b) the more recent results of in situ testing that indicate that contamination-free exposures to electrons show reflectance changes in the infrared region as well.

4.2 RECOMMENDATIONS

This program has provided the basis for making the following recommendations:

(1) A study of the dependence of coating or surface reflectance degradation upon the incident energy of protons and electrons between 2 and 80 keV should be performed as follow-on work to this contract.

(2) A study of rate effects from ultraviolet radiation should be made from one to five or more space ultraviolet suns, to provide baseline data of a scope comparable to electron data available from this program. This will provide a better basis for:

(3) A properly-planned (i.e., related to orbital environments expected to be encountered) multiple radiation environment test program.

(4) A study of in-vacuum (in situ) reflectance changes with time following exposure of thermal control coatings to electromagnetic and particle radiation should be performed to provide more basic data on possible damage mechanisms.

(5) Based upon evidence of micro-pitting in selected coatings following proton exposure, an investigation of light trapping from such pitting as a potential mechanism for increased absorptance (reflectance degradation) should be made.